

DIPLOMARBEIT

Mass spectrometry of pharmacologically active glycoconjugates from *Crocus sativus* L.

Ausgeführt am Institut für

Chemische Technologien und Analytik

der Technischen Universität Wien

unter der Anleitung von

Univ.Prof. Mag.pharm. Dr.rer.nat. Günter Allmaier

durch

Edita Rados

Wallensteinstraße 42/17, 1200 Wien

April 2016

Edita Rados

Abstract

Crocus sativus L. is one of the most expensive spice plants in the world, better known under the name "saffron". It has been used for thousands of years not only as a spice and food colorant, but also for various folk medical purposes. Especially the dried saffron stigmas, which contain crocins being responsible for its color and acting as potential pharmacological active compounds, were structurally analyzed by LC-ESI-MSⁿ (n=1-3). Previous studies showed that crocins constitute ester glycosides with one and two glycosylation sites, respectively, containing up to five glucose units in total, but only up to three glucose units per site.

In order to further investigate crocetin ester glycosides reverse-phase HPLC was coupled to ESI MS. For optimum separation a method with a long gradient with water/methanol as mobile phase was developed. The addition of formic acid to the mobile phase was necessary in order to get improved LC peak shapes, especially for those peaks related to compounds exhibiting one free carboxylic acid group.

During extensive LC-MS² and -MS³ experiments a large number (> 10) of previously undescribed new crocetin ester glycosides was found including a second type of apocarotenoid aglycon (a C₁₇ backbone, which we termed "norcrocetin" in contrast to the known C₂₀ apocarotenoid aglycon crocetin) as well as highly glycosylated monosubstituted crocetin ester glycosides with up to 11 glucose units. Several other low abundant crocins with already known molecular mass, but representing non-described crocin isomers, were found, too.

In the second part of this thesis, an attempt to locate crocins on the surface of saffron stigmas was made. For this purpose MALDI imaging mass spectrometry was used. It delivers spatial distribution of the analytes on the desired surface. Experiments with two different matrices, DHB (2,5-dihydroxy benzoic acid) and THAP (2,4,6-trihydroxyacetophenone) were performed.

Best results were obtained using the DHB matrix but the location of crocetin glycosides was different from stigma to stigma and because of this a general fixed location of crocins could not be determined.

For the determination of any specific changes of the matrix distribution on the surface of saffron stigmas when these two matrices were applied prior to/after storage under vacuum conditions, EM experiments were performed. Because of the uneven surface of the saffron stigmas it was not possible to conclude that better/worse distribution of the matrix was the result of the way the stigmas were stored before the matrix was applied.

Zusammenfassung

Crocus sativus L. ist eine der teuersten Gewürzpflanzen der Welt, besser bekannt unter dem Namen "Safran". Es wird seit tausenden von Jahren nicht nur als Gewürz und Lebensmittelfarbstoff, sondern auch für verschiedene volksmedizinische Zwecke verwendet. Vor allem die getrockneten Safran-Stigmas, die Crocine enthalten und die für die Farbe verantwortlich sind, werden als potenzielle pharmakologische Wirkstoffe gesehen und wurden strukturell mit LC-ESI-MSⁿ (n=1-3) analysiert. Frühere Studien zeigten, dass Crocetinesterglykoside eine oder zwei Glykosylierungsseiten haben können, mit insgesamt bis zu fünf Glucoseeinheiten, aber nur bis zu drei Glucoseeinheiten pro Glykosylierungsstelle.

Um Crocetinesterglykoside weiter zu untersuchen, wurde eine Umkehrphasen-HPLC mit ESI MS gekoppelt. Für eine optimale Trennung wurde eine Methode mit einem langen Gradienten mit Wasser/Methanol als mobile Phase entwickelt. Die Zugabe von Ameisensäure zur mobilen Phase war notwendig, um bessere LC-Peakformen zu bekommen, insbesondere bei jenen Peaks, die von den Verbindungen stammen, die eine freie Carbonsäure-Gruppe enthalten. Während umfangreicher LC-MS² und -MS³ Experimente wurde eine Vielzahl (> 10) der bisher nicht beschriebenen neuen Crocetinesterglykoside gefunden, sowie eine zweite Art von Apocarotenoid Aglycon (mit C₁₇- Grundkörper, das wir "Norcrocetin" genannt haben im Gegensatz zum bekannten C₂₀ Apocarotenoid Aglycon Crocetin) und hochglykosylierte monosubstituierte Crocetinesterglykoside mit bis zu 11 Glucose-Einheiten. Mehrere andere gering vorkommende Crocine mit bereits bekannten Molekülmassen, die aber nicht beschriebenen Crocin Isomeren zuzuordnen sind, wurden auch gefunden.

Im zweiten Teil dieser Arbeit wurde versucht, Crocine an der Oberfläche der SafranßStigmas zu lokalisieren. Zu diesem Zweck wurde MALDI Imaging Massenspektrometrie verwendet. Sie liefert die räumliche Verteilung der Analyten auf der gewünschten Oberfläche. Versuche mit zwei verschiedenen Matrices , DHB (2,5-dihydroxy benzoic acid) and THAP (2,4,6-trihydroxyacetophenone).

Die besten Ergebnisse wurden mit der DHB-Matrix erreicht. Die Position der Crocetinglykoside war unterschiedlich für jedes untersuchte Stigma und aus diesem Grund konnte keine allgemeine Aussage über die Lokalisation der Crocine getroffen werden.

Um zu sehen, ob Veränderungen auf der Oberfläche der Safranfäden passieren, wenn diese beiden Matrizen angewendet wurden und wie sich die Lagerung von Safranfäden unter Vakuum, vor der Matrix Applikation, auf die Matrixverteilung auf der Oberfläche auswirkt, wurden EM-Experimente durchgeführt. Wegen der unebenen Oberfläche der Safranfäden war es nicht möglich mit Hilfe von EM, zum Entschluss zu kommen, dass die bessere/schlechtere Verteilung der Matrix das Ergebnis ist, wie die Safranfäden vor der Matrix auftragung gelagert wurden.

Danksagung

Für meine Mutter und meinen Vater, die auf vieles verzichtet haben um mir das Studium zu ermöglichen.

Sehr großer Dank gilt Professor Günter Allmaier, dessen Vorträge mich inspiriert haben bei ihm die Diplomarbeit zu schreiben, Ernst Pittenauer, der mir viel geholfen hat und immer bereit war, meine Fragen zu beantworten, der gesamten Arbeitsgruppe und allen anderen, die mir geholfen haben.

Danke auch an meinen Bruder, der für mich nur das Beste will.

Table of Contents

1. Introduction	1
1.1 <i>Crocus sativus</i> L. – Saffron	1
1.1.1 Building components.....	3
1.1.1.1 Crocin.....	4
1.1.2 Pharmacological usage	7
1.1.2.1 Possible use of crocins in the treatment of Alzheimer disease.....	7
1.2 Scope of this study	9
1.3 Mass spectrometry.....	10
1.3.1 Ionization Techniques.....	11
1.3.1.1 MALDI	12
1.3.1.2 ESI	13
1.3.2 Mass spectrometric analyzers	16
1.3.2.1 Time of flight (TOF) mass analyzer	17
1.3.2.2 Reflectron time of flight (RTOF) mass analyzer.....	19
1.3.2.3 Quadrupole ion trap (QIT)	21
1.3.2.4 Tandem MS, multistage MS and Collision Induces Dissociation (CID)	23
1.3.3 Detectors	24
1.4 Imaging mass spectrometry (IMS).....	27
1.5 LC-ESI MS	28
1.6 Electron Microscopy (EM)	30
1.7 Carbohydrate product ion nomenclature	31
2. Experimental	33
2.1 Saffron	33
2.2 LC-ESI MS	34
2.2.1 Sample preparation	34
2.2.2 LC-ESI MS instrumentation and parameters	34
2.3 Imaging MALDI MS	38
2.3.1 Sample preparation	38
2.3.2 Imaging MALDI MS parameters.....	40
2.3.2.1 UltrafleXtreme.....	40
2.3.2.2 Axima TOF ²	41
2.4 Electron Microscopy	43

2.4.1 Sample preparation	43
2.4.2 EM parameters	43
3. Results and discussion	45
3.1 LC-ESI MS	45
3.1.1 Crocin glycosylation pattern including aglycon pattern	48
3.1.1.1 Crocetin structures	49
3.1.1.2 Norcrocetin structures	54
3.1.2 Highly glycosylated crocetin	58
3.1.3 Summary	60
3.2 Imaging MALDI MS	64
3.2.1 UltrafleXtreme	66
3.2.2 Axima TOF ²	74
3.3 Electron Microscopy	84
4. Conclusion	89
5. References	92
6. Equipment / Instruments / Materials	96
7. List of Figures	97
8. List of tables	101
9. List of abbreviations	102
10. Appendix	104
10.1 Mass spectra of identified crocins containing crocetin aglycon	104
10.2 Mass spectra of identified crocinc containing norcrocetin aglycon	116
10.3 Axima TOF ² and UltrafleXtreme IMS results	119
10.4 Electron Microscopy results	126

1. Introduction

Substances that can influence the activity of living organisms or the function of an organism are called pharmacologically active substances. They can be formed naturally or be manufactured. Such substances have large importance in the medicine because they can be used in treatment of different diseases. The pharmacologically active glycoconjugates refer to the substances that are composed of carbohydrates linked covalently to aglycons e.g. steroids, lipids or peptides.

When a sugar, which is a carbohydrate, is linked to some functional group via O-glycosidic bond, then these molecules are called glycoside. The focus of this thesis will be especially on crocetin glycosides found in the stigmas of *Crocus sativus* plant which are considered as pharmacological active compounds.

1.1 *Crocus sativus* L. – Saffron

Saffron is one of the most expensive spices of the world, produced from the stigmas of the *Crocus sativus* L. flowers (Figure 1). Belonging to the large *Iridaceae* family this plant is its only member that can be used as a spice [1].



Figure 1: *Crocus sativus* L. – Saffron, drawn after a photograph from [48]

It is characterized through purple flower and the fact that it is an autumn flowering plant that can only be reproduced vegetatively. The parts of interest of the flower are the dark red colored threads representing the stigmas of the flower (Figure 2). Each flower has only 3 stigmas, which means that a large number of the flowers are necessary in order to produce 1 gram of the final product [1].



Figure 2: Saffron stigmas

Crocus sativus has been cultivated in many countries, but the plant originated from *Crocus cartwrightianus* located in the eastern Mediterranean region [2].

For thousands of years saffron has been used not only as a spice and food colorant, but also for various folk medical purposes e.g. for the treatment of kidney problems, to cure colds, reduce inflammations or for the treatment of diabetes patients [1-7]. Because of that it has always been seen as very valuable plant which leads to extremely high prices of the stigmas. For the harvest the stigmas need to be plucked by hand and stored for drying. During the dehydration chemical and physical reactions occur which lead to the end product, the saffron spice. The different dehydration time and the time of harvest influence the quality of the saffron [3]. Because of its wide range of application saffron has become the focus of scientific research.

1.1.1 Building components

Saffron is well known as a spice that can give food color, flavor and aroma. The 3 main components of the dried saffron stigmas responsible for that are crocin, picrocrocin and safranal (the major component of the essential oils).

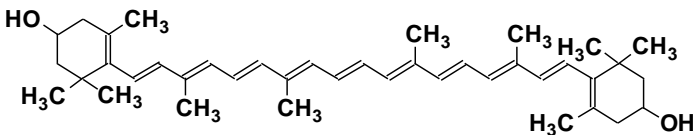
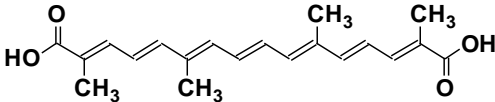
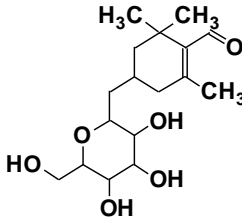
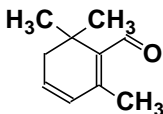
Name	Chemical structure
Zeaxanthin (a C ₄₀ -carotenoid-alcohol)	 <p>Monoisotopic mass: 568.43 Da</p>
Crocetin (a C ₂₀ -apocarotenoid)	 <p>Monoisotopic mass: 328.17 Da</p>
Picrocrocin	 <p>Monoisotopic mass: 330.17 Da</p>
Safranal	 <p>Monoisotopic mass: 150.10 Da</p>

Table 1: Chemical structure of the most important saffron components

Some other elements that are found in the stigmas are water, protein, mineral matter, fat, reducing sugars, crude fiber and others [1]. For medical purpose maybe the most important component of the saffron is crocin. It is a natural apocarotenoid that is water soluble, which is non-typical for carotenoids [5]. It is formed when zeaxanthin is enzymatically cleaved down into smaller components a C₁₀ apocarotenoid hydroxy-β-cyclocitral and C₂₀ apocarotenoid crocetin dialdehyde. These components are then modified through oxidative modifications and glucosylation reactions leading in the end to formation of crocetin aglycon and picrocrocetin which is further transformed into safranal [2]. In Table 1 chemical structures of zeaxanthin, crocetin, picrocrocetin and safranal are given [6].

The bitter taste of saffron comes from picrocrocetin which is a colorless glycoside [1]. During the drying process this picrocrocetin splits into D-glucose and safranal which is a major component of the essential oil responsible for the specific aroma and odor of saffron [1, 4].

1.1.1.1 Crocin

As mentioned earlier, crocin is a natural carotenoid found in the saffron stigmas. It is a glycoside meaning that it is composed of an aglycon and different sugar components. The aglycon C₂₀H₂₄O₄ named crocetin, is the backbone of crocin. The transformation of carotenoids to crocetin is performed by oxidative cleavage and catalyzed by carotenoid cleavage dioxygenases which are highly selective enzymes [2].

This crocetin, according to previous studies [2], can have one or two glycosylation sites allowing glycosylation with up to 3 glucose units per site, but only five glucose units in total. So the glycosylation can happen with glucose, gentiobiose, neapolitanose and gentiotriose.

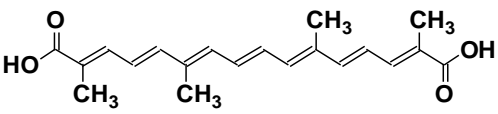
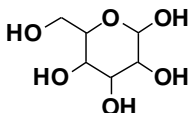
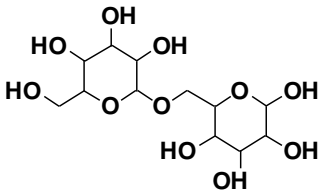
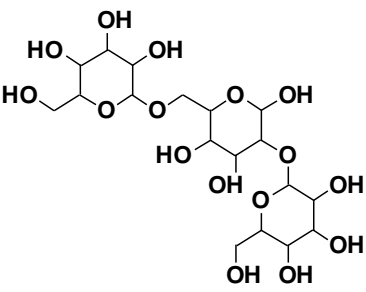
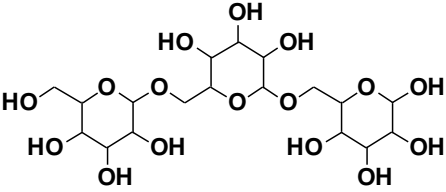
Name	Type	Chemical structure
Crocetin (a C ₂₀ -apocarotenoid)	Aglycon	
Glucose	Oligosaccharide portion	
Gentiobiose (a disaccharide, 1→6 linked)	Oligosaccharide portion	
Neapolitanose (a branched trisaccharide, 1→2 and 1→6 linked)	Oligosaccharide portion	
Gentiotriose (a linear trisaccharide, 1→6 linked)	Oligosaccharide portion	

Table 2: Chemical structure of the aglycon and oligosaccharide portions described so far [2]

One study performed on early-spring flowering *Crocus* showed that crocins, which were found in the stigmas, can have up to 8 glucose units [19]. Therefore this indicated that autumn flowering *Crocus* could also be glycosylated with more than 5 monosaccharide units. The most abundant crocetin ester glycoside in the stigmas of saffron has the molecular formula C₄₄H₆₄O₂₄ and it is a bis-gentiobiosyl crocetin (Figure 3) [7].

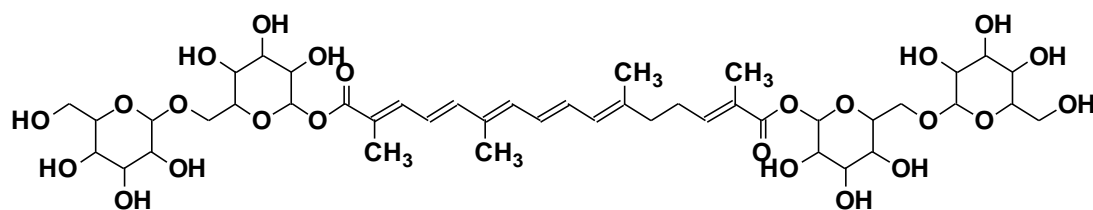


Figure 3: Chemical structure of bis-gentiobiosyl crocetin $C_{44}H_{64}O_{24}$ (Monoisotopic mass: 976.3787 Da)

Crocins are soluble in water forming red to yellow solution (Figure 4). Opposite to crocin, the aglycon crocetin is hydrophobic.



Figure 4: *Crocus sativus* solution obtained by extracting 10 saffron stigmas in two ml of H_2O

Crocins have been characterized as phytotherapeutical drug to treat cancer (antiproliferative), as antioxidant and antidepressant agent, with the important feature that no side effects were reported [8]. Studies showed that when consumed orally, crocins could not be absorbed directly in the gastrointestinal tract (GI tract), but were rather hydrolyzed to crocetin in the intestinal region [8]. These crocetins are then metabolized to some extent to mono- and diglucuronide conjugates [8].

1.1.2 Pharmacological usage

In the past, saffron has been used not only in the culinary world, but also for treatment of different diseases, as well as stimulant or aphrodisiac [1]. A papyrus dating from ca 1550 BC shows the usage of saffron in the treatment of kidney problems [7]. As folk medicine saffron is used to cure colds and coughs, to reduce inflammation, for treatment of diabetes patients or to treat alcoholism and liver problems [7].

The efficacy of saffron extracts when used as a therapy against depressions has been confirmed in different clinical trials [11].

In Arabic countries, China and India saffron has been used as a remedy for cancer [12].

Until now positive effects of saffron extract on breast, cervical, lung, pancreatic and skin cancer have been reported. But it has to be considered that more studies are needed before the clinical trials could be started and the applied extracts are not very well defined.

1.1.2.1 Possible use of crocins in the treatment of Alzheimer disease

Alzheimer disease causes the loss of memory, disorientation, in the end death and has not yet been completely understood and a cure has yet to be found. Because of that it is very important to find new pharmacologically active substances and saffron could help in treatment of patients with Alzheimer disease because crocins could block the aggregation and deposition of β -amyloid beta peptide fibrils leading to Alzheimer disease [14].

Amyloid protein is a fibrous protein that is mainly made out of β -sheets. When found in organs and tissues it is considered abnormal because it indicates a disease like Alzheimer or type II diabetes [13].

Amyloid fibril formation has two phases which are shown in Figure 5. The first phase is the lag phase where the conversion of soluble monomers into small oligomers happens and it comes to formation of amyloid seeds. The second phase is the growing phase in which a rapid assembly of amyloid seeds into filaments and fibrils occurs.

It is assumed that crocin compounds could bind specifically to amyloid beta fibrils and inhibit amyloid formation [14].

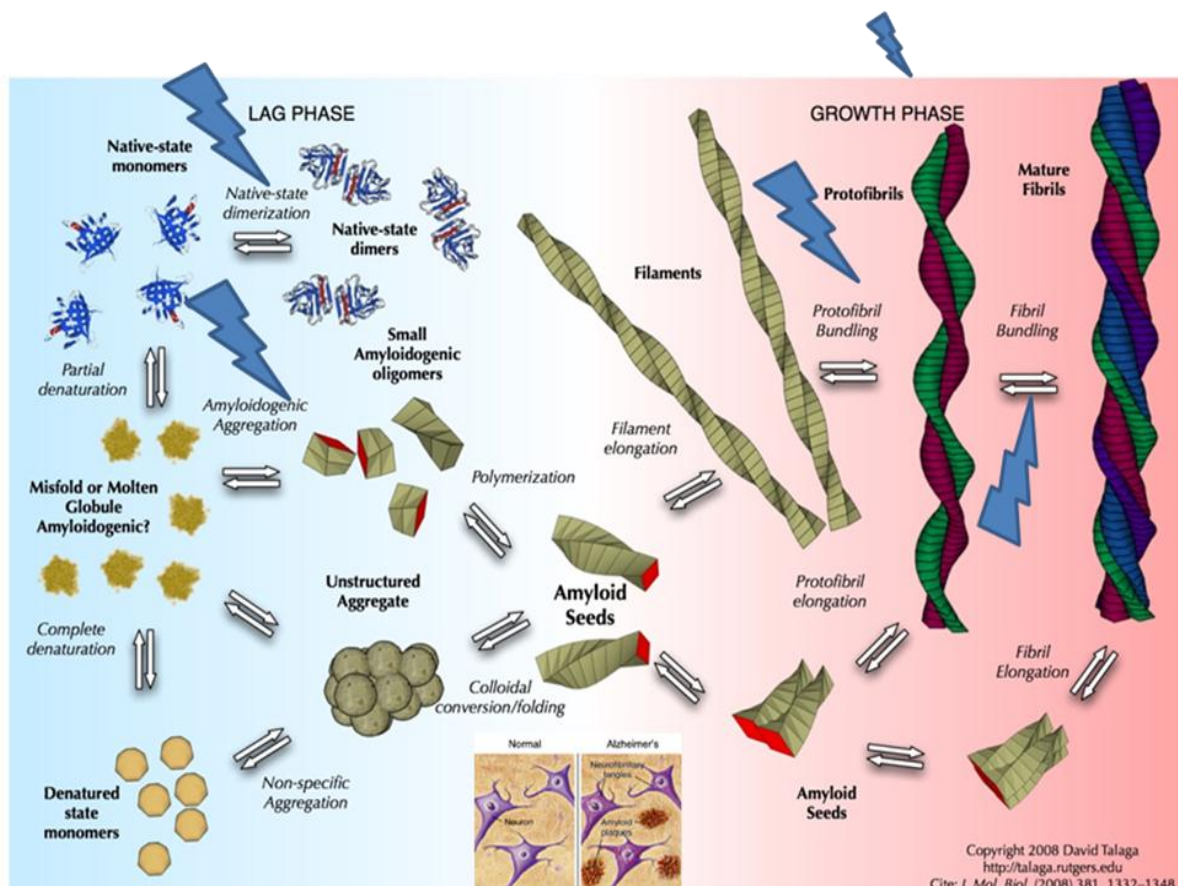


Figure 5: Formation of the amyloid fibrils, lag and growth phase. Adapted from [15, 36]

Also some experimental studies have shown that crocin decreased the number of fibrils formed and significantly reduced the average fibril lengths of amyloid β fibrils [14].

Although these studies have been performed *in vitro*, they have shown positive effect of crocins and could be used for possible *in vivo* studies [14]. It should be noted that crocetin ester glycoside cannot be absorbed when orally applied, because of the hydrolysis to crocetin which occurs in the gastrointestinal tract. So a different application way might be necessary and how far the crocins can cross the blood-brain barriers is still open.

1.2 Scope of this study

As mentioned the saffron extracts applied for pharmacological testing were not well characterized and therefore more detailed information on the extract compositions were urgently required.

In that respect finding new crocin structures among already known structures has great importance for the development of pharmacological tests and final new drugs. As the use of saffron in treatment of many different diseases dates back to ca 1550 BC [17], it is not a surprising that it has been the main topic of many researches. Especially the crocins found in the stigmas of saffron have been of great interest for medical purposes because until now no side effects could be shown.

The first scope of this study was to obtain the complete glycosylation pattern of crocins from a well-defined extract of saffron stigmas using liquid phase separation online coupled to MS (RP-HPLC-ESI multistage MS (MS^n $n=1-3$)) by finding a method that will allow the optimal detection of crocetin glycosides.

The second scope was to develop a visual location of crocetin glycosides on the surface of saffron stigmas using MALDI based imaging mass spectrometry. It was also of interest to find out if the crocetin glycosides are located only on specific surface parts of the stigmas or if they are randomly distributed across the whole surface.

1.3 Mass spectrometry

Mass spectrometry (MS) is widely used as analytical technique for detection, characterization and identification of bioactive compounds by formation of intact molecular ions and detection of them.

The separation of the ions has to be performed in a high vacuum system. This is important in order to reduce the collision between the ions and other gaseous residues which can be found in the MS analyzer [16].

The process during which the ions are formed is called ionization or desorption/ionization process. In order to get ionized the sample molecules need to be transferred into the gas phase. They can then be transformed into positive or negative ions, singly or multiply charged, before being separated in a mass analyzer.

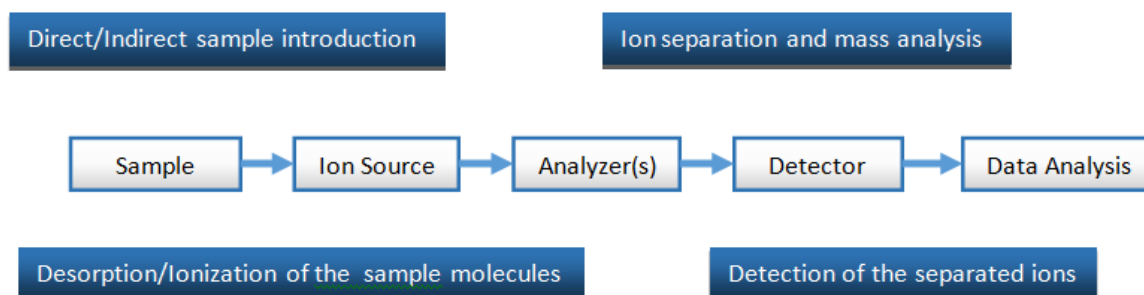


Figure 6: Scheme of a mass spectrometer

The main building blocks of the mass spectrometer are the ion source, the mass analyzer and the detector (Figure 6).

1.3.1 Ionization Techniques

Due to the fact that the MS analyzer can only separate and detect ions, the first step in mass spectrometry is the generation of ions of the sample molecules. Ionization is possible only if the sample is present in the gas-phase. Based on the sample properties, the appropriate technique needs to be selected because that will allow the final formation of molecular ions.

There are different kinds of techniques that can be used and they can be separated in two groups [17]:

- Hard ionization techniques – gas phase ionization techniques like
 - Electron impact (EI)
 - Chemical ionization (CI)
- Soft ionization techniques – desorption/ionization techniques like
 - Matrix Assisted Laser Desorption/Ionization (MALDI)
 - Desorption Electrospray Ionization (DESI)
 - Electrospray Ionization (ESI)
 - Nano Electrospray Ionization (nESI)

The difference between these two groups is that the mentioned soft ionization techniques principally produce intact molecular ions of different type with a small number or no fragment ions at all. On the other hand, the hard techniques generate a large number of fragment ions but not all the times intact molecular ions are formed or only at very low abundance.

MALDI and ESI were selected for this work and they will be explained in detail in the following chapters.

1.3.1.1 MALDI

Matrix-assisted laser desorption/ionization technique (MALDI) is being used for more than 25 years for the desorption/ionization of intact biomolecules [18]. In 2002 Koichi Tanaka was awarded with $\frac{1}{4}$ of the Nobel Prize for development of this desorption/ionization method. MALDI belongs to the soft ionization techniques, meaning that the ionization process produces a very low number of fragment ions allowing the detection of large, non-volatile and thermo labile molecules [17]. In order to generate ions the analyte molecules have to be incorporated into matrix molecules, which represent the essential part of this method. This is done by mixing the matrix solution with the sample solution before or direct on the sample plate. The solvent from the mixture is then allowed to evaporate before the plate can be introduced into the in source of the instrument. After the solvent evaporation matrix crystals in which analyte molecules are embedded are formed.

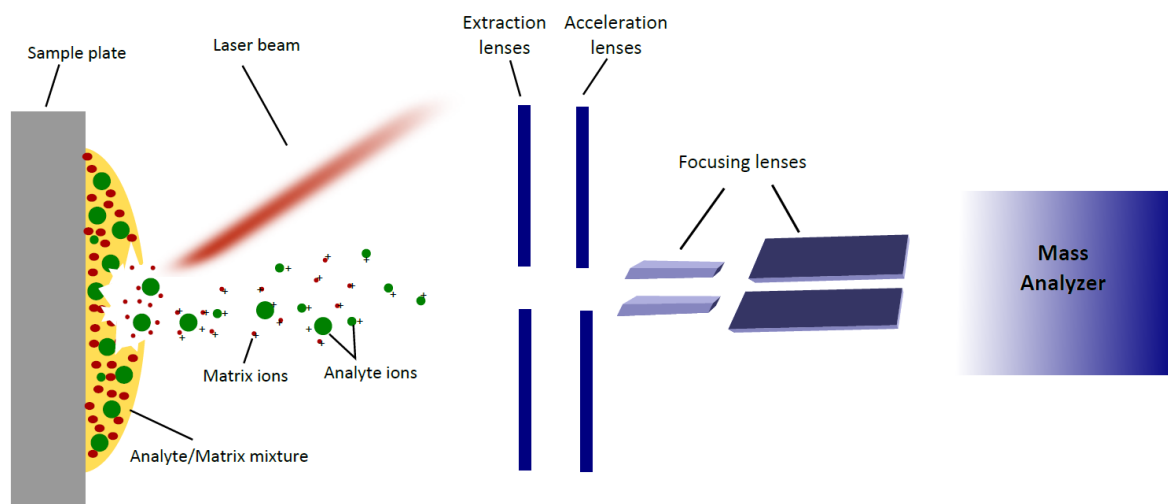


Figure 7: Illustration of desorption/ionization process using MALDI technique

Figure 7 shows the desorption/ionization process using MALDI. When the laser beam hits the matrix/analyte surface it comes to ablation and desorption/ionization in the surface

plume. Desorption and ionization takes place almost simultaneously, so it is very difficult to separate these two steps [17]. Ions are then accelerated in an electrical field and are directed to the mass analyzer which is typically a linear or reflectron time of flight analyzer (TOF).

Different matrices absorb at different laser wavelength, so the selection of the proper matrix is essential for the measurement to work because there is no universal matrix [18]. Two types of lasers used for MALDI are N₂ (nitrogen) laser with wavelength of 337nm and Nd-YAG (neodymium-doped yttrium aluminum garnet) laser at wavelength of 355 nm. Nd-YAG laser is frequency tripled which means that 355nm represents one third of its original wavelength.

1.3.1.2 ESI

In 2002 John Fenn was awarded with a shared Nobel Prize with Koichi Tanaka for the invention of ESI which gained great significance in the analysis of large biomolecules like peptides, proteins, oligosaccharides, glycolipids, etc. [20]. Like MALDI, ESI belongs to the group of soft ionization techniques. The introduction of the sample, which needs to be in the liquid state or dissolved in solution, can be done directly with a syringe pump or indirectly via high-performance liquid chromatography (HPLC).

The sample solution is pumped through a spray capillary (which functions as an electrode) and an aerosol is formed (Figure 8). On the opposite side of the capillary is the second electrode with a small gap in the middle through which the formed ions are being transported into the analyzer. The ions are formed because of the applied voltage between these two electrodes, which causes the formation of a Taylor cone on the tip of the spray capillary. However, because of the field small aerosol droplets containing the analyte are torn away from the Taylor cone and are moving in the direction of the second electrode because of the potential difference between these two electrodes. During the flight the droplets lose the solvent due to the evaporation and what remains are singly or multiply

charged analyte molecules which continue their way to the analyzer. This process takes place at atmospheric pressure.

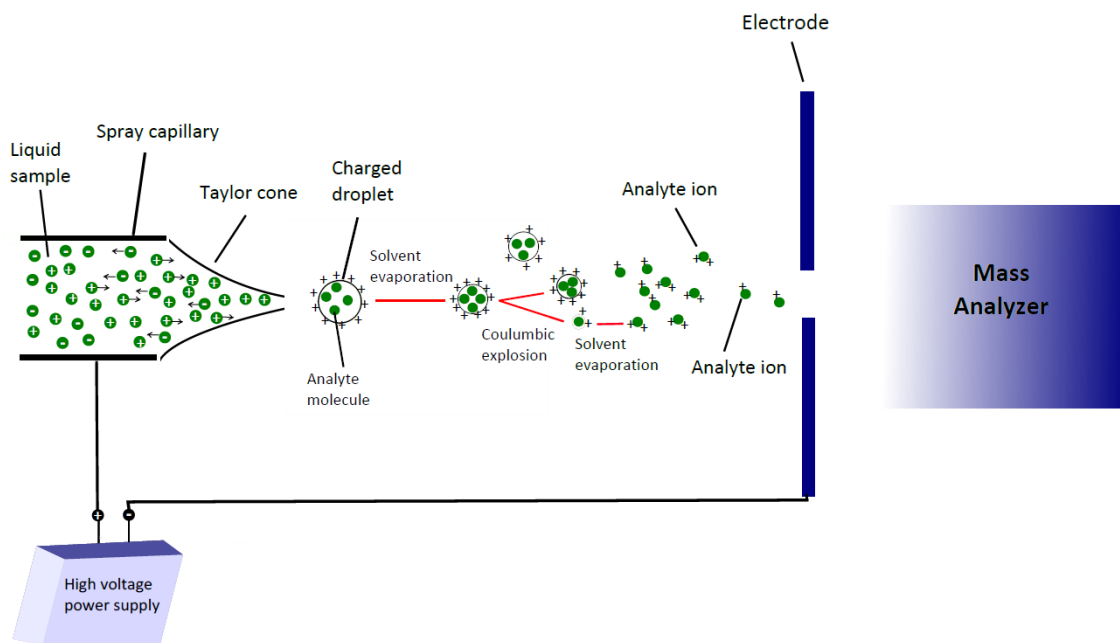


Figure 8: Illustration of electrospray ionization process, ion formation according to ion evaporation model

There are two suggested models for the ion formation: charge residue model and ion evaporation model [21]. Charge residue model, developed by M. Dole is applicable for the large analyte molecules (Figure 9) [22].

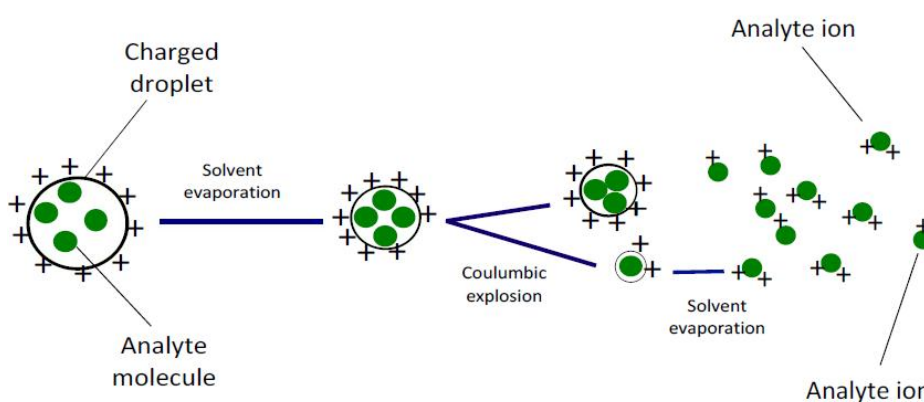


Figure 9: Ion formation based on charge residue model (CRM)

As stated earlier the aerosol droplets containing the analyte are positively or negatively charged and the charge is distributed over the whole surface of the droplet. When the solvent molecules start to evaporate, the distance between the charges starts to reduce until it comes to the repulsion between the charges and the Coulombic (Rayleigh fission) explosion happens. The point at which this starts to happen is called the Rayleigh limit. It means that the large droplet falls apart into smaller droplets and the process continuous until the solvent is evaporated completely and only one positively or negatively charged analyte molecules remain. Very large molecules can hold larger number of charges than the smaller ones and very small molecules can have only one charge.

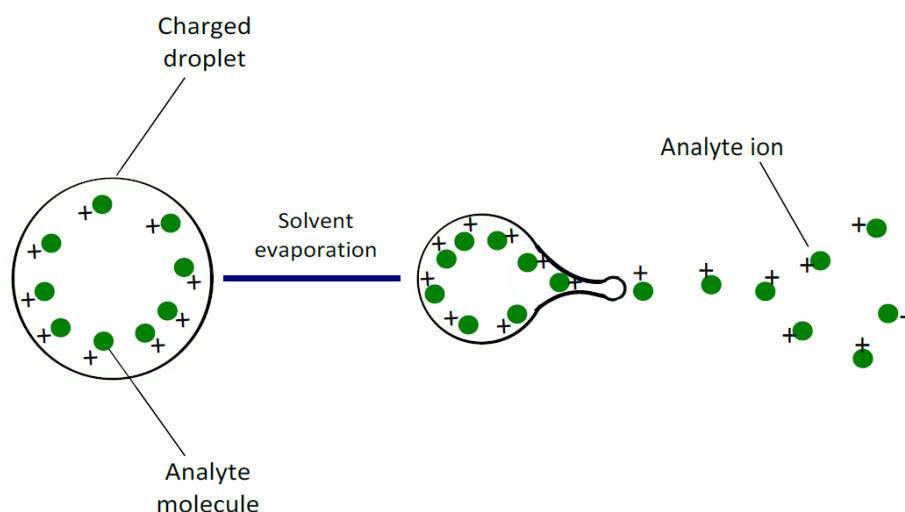


Figure 10: Ion formation based on ion evaporation model (IEM)

The second model, the ion evaporation model is applicable for small analyte molecules. Figure 10 shows the principle of ion evaporation model. The droplets that are moving toward the analyzer have multiple charges on the surface. During the flight the solvent is evaporating and the distance between the charges is reducing. When the charge-to-surface ratio becomes too high, the charged ions are directly ejected from the droplet.

ESI allows positive and negative ionization mode and depending on the mode the formed molecular ions containing analyte can be: protonated $[MH]^+$ or $[M + nH]^{n+}$, adduct ions e.g. $[M + Na]^+$ or deprotonated $[M - H]^-$ or $[M - nH]^{n-}$ [17], [32].

1.3.2 Mass spectrometric analyzers

The main function of the analyzer is separating the ions that are coming from the ion source with a certain kinetic energy based on their mass to charge ratio. There are different types of analyzers which are distinguished according to different physical principles used for the separation of the ions, like electric/magnetic field deflection, alternating fields based separation or different flight times. The mass analyzer is the part of the mass spectrometer that is always under vacuum. Different analyzers require different vacuum qualities, varying from rough vacuum of $\approx 10^{-3}$ mbar to very high vacuum of $\approx 10^{-9}$ mbar.

The ability of the mass analyzer to separate the ions is called the resolution (R) and today one definition for the resolution is commonly used for all types of analyzers: R_{FWHM} (full width half maximum) definition (Figure 11). For the FWHM definition no neighboring signal is required compared to the R_{valley} definition which requires two neighboring peaks of similar height.

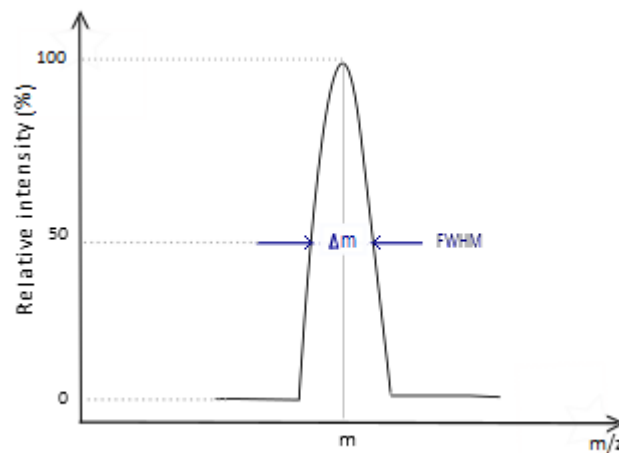


Figure 11: Definition of mass resolution using full width half maximum definition (FWHM), where Δm is full width of the signal at 50% of the maximum height

The resolution by FWHM is defined as quotient of the ion mass and the full width of the signal at 50% of the maximum height (equation [1.1]).

Where:

$$[1.1] \quad R = \frac{m}{\Delta m}$$

R - resolution

m - m/z value of ion

Δm - width of the ion peak at 50% of the height

Obtainable resolution differs from analyzer to analyzer but the highest resolution can be obtained with FTICR (Fourier Transform Ion Cyclotron Resonance) mass analyzer ($R_{FWHM} = 500\,000$) [23], [24]. Linear time-of-flight (TOF) ($R_{FWHM} = 5\,000$), reflectron time-of-flight (RTOF) ($R_{FWHM} = 20\,000$) and quadrupole ion trap (QIT) ($R_{FWHM} = 4\,000$) mass analyzer are the analyzers used for the Saffron experiments and will be explained in more detail [24].

1.3.2.1 Time of flight (TOF) mass analyzer

A linear TOF mass analyzer as the name states separates the ions according to their different flight times through the flight tube without the influence of an external field or force. These analyzers are typically used in combination with MALDI, but can be used also with other ionization techniques as e.g. ESI or EI.

There are two types of TOF analyzers: linear TOF (TOF) and reflectron TOF (RTOF). In the Figure 12 a scheme of linear TOF can be seen.

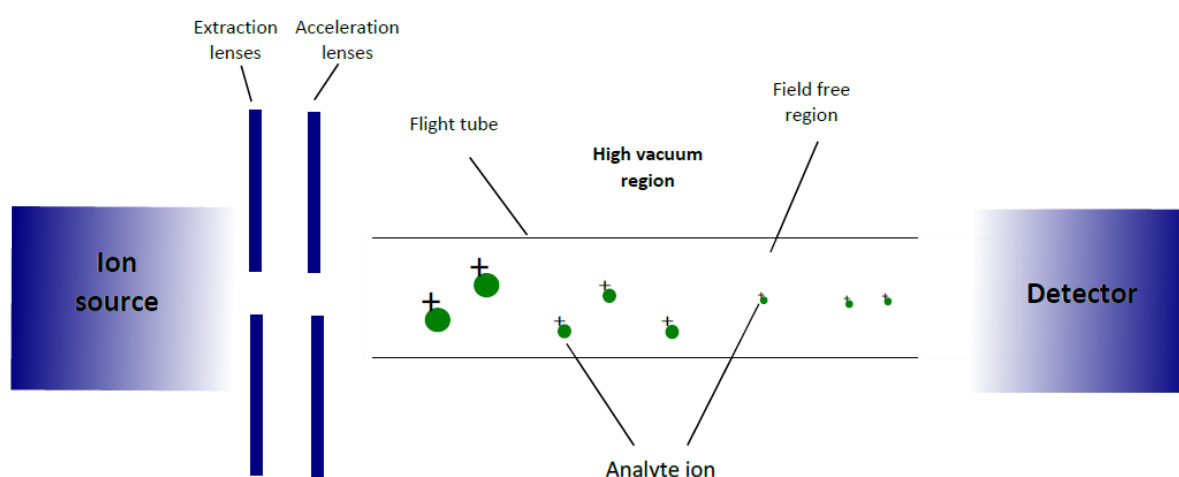


Figure 12: Illustration of a linear TOF mass analyzer

The core of this analyzer is a tube which is empty and there is no electrical or magnetic field influence. The ions from the ion source are accelerated with a certain potential (except gravitational force) (e.g. 20 kV) and are all given certain kinetic energy (e.g. 20 keV). The ions that have low mass to charge ratio will fly with higher speed through the tube while large ions will fly at slower speed.

The length of the tube can vary from 0.5 m to few meters [37]. This parameter is important because the longer the tube the more time the ions will spend flying and will arrive at different times at the detector which means they will be better separated, i.e. show an increased resolution of the ion.

The problem with this setup is that in the real world the ions do not start at the same time from the acceleration point and their own energy is dependent the internal energy they have. This will influence the flight time and the resolution. That means that ions which have the same m/z ratio will have different kinetic as well as internal energy. They will reach the detector at different times and the result will be a broad peak. This problem can be solved with delayed extraction and the use of a reflectron [24].

After desorption/ionization the ions are immediately extracted with the extraction lenses and accelerated in the direction of the mass analyzer. The delayed pulsed extraction allows the ions to move, for a short time of period in a field free region before being extracted from the ion source. This means that for few nanoseconds the ions are being separated according to their initial velocity and the faster ions will move further than the slower ones. When the extraction/acceleration field is turned on the ions that are closer to the flight tube will be accelerated at lower potential than those that had slower initial velocity. Thanks to this delayed extraction the slower ions will catch up the ions with initially higher velocity. This leads to the improved resolution but the delayed extraction works only for the ions with a narrow m/z range.

1.3.2.2 Reflectron time of flight (RTOF) mass analyzer

In order to improve the resolution a reflectron can be used for ion separation. The reflectron represents an electrostatic ion mirror which means that it deflects the ions in the direction of the detector increasing the flight time. In the Figure 13 illustration of RTOF analyzer is shown.

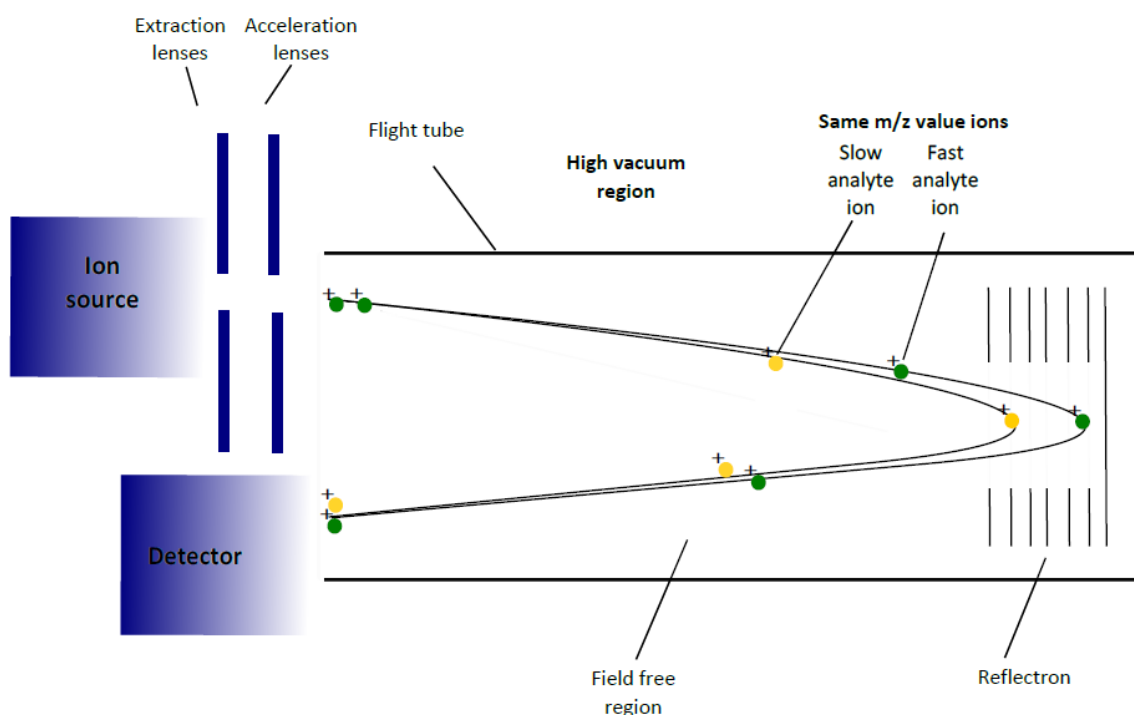


Figure 13: Illustration of reflectron TOF mass analyzer (RTOF)

Just like with the linear TOF the ions coming from the ion source are being accelerated with certain acceleration voltage. They fly through the flight tube until they reach the reflectron and are then sent back through the flight tube to the detector. The reflectron is actually a group of additionally lenses (electrodes) which are placed at the end of the flight tube and they represent a voltage gradient. The advantage of this method is that the ions that have the same m/z but different kinetic and internal energy will still be detected at the same time. The reason for this is that the ions with different energy penetrate the voltage gradient differently, meaning that the ions with higher energy will go further into the field than those with lower energy [21]. In other words, the ions with higher velocity will have longer flight

time than the ions with the same m/z ratio but slower velocity. A static electric field is used to reverse the ions back through the flight tube in the direction of the detector. With this the energy distribution of individual ions is reduced not only because of the longer flight path, but also due to energy and space focusing leading to increased time and therefore mass spectrometric resolution.

The type of reflectron that uses only one electric field region is called single stage reflectron. There are also reflectrons with two different electric field regions called dual stage reflectron, meaning that the first region has stronger electric field than the second. Third type of the reflectron is the curved field reflectron which has a nonlinear electric field gradient thus allowing the separation without the need to step the reflectron voltage. It is made out of a large number of lenses which allow steadily increase of the voltage difference creating the field.

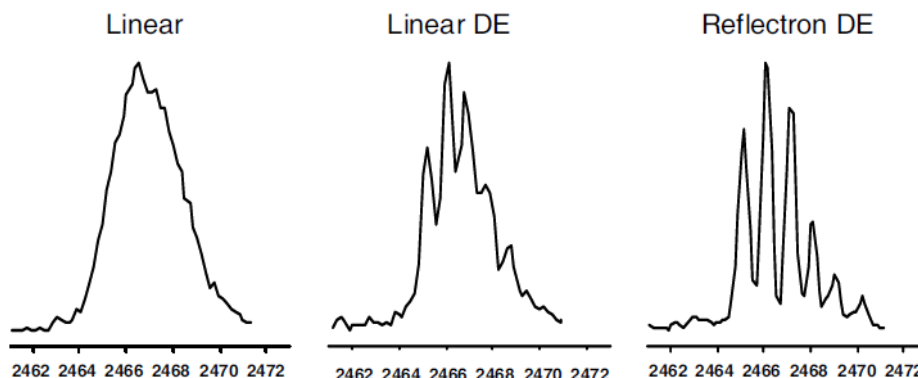


Figure 14: Comparison of MALDI mass spectra obtained in linear mode, linear mode with delayed extraction and reflectron mode with delayed extraction. Figure taken from J. T. Watson and O. D. Sparkman [25]

Figure 14 shows that the best mass spectrum in terms of R_{FWHM} is achieved when a reflectron in combination with delayed extraction is used (right mass spectrum). This means that the resolution is increased and with that the isotope pattern separation.

1.3.2.3 Quadrupole ion trap (QIT)

Quadrupole ion trap, also called Paul trap, got its name after its inventor Wolfgang Paul in the 1950s [26]. There are two types of ion traps: the 3D QIT, which works with three dimensional quadrupole fields and linear ion trap (LIT) which works with two dimensional quadrupole fields [26]. The instrument used for the measurements in this work constitutes a 3D ion trap, which is shown in the Figure 15.

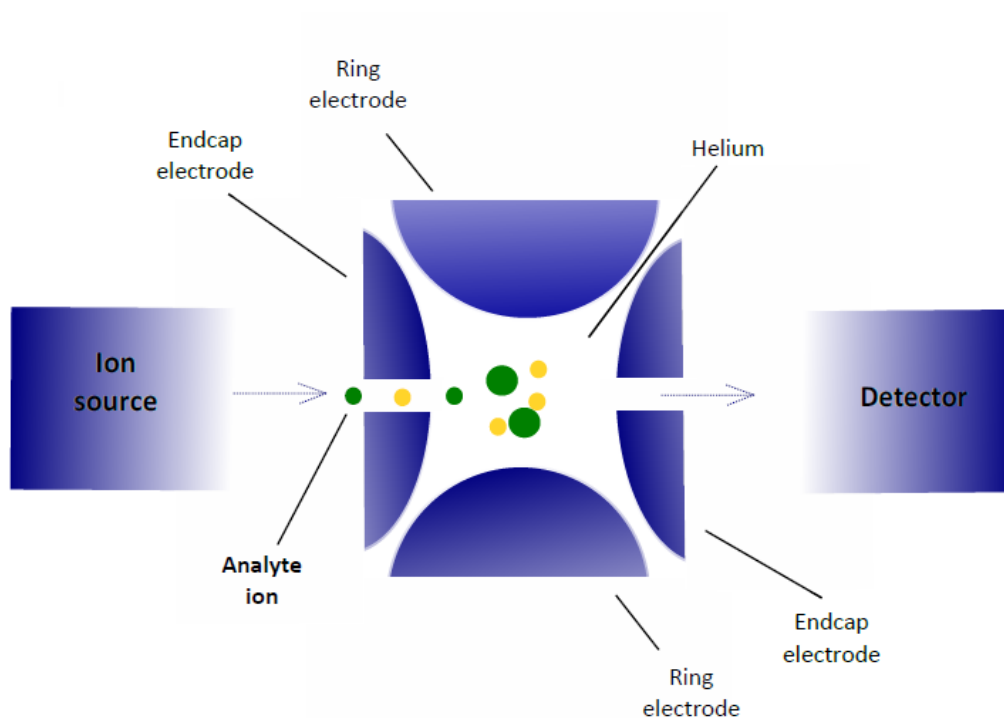


Figure 15: Illustration of the quadrupole ion trap mass analyzer, cross-section view

The transfer of the ions into the ion trap is performed by low voltage acceleration followed by using a set of two octapoles. The ion trap itself consists of three electrodes: one ring electrode and two end cap electrodes. Both end cap electrodes have small openings through which the ions that come from the ion source can enter the ion trap and later leave the trap in the direction to the detector [27].

The specific arrangement of the electrodes ensures that the ions are trapped within the quadrupole field which is formed by applying RF voltage to the ring electrode [28]. Inside the ion trap there is helium gas which has the function to cool and slow down the ions by the means of collision. The helium gas does not interact chemically with the ions, it only absorbs their kinetic energy, causing them to group in the center of the trap [29]. By ramping the RF voltage the quadrupole field is changing and resonance excitation is generated which causes the ions to move up and down and then finally leave the ion trap. First, the small ions leave the trap and then those with higher m/z are moving towards the detector [28]. The amount of ions that can be stored inside the trap is limited, but because the whole procedure takes only short time (ms) the next batch of ions can be injected into the ion trap [26]. This means that in the end a great number of scans are added to one mass spectrum.

The advantage of the 3D QIT is that there is no need for the second analyzer if MS^n or MS/MS measurements are required. Usually for the MS^n measurements two, three or more analyzer are needed but QIT MS enables tandem mass spectrometry (MS^2) and multistage MS (MS^n , $n = 2, 3, \dots$) without the use of a second analyzer. This is called tandem-in-time because every stage of mass spectrometric experiment is performed sequentially inside the one and only mass analyzer, the ion trap. After the first set of product ions from the precursor ion have been generated a desired product ion can be kept in the ion trap and collided with the gas molecules creating so second generation product ions. Instruments using other mass analyzers perform tandem-in-space MS because the analyzers are spatially separated one from another. The transition of ions between the mass analyzers causes ion losses which is not the case with the ion trap. For more information on tandem mass spectrometry see chapter 1.3.2.4.

1.3.2.4 Tandem MS, multistage MS and Collision Induces Dissociation (CID)

Tandem mass spectrometry is a method used to select the ions of specific m/z value, fragment them and then analyze the product ions. It can deliver structural unique and partly complete information about the intact molecules at high sensitivity.

When only two steps are involved the process is also called MS/MS. There is also the possibility to select these first step fragment ions, perform second fragmentation and then analyze the resulted fragment ions or go even further and perform another fragmentation. This is called multistage MS (MS^n , $n = 2, 3...$) experiment. There are two types of tandem mass spectrometry: tandem-in-time and tandem-in-space.

In tandem-in-time mass spectrometers every stage of mass spectrometric experiment is performed sequentially inside the one and only mass analyzer. After the first set of product ions from the precursor ion have been generated a desired product ion can be kept in the ion trap and collided with the gas molecules creating so second generation product ions. This can be done in a linear ion trap (LIT), quadrupole ion trap (QIT), Orbitrap or Fourier transform ion cyclotron resonance (FT - ICR) mass spectrometers [24].

In tandem-in-space mass spectrometers more than one mass analyzer is used. The analyzers are spatially separated one from another. The first analyzer is used for the selection of desired ions. These ions are then ejected from the first analyzer and transferred into the collision cell where the fragmentation takes place. The generated product ions are then transferred into the second analyzer where they can be analyzed or selected for further fragmentation. Because the transition of ions between the mass analyzers causes ion losses the number of ions transmitted is getting lower with the higher number of analyzers. Because of that usually not more than four analyzers are used [24]. The most common tandem-in-space mass spectrometers are triple – quadrupole and TOF based instruments [24].

A collision cell, which is located between two analyzers is a small chamber filled with the collision gas (e.g. helium, nitrogen or argon). The precursor ions that come into the cell through a small opening collide with the gas molecules and the energy transfer occurs increasing the internal energy of the ions and causing them to fall apart [41]. This kind of

decomposition which is caused by collision is called collision induced dissociation (CID) [24]. The CID can occur in both tandem-in-space and tandem-in-time instruments with the difference that tandem-in-time instruments require collision cell while in the tandem-in-space instruments the whole process occurs in the ion trap or ICR [24]. There are two types of CID: low energy CID and high energy CID.

In low energy CID the ions are excited through vibrational excitation which occurs when the ions interact with the gas molecules. The energy transmitted is in the range of eV but that is enough to break weak bonds in the ions and cause fragmentation [42]. Low energy CID spectra can be obtained with instruments containing quadrupole, ion trap or ICR analyzer [24].

In high energy CID the energy transferred to the ions is $> \text{keV}$. Because of this high energy the collision with the gas molecules happens in very short time causing the breakage of the internal bonds and fragmentation of the ions. The excitation that occurs in this case is mostly electronic, meaning that the ions go to higher excited electronic state during the collision [43]. The high energy CID is possible only in the instruments that allow high translational energy of the ions like the ones containing electromagnetic or TOF analyzers [24].

1.3.3 Detectors

The ions that survive the transfer from the ion source and through the analyzer are being detected with an ion detector, which can be a so called secondary electron multiplier (SEM) or microchannel plates (MCP). There are two types of SEM detector used in MS: discrete dynode and continuous dynode electron multiplier and they are shown in the Figure 16.

The dynode material is able to interact with the incoming ions. So when the first ion hits the dynode surface 2 electrons are being generated. These two electrons are accelerated towards the next dynode and generate four electrons after hitting the dynode.

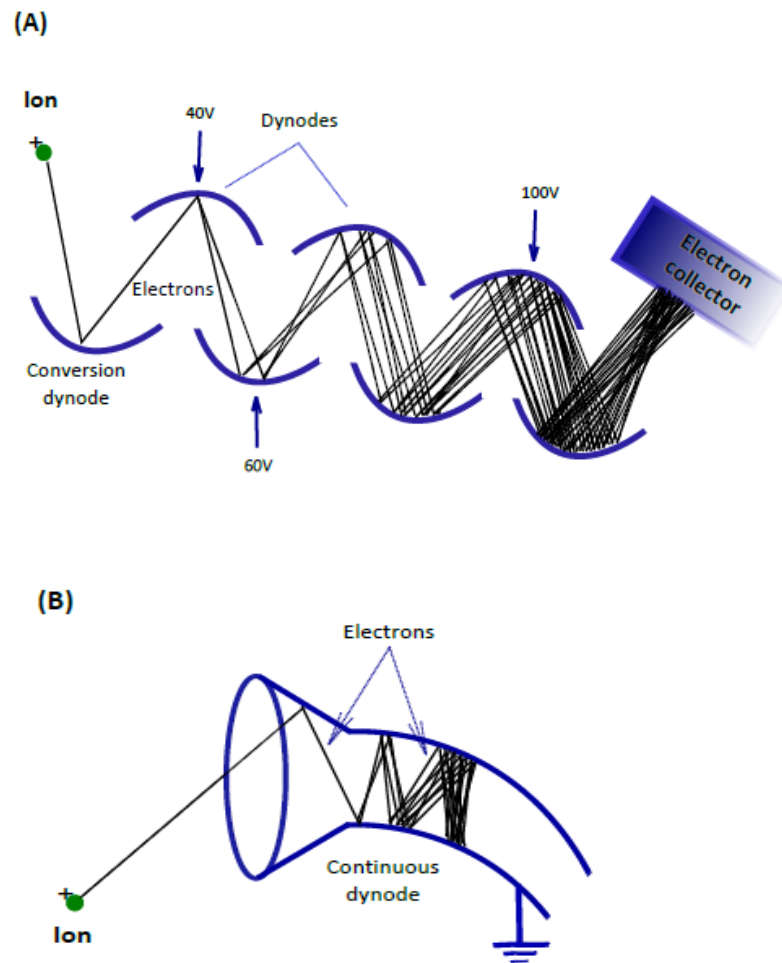


Figure 16: Illustration of secondary electron multiplier with
(A) discrete dynode and (B) continuous dynode

In the case of discrete dynode the electrons move to the next dynode under the influence of a magnetic field. If the continuous dynode is used then the continuous voltage drop along the dynode will ensure that the electrons keep moving towards the end of the dynode, while hitting the walls of the dynode. The whole process is repeated multiple times until in the end between 10^5 and 10^6 electrons are generated and the current which can be detected is produced [35]. This working principle is called secondary electron emission. The measured current represents the number of ions detected.

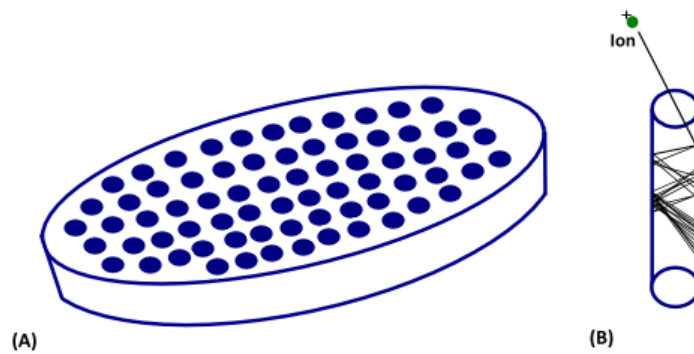


Figure 17: Illustration of (A) microchannel plates and (B) channel

MCPs are usually used in TOF instruments. They are made out of glass plates with a large number of channels which are tilted under $10\text{-}20^\circ$ angle to the surface normal (Figure 17) [39]. This is necessary to ensure that ions hit the walls of the channels and not just fly through. The surface and the channels are covered with semiconductor material allowing the interaction with the incoming ions [24].

The working principle is similar to the SEM. The incoming ions hit the surface of the plate causing the generation of the electrons which travel down the channel causing more electrons to be generated. At the end around 10^6 electrons are generated. The advantage of MCP is very fast response time ($< 1\text{ ns}$) due to the very short channels [39]. Usually two or three MCPs are connected to one another which can increase the amplification up to 10^8 [24]. The disadvantage is that they reach the saturation very fast and the prices are much higher than of the SEM [24].

1.4 Imaging mass spectrometry (IMS)

IMS is a powerful technique developed in 1994 by Caprioli Richard and in the recent years it has become very important for medical and scientific analysis [30]. It is a technique that delivers the visual information about the localization of the biological compounds (peptides, proteins, lipids, metabolites etc.) on the sample surface. Because of these properties it has been used in e.g. diagnostics to identify tumor regions [30] or for the detection of drugs in tissues [18]. IMS is usually performed using the same instruments which are used for standard MALDI-MS measurements.

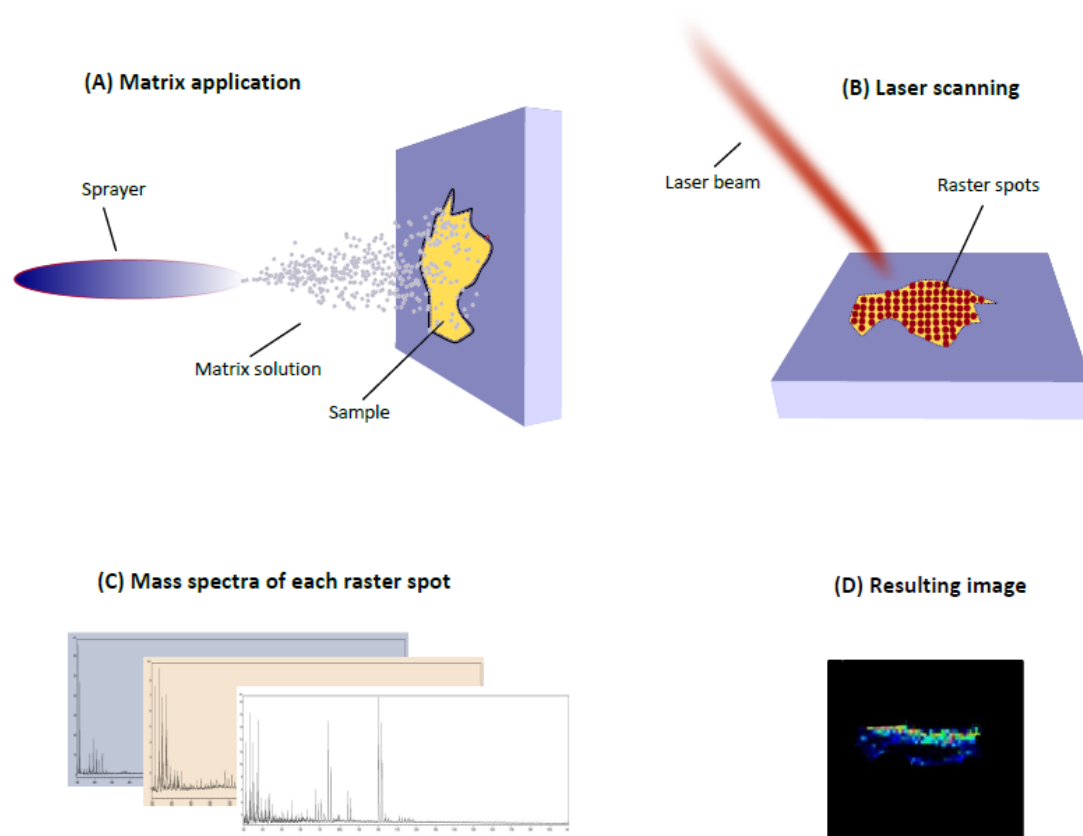


Figure 18: Illustration of MALDI IMS steps

In MALDI IMS (Figure 18) a laser beam scans the surface of the sample in raster pattern and a full mass spectrum is recorded for each analyzed point. The analyzing and the detecting

principles in IMS are equal to those in MALDI MS. IMS leads to the partly destruction of the sample surface, so it is not always possible to use the same sample twice but usually only a few molecular monolayers are being destroyed so the sample can be reanalyzed [30].

When MALDI IMS is used the matrix solution and analyte solution are not mixed together like it was the case with the conventional MALDI, but the matrix solution is e.g. being sprayed homogeneously over a sample surface. This leads to *in situ* extraction of molecules from the sample [31]. The limitation of using MALDI IMS is that the matrix solution needs to be deposited homogeneously on the surface of the sample so that the analyte can be extracted vertically into the matrix crystals. Too much of matrix solution will lead to the horizontal diffusion of the analytes so their original position will be changed and the result will not be trustworthy.

That means that achieving homogeneous layers of matrix is important for efficient desorption/ionization. The matrix can be deposited on the surface of the sample using different techniques such as electrospray deposition, chemical inkjet printing, deposition of the matrix using an airbrush (spray nebulizer) or sublimation [18].

1.5 LC-ESI MS

Combining two different techniques, a separation technique (e.g. HPLC) and MS, allows us to detect components that are otherwise suppressed by other more abundant components in the ion generation process. HPLC can be used for separating, analyzing and purifying mixtures that are in liquid state or that can be dissolved in a solvent [20].

This means that the purification will remove some of the components that cause background ions or suppress ionization [32]. LC/MS refers to the combination of liquid chromatography as a separation technique combined with a mass spectrometer, in this case with electrospray as desorption/ionization technique. Building blocks of an LC-ESI system are showed in the Figure 19.

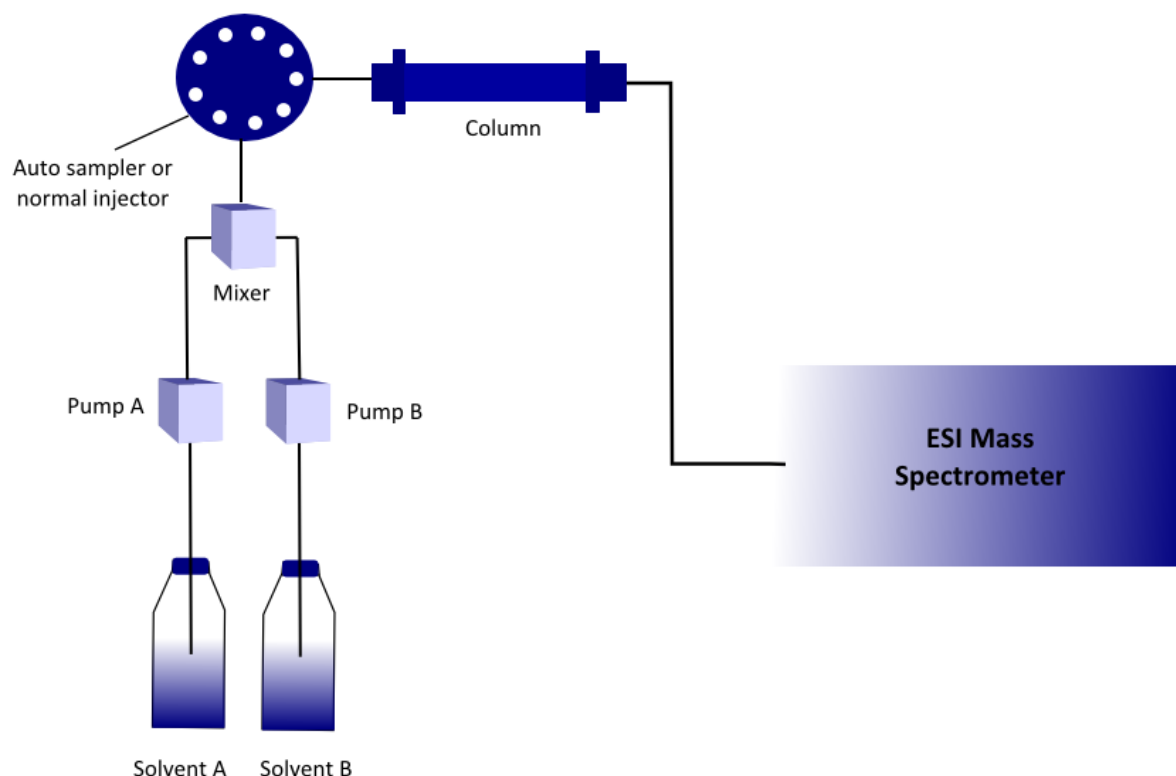


Figure 19: Illustration of LC-ESI MS

The main part of the LC system is the chromatographic column in which the stationary phase is located. The column can have different length (usually 3 - 25 cm) and different inner diameter (usually 75 μm - 5 mm) which influences the flow rate [20]. They are usually filled with silica material. Through the column a mobile phase containing the sample is transported and it comes to interaction between the sample and the stationary phase [34]. The HPLC has a high selectivity because the sample analyte interacts not only with the stationary phase but also with the mobile phase [20]. Because of that the choice of the mobile phase composition is very important.

The composition of mobile phases depends on the type of the sample that needs to be analyzed. In the case of two mobile phases, two separate pumps are used to pump the mobile phases to the mixer where they are mixed together. The injector is used to inject the sample into the mobile phase, and the new mixture moves towards the column which is filled with the stationary phase which can be a solid or gel. The sample analytes have different attractions toward the stationary phase and some will interact stronger with the

stationary phase and be retained longer and some shorter. There are also components that do not interact with the column and they will be eluted at the so called “dead time” [20]. There are different types of chromatographic principles that can be used as e.g. reversed phase, normal phase, ion exchange, size exclusion or ion pair.

For the saffron measurements a reversed phase (RP) HPLC was used, meaning that the stationary phase was hydrophobic while the mobile phase was hydrophilic. RP is used for the separation of small, polar molecules up to intact proteins. The separation occurs based on the hydrophobic properties of the analyte because the stationary phase is usually hydrophobic.

After the HPLC separation the components, including the solvent, need to go into the mass spectrometer for the analysis. They are introduced through the inlet into the ESI ion source where the desorption/ionization and solvent evaporation occurs. For more information on ESI see chapter 1.3.1.2

1.6 Electron Microscopy (EM)

Electron microscopes enable high resolution visualization of different samples by using beams of electrons instead of light rays as it is the case with traditional optical microscopes. This means that EM allows much higher magnification (up to two million times) thus producing images with clearer details of the examined objects. There are different types of electron microscope and the one used for the measurements in this work is scanning electron microscope (SEM) which produces images of the surface of very small objects [44].

The working principle of SEM is based on an electron gun, located on top of the instrument, which produces a beam of electrons which then travel down the instrument towards the sample. Different electromagnetic and/or electrostatic lenses are used to focus the electron beam [45]. When the electron beam hits the surface of the sample it causes emission of secondary electrons and X-rays from the surface. The beam moves back and forth, scanning the surface of the sample [46]. A detector is used to collect these particles including the

backscattered electrons from the primary beam. As a result a sharp 3D picture of the sample is generated on the screen.

The inside of the SEM needs to be under vacuum in order to allow the electron beam to travel in a straight path and the conductivity of the sample must be provided [44].

1.7 Carbohydrate product ion nomenclature

Glycoconjugates are biological molecules, where carbohydrates are linked to non – sugar components (aglycons), which can be various origin as a lipids, steroids or peptides [9]. Saffron contains a large number of glycoconjugates because its aglycon crocetin can be glycosylated with different carbohydrates. Although various tandem mass spectrometric techniques have been used in the past for the determination of product ions of glycoconjugates, in this study low energy CID in combination with ion trap multistage mass spectrometry has been applied.

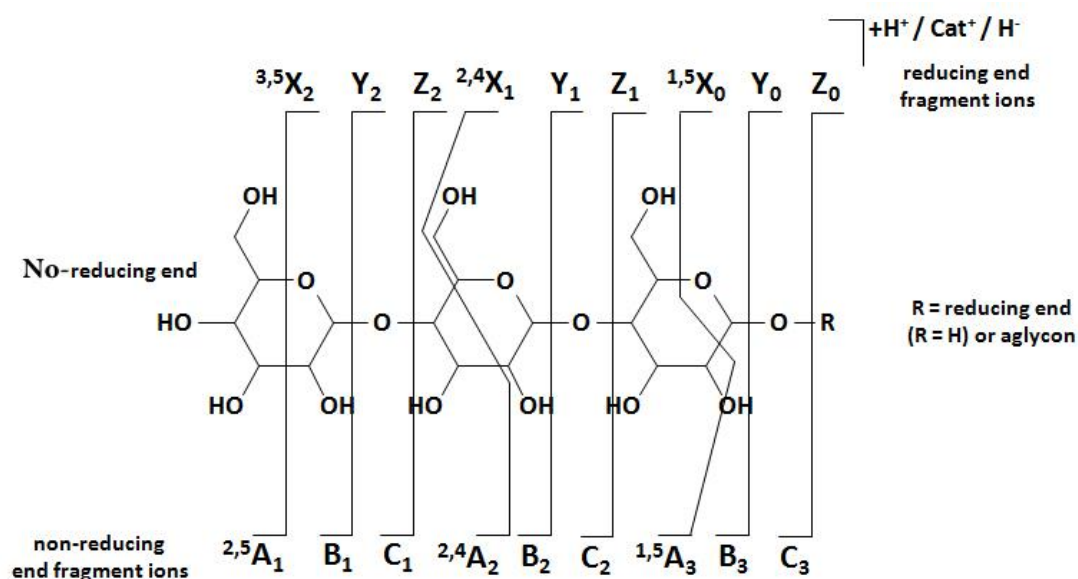


Figure 20: Carbohydrate product ion nomenclature. Adapted from [10]

The nomenclature used for the labeling of the fragment ions still containing the carbohydrate portion is the one developed by Domon and Costello in the late 1980s (Figure 20) [10].

Based on this nomenclature the fragments retaining the reducing end are called X, Y, and Z, while A, B and C are fragments containing the non-reducing end (Figure 20). Fragmentations A and X represent the cross ring cleavages by two bond cleavage. Y, Z, B and C are on the other hand the fragmentations around the interglycosidic bond. Lower case numbers represent the number of glycosidic bond cleavages while the upper case numbers represent the cleavages inside of the carbohydrate ring [10].

2. Experimental

2.1 Saffron

Crocus sativus L. dried stigmas used for the analysis in this work were produced in two different countries. In Table 3 the origin of saffron and its use in this work is shown.

Name	Country	Used for
Safran (Saffron)	Greece	LC-ESI MS
Kashmiri Saffron	India	MALDI IMS

Table 3: Saffron stigmas origin and their use for the MS measurements in this work

The reason for choosing saffron stigmas from two different origins was because the Greece saffron did not have the appropriate shape (straightness and flatness) for the imaging experiment (Figure 21), whereas the Indian saffron fulfills better the requirements.



Figure 21: Saffron stigmas; the upper stigma was produced in India and the lower in the Greece

2.2 LC-ESI MS

2.2.1 Sample preparation

The saffron stigmas used for the experiment were obtained from Greece. In order to analyze crocins, dried saffron stigmas were extracted with 2 ml of ultrahigh quality water.



Figure 22: Saffron extract

For the extraction 10 stigmas were used with the weight varying from 16 mg to 18 mg. For a more complete extraction the mixture was put in an ultrasonic bath (USC200TH VWR, Radnor, Pennsylvania, USA) for 15 min. 1 ml of extract was taken for the centrifugation (1 min at 6 000 rpm) and was then used for the measurement.

A small amount of sodium chloride (Merck, Darmstadt, Germany) was added to the extract to improve the ionization of the analytes. The final saffron extract has a deep orange color as it can be seen in the Figure 22.

2.2.2 LC-ESI MS instrumentation and parameters

The measurements of saffron extract were performed on Bruker Esquire 3000^{plus} 3D-quadrupole ion trap mass spectrometer fitted with a standard electrospray ions source (Bruker Daltonics, Bremen, Germany) coupled to HPLC system (Hitachi LaChrom Elite, Tokyo,

Japan). The Bruker Esquire 3000^{plus} is equipped with an SEM detector. It allows data acquisition throughout MS and MSⁿ experiments (manual or automatic mode). The separation column used for the HPLC was a polar end-capped, reversed phase XTerra MS C8 column (Waters, Milford, MA, USA). The stationary phase of the column contains spherical shaped 3.5 µm particles with a pore size of 125 Å with a dimension of 150 mm in length and a diameter of 2.1 mm. For all LC-MS experiments the LC was directly coupled to the mass spectrometer without using the UV detector.

The sample extract was transferred into a 1.5 ml vial and placed into the autosampler of the HPLC. The used HPLC settings are showed in Table 4.

Parameter	Value
Oven Temperature	40 C°
Column temperature	40 C°
Flow rate	200 µl/min
Injection volume	10-20 µl

Table 4: HPLC settings used for the separation of saffron solution

For the HPLC two solvent systems were used: solvent system 1 consisted of ultra high quality water (UHQ) and 0.05% formic acid and solvent system 2 consisted of methanol (Merck, Darmstadt, Germany) and 0.05% formic acid.

Because of the complexity of the aqueous extract a method with a long gradient for optimum separation was required (Table 5).

Time (min)	Solvent 1	Solvent 2
00:00	70	30
45:00	5	95
55:00	5	95
60:00	70	30

Table 5: Values of the gradient flow used in HPLC

The diagram of the gradient used for the measurements is showed in Figure 23.

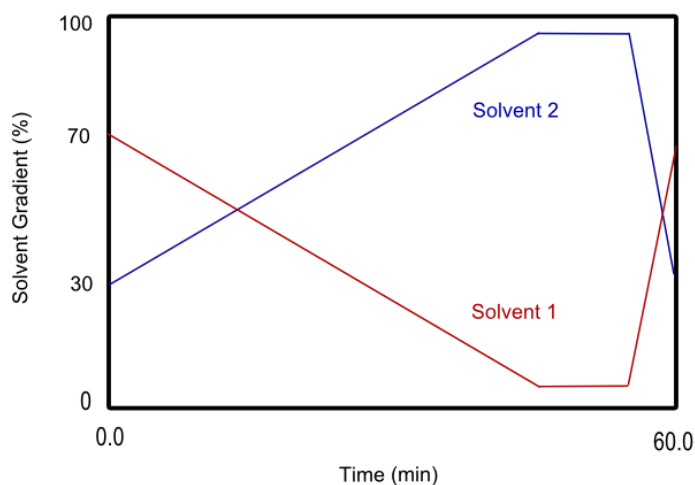


Figure 23: Illustration of HPLC mobile phase gradient

Table 6 and 7 give an overview of the most important ESI settings.

Parameter	Value
Ion source temperature	300 C°
Nebulizer gas pressure	16-18 psi
Dry gas flow rate	10-12 l/min
Polarity	positive
Mass range	m/z 100-2000

Table 6: ESI parameters used for the separation of saffron analytes

Parameter	Value
Fragmentation amplitude	0.6-1 V
Cut off	23 %
Isolation width	4 Da

Table 7: ESI Manual MSⁿ parameters used for the separation of saffron analytes

For all LC-ESI measurements manual MSⁿ experiments were performed. This means that during the entire gradient only one precursor ion mass was monitored.

The precursor ion masses selected for all MSⁿ measurements were performed based on calculated molecular masses, meaning that in order to find crocins with a different number of glucose, the precursor ion mass was increased by +162 Da, which corresponds to one glucose unit (Table 8).

[M + Na]⁺ (calc. monoisotopic m/z values)	Elemental composition
2133.74	C ₈₆ H ₁₃₄ O ₅₉
1971.69	C ₈₀ H ₁₂₄ O ₅₄
1809.63	C ₇₄ H ₁₁₄ O ₄₉
1647.58	C ₆₈ H ₁₀₄ O ₄₄
1485.53	C ₆₂ H ₉₄ O ₃₉
1323.47	C ₅₆ H ₈₄ O ₃₄
1161.42	C ₅₀ H ₇₄ O ₂₉
999.37	C ₄₄ H ₆₄ O ₂₄
837.32	C ₃₈ H ₅₄ O ₁₉
675.26	C ₃₂ H ₄₄ O ₁₄
513.21	C ₂₆ H ₃₄ O ₉

Table 8: Calculated monoisotopic mass values of crocetin ester glycosides

2.3 Imaging MALDI MS

Imaging experiment was carried out on two MALDI based mass spectrometers: the UltrafleXtreme TOF/RTOF mass spectrometer (Bruker Daltonik, Bremen, Germany) and the Axima TOF² TOF/RTOF mass spectrometer (Shimadzu Kratos Analytical, Manchester, UK). UltrafleXtreme uses a 2 kHz Smartbeam laser which is a modified Nd:YAG laser with a wavelength of 355 nm and is fitted with a dual stage reflectron.

The Axima TOF² instrument uses a 337 nm wavelength nitrogen laser with a repetition rate of 20 Hz. In contrast to the UltrafleXtreme, the Axima TOF² uses a curved field reflectron.

Whereas the UltrafleXtreme instrument allows imaging of the entire sample in a single data file (limited by the target size/size of the glass slide), imaging of the sample using Axima TOF² covers only an area of 2 × 2 mm by software limitation. Therefore, for bigger samples several separate/overlapping images are required as individual files, which are finally merged to a complete sample image.

2.3.1 Sample preparation

The sample preparation for both instruments was identical. Because Kashmiri Saffron from India has a more flat surface than the Greece one which was used for ESI measurements, it was chosen for the imaging experiments. To ensure that both types of saffron delivered identical results an LC-ESI MS experiment additionally of Kashmiri Saffron was performed. The sample preparation and instrument settings were identical to those for Greece saffron which are described in the chapter 2.1.

Saffron stigmas were put on the ITO slides (indium tin oxide coated glass slides) (Delta Technologies, Loveland, Colorado, USA) which carried a conductive tape piece for adhesion of the stigmas. The slides were then put overnight in a desiccator for better drying.

Two different matrices DHB (2,5-dihydroxy benzoic acid) and THAP (2,4,6-trihydroxyacetophenone) were used. Both matrices were obtained from Sigma-Aldrich (St. Louis, MO, USA). They were chosen because THAP proved to be a good choice for MALDI

measurements of saffron extracts [40] while DHB matrix worked well for peptides and lipids measurements [30]. The matrix solutions were mixed according to the ratios from Table 9. To both matrix solutions a small amount of sodium chloride (Merck, Darmstadt, Germany) was added. The addition of NaCl is important because it improves the ionization of the analytes as these compounds of interest do not contain basic nitrogen.

Matrix solution 1
1000 mg in 5 ml H ₂ O:MeOH (1:4, v/v) doped with NaCl
Matrix solution 2
250 mg in 5 ml MeOH doped with NaCl

Table 9: Composition of matrix solution 1 and 2

After the drying process the stigmas were taken out from the desiccators and sprayed with matrix solution. For this purpose an airbrush system from Sparmax (Taiwan) consisting out of TC-610H EURO-TEC 16A compressor and SP 575 airbrush was used. The matrix was sprayed with roughly a 20 cm distance from the sample and spraying was performed in several steps allowing the matrix to dry before the next layer was deposited. These steps were repeated until the MALDI matrix solution was consumed and an almost homogenous surface coverage was attained.

The homogeneity of the sprayed matrix is very important because:

- Too high amount of solvent leads to transfer of analytes from their original place and
- Too little of solvent will not lead to sufficient analyte extraction from the sample

For the calibration of UltrafleXtreme and Axima TOF² a mixture of saffron extract and matrix solution was used. The saffron stigmas were extracted according to the chapter 2.2.1 with the difference that in this case Indian instead of Greece saffron was used. The matrix solution was obtained by mixing 15 mg of THAP matrix with 1 ml of MeOH. A small amount of sodium chloride (Merck, Darmstadt, Germany) was added to the matrix solution. Because NaCl cannot be dissolved easily in MeOH, the matrix solution was put in an ultrasonic bath

(USC200TH VWR, Radnor, Pennsylvania, USA) for 1 min. The matrix solution was then mixed with the saffron extract 1:1 (v/v) and 0.5 µl of the mixture was spotted on the conductive tape on the ITO slide.

2.3.2 Imaging MALDI MS parameters

2.3.2.1 UltrafleXtreme

For the imaging experiments all measurements were performed with the use of AutoXecute mode from flexControl (Bruker Daltonics), which allows automatic data acquisition. Two methods were applied, a flexControl and AutoXecute method with the settings showed in Table 10.

Parameter	Value
flexControl method settings	
m/z range	m/z 300-2000
Polarity	Positive
Matrix suppression	100 Da
Laser intensity	83-90 %
Analyzer mode	Reflectron
Acceleration voltage	25 kV
AutoXecute method settings	
Accumulation: MS/Parent Mode	Off
Movement	Random walk
Number of shots per raster position	100

Table 10: flexControl and AutoXecute method settings

The settings used in flexImaging (Bruker Daltonics), a program used to acquire and analyze the mass spectra of the sample, are given in Table 11.

Parameter	Value
Sample preparation	Uniformly distributed coating
Raster width	40 μm

Table 11: flexImaging settings

The duration of the measurements was dependent on the size of the sample varying from two to three hours.

2.3.2.2 Axima TOF²

For the Axima TOF² measurements MALDI-MS software (Launchpad 2.8.4) from Shimadzu is used. The settings of the Acquisition-Firing window are showed in Table 12.

The acquired data was visualized using BioMap Version 3804 by Novartis (Basel, Switzerland). This software was originally developed for MRI data analysis but, over the years, it was modified to support data from any source by adding different software packages [38].

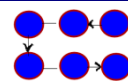
Parameter	Value	
Acquisition		
Laser intensity (0 - 180)	85-95 arbitray unit	
Profiles per sample	Identical to number of raster points	
Number of shots accumulated per profile	5	
Matrix Suppression ("blanking")	Up to m/z 300	
Exp. Tech.		
m/z range	m/z 100-1300	
Analyzer mode	Reflectron	
Polarity	Positive	
Storage		
Average profiles	1	
Store profiles	All	
Raster		
Raster Type	Regular Rectangular	
Raster Style	Serpentine raster	
Extent of the raster	Defined by width and height	
Spacing	40 μm	
Calculate raster	Based on spacing	

Table 12: Axima TOF² acquisition-firing window settings. Regular raster defines the regularly spaced distribution of fired shots around the raster center. Raster style determines the direction of the raster

2.4 Electron Microscopy

2.4.1 Sample preparation

Three different approaches were used for the sample preparation:

- Approach 1

Three saffron stigmas were taken for the measurement, cut in half with a scalpel and left part of each stigma was annotated and stored in a plastic box for 24 hours. The right half's of the stigmas were put into a desiccator for 24 hours.

- Approach 2

For the second approach 4 stigmas stored under ambient conditions were used. Two stigmas were covered with a DHB matrix solution prepared according to the chapter 2.2.1 and two were covered with THAP matrix solution also prepared according to the Chapter 2.2.1. Both solutions were sprayed using the airbrush system.

- Approach 3

In third approach one stigma was taken, cut in half with a scalpel and stored into a desiccator for 24 hours. After the drying process the left part of the stigma was covered with DHB matrix solution and the right one with THAP matrix solution. Both solutions were prepared according to Chapter 2.2.1 and sprayed using the airbrush system.

2.4.2 EM parameters

Electron microscope measurements were carried out on the Quanta 200 SEM instrument (FEI, Oregon, USA). This instrument allows working in three different imaging modes: high-vacuum (special preparation of sample needed), low vacuum (for nonconductive samples) and ESEM mode (environmental scanning electron microscope for wet samples). It uses a larger number of detectors like Secondary Electron (SE), Back Scattered SE, Gaseous SE Detector etc. The settings used to acquire the images of the sample, are given in Table 13.

Parameter	Value
Operating vacuum mode	High Vacuum (HiVac)
Acceleration voltage	10 kV
Beam spot size	2 (\triangleq 2.6 pA) – 4 (\triangleq 28 pA)

Table 13: Electron microscope settings

The beam spot size which represents the focused area of the electron beam can be selected individually for every measurement from the factory preset list (numbered 1 – 10). Lower number leads to smaller beam current. Based on the selected spot size the beam current can vary between 0,81 pA and 30 nA.

3. Results and discussion

3.1 LC-ESI MS

In order to acquire detailed structural information of crocetin ester glycosides, an aqueous extract of saffron was used for the LC-ESI MS measurements. Because of the complexity of the saffron extract a HPLC system was necessary in order to get separated and thereafter well-defined compounds. Extraction of crocins using water is the best way to do it because crocins are highly water soluble but it must be considered that this extraction method is not selective meaning that not only crocins but also other water soluble components are being extracted.

It was observed that the color of the extract became less intense becoming more yellow over a longer period of storage. Because of color change of the extract and measured changes (crocins could not be detected anymore), caused possible due to photodegradation and hydrolytic cleavage, a new extract needed to be prepared every 3 days.

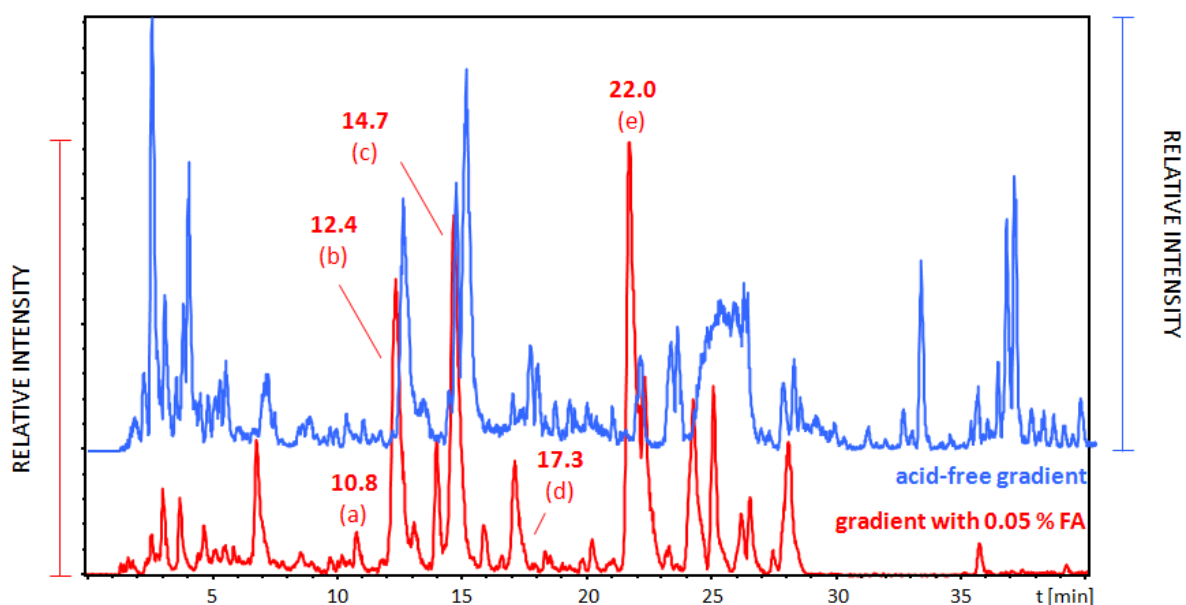


Figure 24: Segment of the base peak chromatogram of the full scan LC/ESI MS separation of an aqueous extract of saffron by two different elution solvent systems: acid free solvent gradient (blue) and solvent gradient with 0.05% FA (red). Some peaks are labeled and represent known structures: crocin with 5 glucose units (a), crocin with 4 glucose units (b), crocin with three glucose units (c), crocin with two glucose units (d, e). Other peaks represent crocins with low intensity or unknown structures as well as different unknown compound classes

A method with a long gradient for optimal separation was developed as described in chapter 2.1.2. An initial method with a shorter gradient indicated that some components eluted later in time and were not well-separated which was the reason for development of a longer gradient which was then used for all measurements.

Using H₂O and MeOH as a mobile phase resulted in good separation but it was clear that not all components were separated completely. The addition of 0.05% of formic acid to both solvents improved the separation of particular compounds exhibiting one free carboxylic acid group and resulted in sharper and more abundant peaks as it can be seen in the Figure 24. When a mobile phase gradient consists only of water and methanol the carboxyl group (COOH groups) can dissociate into carboxylate ions and protons, which leads to broadening of the peaks in the chromatogram. On the other hand when formic acid is added the carboxyl group becomes undissociated resulting in better, i.e. narrower peak shape.

Crocins which contain more glucose units elute much earlier than those with less, but this is not the case with the monosubstituted crocins because of one free carboxylic acid group of the aglycon.

One consequence of adding formic acid has also to be considered as disadvantage: not only the desired components, but also other components which had nothing to do with crocins were now eluting additionally creating more peaks in the chromatogram. Nevertheless, the improvement of the quality of the chromatographic separation was observed not only in the MS but also in MS² and MS³ experiments, which was necessary in order to explain the structure of yet unidentified glycosylated crocetin.

Figure 25 shows LC-MS² traces (base peak chromatograms) of the precursor ion with m/z 675.3 (theoretical m/z 675.26, $\Delta m = 0.04$) which represents crocins with 2 glucose units.

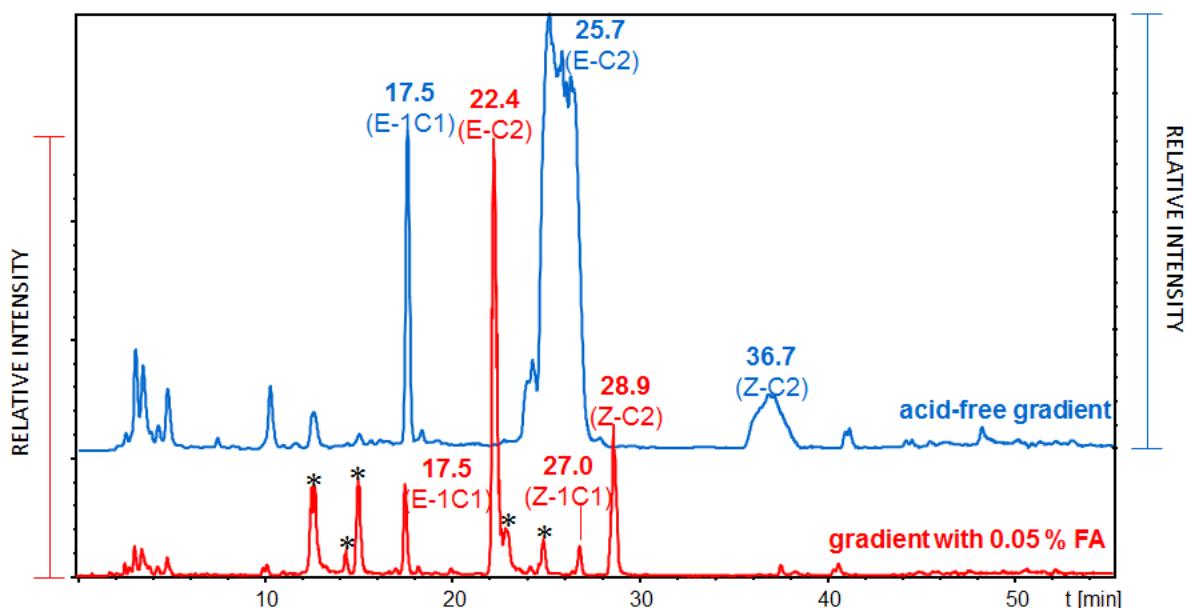


Figure 25: LC-MS² traces (base peak chromatograms) of the precursor ion m/z value 675.3 (theoretical m/z 675.26, $\Delta m = 0.04$) (isomers of crocetin [C] plus two glucose units), (*) represents other isomers of diglycosylated crocetin as well as in-source fragment ions of higher mass crocins. E stands for trans, Z for cis and the numbers represent the number of glucose units, example: E-1C1 represents trans crocetin with 1 glucose on one side and 1 glucose on the other side of the crocetin C, Z-C2 represents cis crocetin with 2 glucose units on one side of the crocetin

Crocins are present as trans (E) and cis (Z) isomers with trans crocins eluting approximately 10 min earlier than cis crocins. It can be observed that the peak at retention time $R_t = 25.7$ min shifts forward to $R_t = 22.4$ min when the gradient with 0.05 % of FA is used and new isomers are eluting. Bis-glucosyl-crocetin (E-1C1) elutes earlier than the mono-gentiobiosyl crocetin (E-C2) because of one free carboxylic acid group of the aglycon in the case of monosubstituted crocetin.

CID (collision induced dissociation) spectra of these two isomeric diglycosylated crocetin are shown in Figure 26. The precursor ion is present at m/z 675.3 (theoretical m/z 675.26, $\Delta m = 0.04$). Both spectra show fragment ion $[M+Na-92]^+$ which indicates the loss of 92 Da. This loss corresponds to C_7H_8 hydrocarbon loss which arises from the in-chain rearrangement of the aglycon [2]. In spectrum A the loss of one glucose can be seen at product ion m/z 513.2 (theoretical m/z 513.21, $\Delta m = 0.01$) $[Y_0+Na+162]^+$ and the loss of second glucose at product ion m/z 351.1 (theoretical m/z 351.16, $\Delta m = 0.06$) $[Y_0+Na]^+$ which represents sodiated Y_0 aglycon product ion.

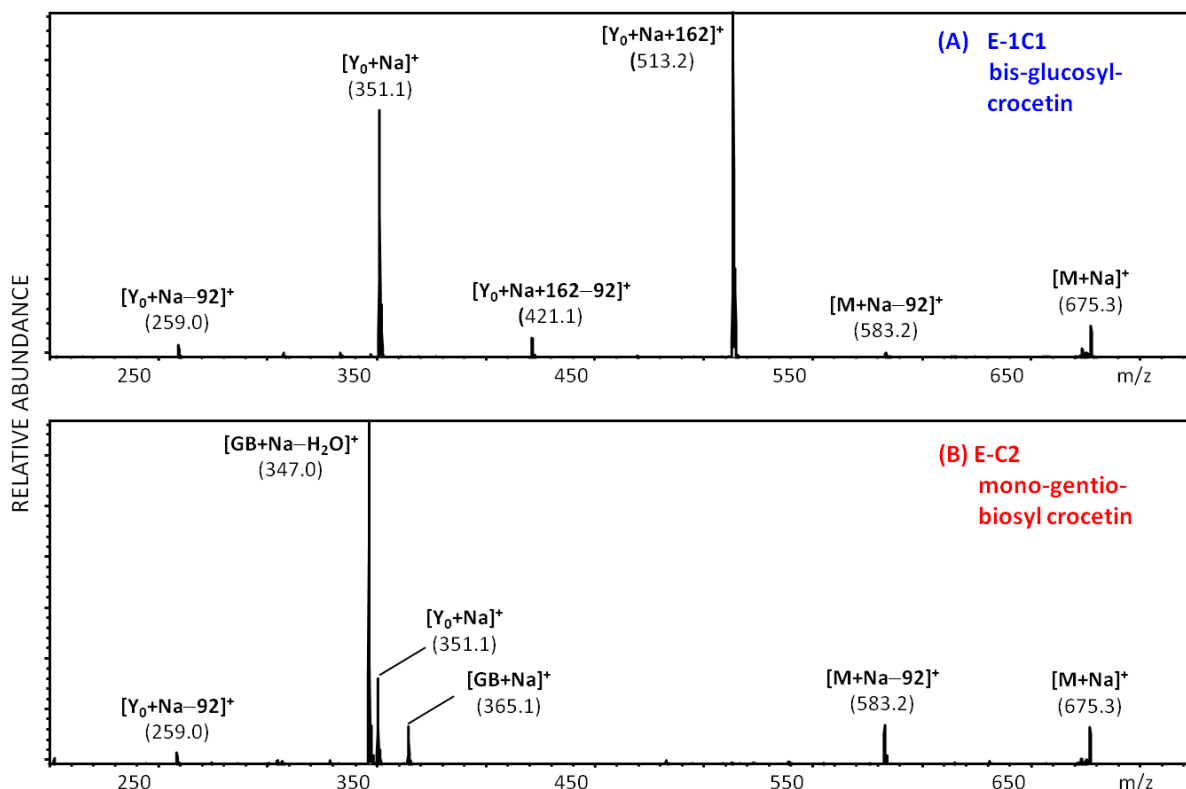


Figure 26: CID mass spectra showing mass spectrometric differences between the two isomeric diglycosylated crocetin bis-glucosyl-crocetin ($R_t = 17.5$ min) (A) and mono-gentiobiosyl crocetin ($R_t = 22.4$ min) (B)

In spectrum B the loss of neutral gentiobiose yields the m/z 351.1 (theoretical m/z 351.16, $\Delta m = 0.06$) ($[Y_0+Na]^+$). The carbohydrate residue can be seen at m/z 365.1 (theoretical m/z 365.1, $\Delta m = 0$) ($[GB+Na]^+$ - which represents intact sodiated gentiobiose) and at m/z 347.0 (theoretical m/z 347.1, $\Delta m = 0.1$) ($[GB+Na-H_2O]^+$ - which represents dehydrated intact sodiated gentiobiose).

3.1.1 Crocin glycosylation pattern including aglycon pattern

Previous saffron investigations done by our group [2] showed that crocetin could be glycosylated with up to 3 glucose units per site but only five glucose units in total. One study performed on early-spring flowering *Crocus* showed that crocins, which were found in the

stigmas, could have up to 8 glucose units but no detailed structural research was performed [19].

This work confirmed all those findings and delivered also new insight into the glycosylation pattern of crocins. New structural isomers of already known crocins were found and also highly glycosylated monosubstituted crocetin ester glycosides with up to 11 glucose units were found. These new glycosides including a new second aglycon will be discussed in more detail.

3.1.1.1 Crocetin structures

All crocins that have more than one sugar unit can have isomers with respect to glycosylation. Besides sharper and more abundant peaks the addition of formic acid lead to the discovery of until now undescribed structural isomers of crocins.

Base peak chromatograms including corresponding MS² and MS³ spectra of crocins with up to 5 glucose units can be found in the chapter 10 Appendix. Crocetin glycosylated with 5 glucose units exhibits a sodiated precursor ion at m/z 1161.5 (theoretical m/z 1161.42, $\Delta m = 0.08$). By increasing the precursor ion for 162 Da, and performing LC-MS² of the precursor ion m/z 1323.5 (theoretical m/z 1323.47, $\Delta m = 0.03$), hexaglycosylated crocetin was confirmed. Figure 27 shows base peak chromatograms of the LC-MS² of the precursor ion m/z 1323.5 (theoretical m/z 1323.47, $\Delta m = 0.03$). It can be seen that when an acid-free gradient is used only one type of isomers is eluting, but by addition of acid to the mobile phase, other isomers were also detected.

In the case of m/z 1323.5 (theoretical m/z 1323.47, $\Delta m = 0.03$) acid free gradient led to discovery of diglucosyl-tetraglucosyl-crocetin isomers (2-C-4), but with the acid gradient also other isomer the mono-hexaglucosyl-crocetin isomer (6-C-0) was discovered.

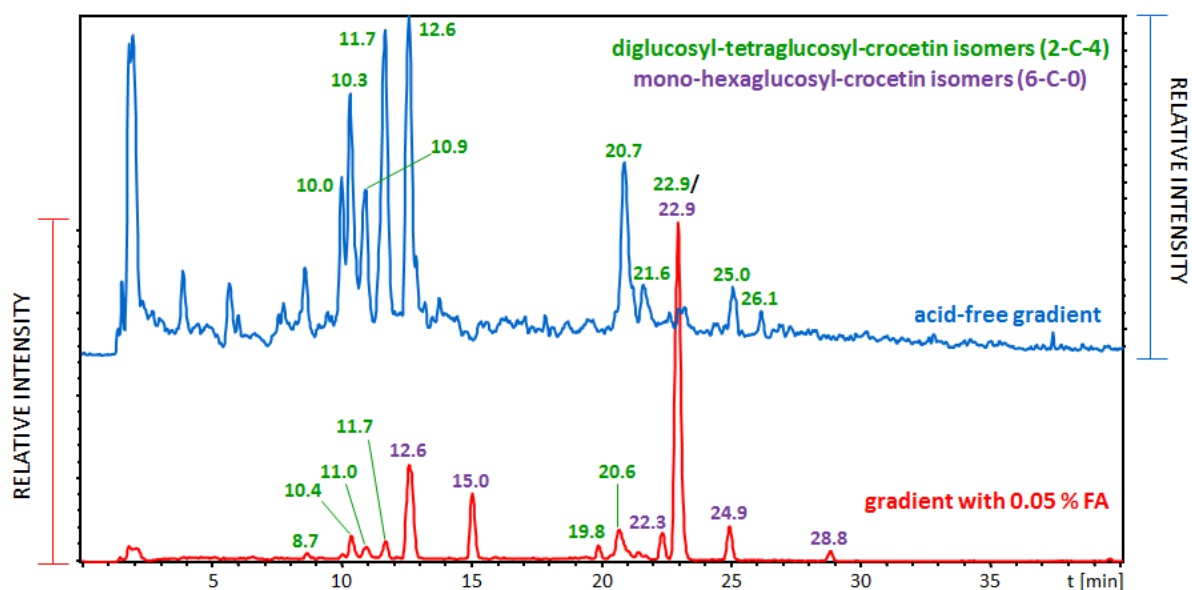


Figure 27: Elution profile of isomeric hexaglycosylated crocetins (MS^2 of m/z 1323.5 (theoretical m/z 1323.47, $\Delta m = 0.03$)) (acid free gradient versus gradient with 0.05% formic acid). Green colored retention times represent diglucosyl-tetraglucosyl-crocetin isomers while the purple colored retention times represent the mono-hexaglucosyl-crocetin isomers.

The already mentioned characteristic loss of 92 Da is present in both spectra as product ion $[M+Na-92]^+$. This loss as stated earlier, corresponds to C_7H_8 hydrocarbon loss which arises from the in chain rearrangement of the aglycon [2].

For better understanding CID mass spectra of two isomeric hexaglycosylated crocetins are shown in Figure 28. The diglucosyl-tetraglucosyl-crocetin eluted at following retention times: 8.7, 10.4, 11.0, 11.7, 19.8 and 20.6 min, while the mono-hexaglucosyl-crocetin eluted at 12.6, 15.0, 22.3, 24.9 and 28.8 min.

In the case of diglucosyl-tetraglucosyl-crocetin in the CID spectrum A, the loss of two glucose is visible at m/z 999.4 (theoretical m/z 999.37, $\Delta m = 0.03$) and a fragment ion B_4 corresponding to four glucose units at m/z 671.3. In the panel B the first fragmentation step is the loss of 328 Da corresponding to the aglycon and a fragment B_6 at m/z 995.4 (theoretical m/z 995.3, $\Delta m = 0.1$) corresponding to 6 glucose units is visible. This confirms the existence of at least two different isomeric structures in the case of hexaglycosylated crocetins.

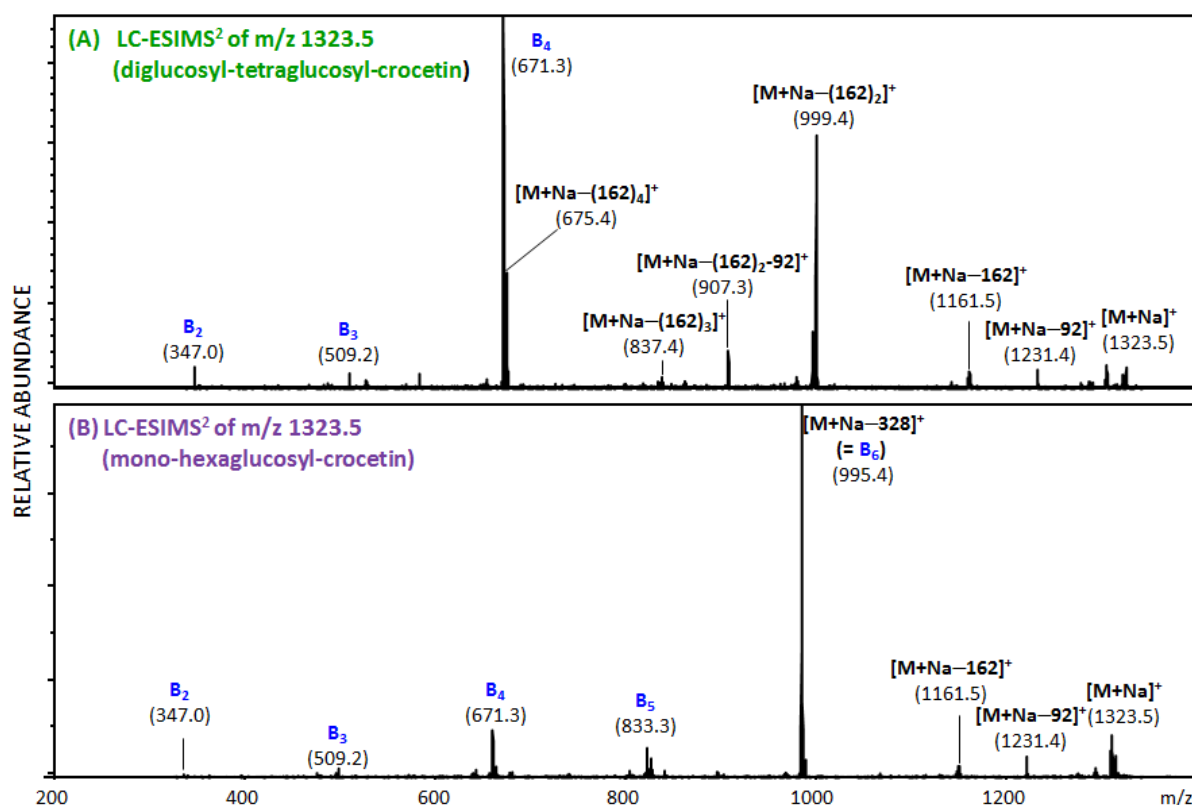


Figure 28: LC-ESIMS² mass spectrum of m/z 1323.5 (theoretical m/z 1323.47, $\Delta m = 0.03$) (sodiated species of hexaglucosylated crocetin), showing two different isomers: diglucosyl-tetraglucosyl-crocetin (A) and mono-hexaglucosyl-crocetin (B)

MS³ measurements were also performed in order to verify the presence of the new isomers because some product ions could have occurred because of the in source fragmentation which cannot be fully excluded.

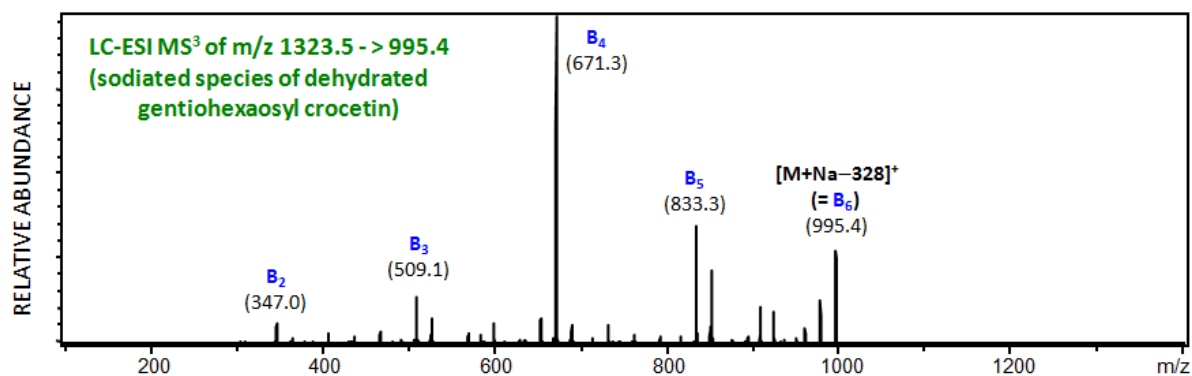


Figure 29: CID MS³ spectrum of the first generation product ion 995.4

LC-ESI MS³ of m/z 1323.5 \rightarrow 995.4 (sodiated species of gentiohexaosyl-crocetin) confirmed that the fragment ion B₅ (five glucose units), B₄ (four glucose units) and B₃ (three glucose units) that can be seen in the Fig. 29 originate from fragment ion B₆.

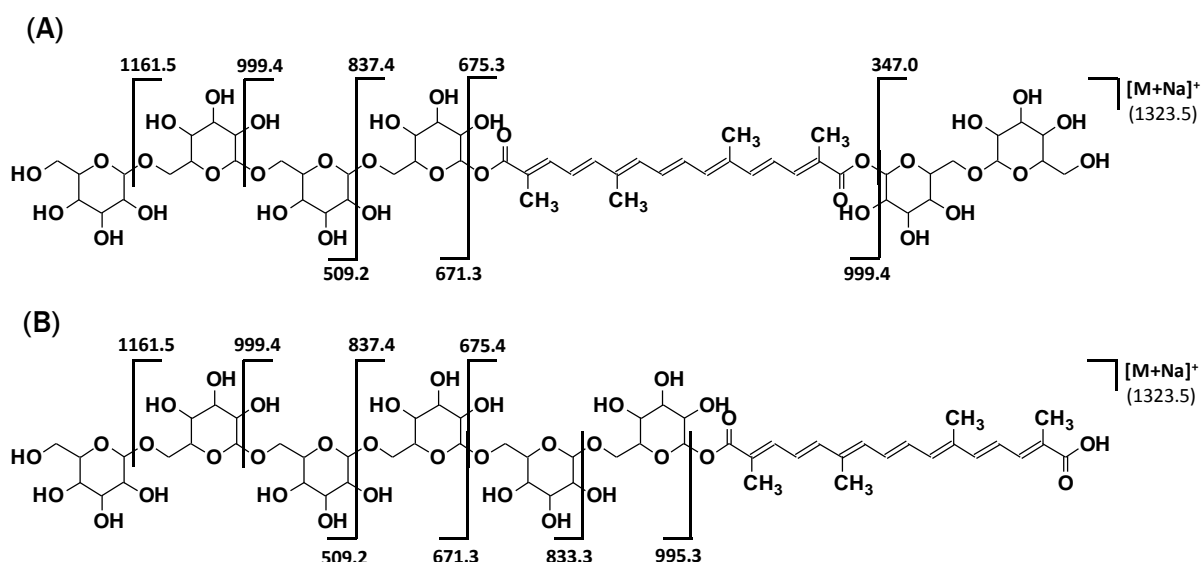


Figure 30: Fragmentation pattern of $[M+Na]^+ = 1323.5$ by LC-ESI MS²; (A) showing fragmentation pattern of diglucosyl-tetraglucosyl-crocetin and (B) of mono-hexaglucosyl-crocetin

For the explanation of the fragmentation pattern of the crocins the Domon-Costello product ion nomenclature for carbohydrates and glucoconjugates which was already explained in chapter 1.6, was used.

The fragmentation of crocins takes place via two different routes depending on the type of the aglycon glycosylation (Figure 30):

- When the aglycon is glycosylated on both sites, then first glucose units are being fragmented
- If the aglycon is glycosylated only on one site, then the first part that is fragmented is the aglycon leaving a linear glucose chain as a fragment ion.

New discovery was also a large number of structural isomers of already known crocins. Using MS³ measurements the difference between gentiotriose and neapolitanose could also be observed (Figure 31).

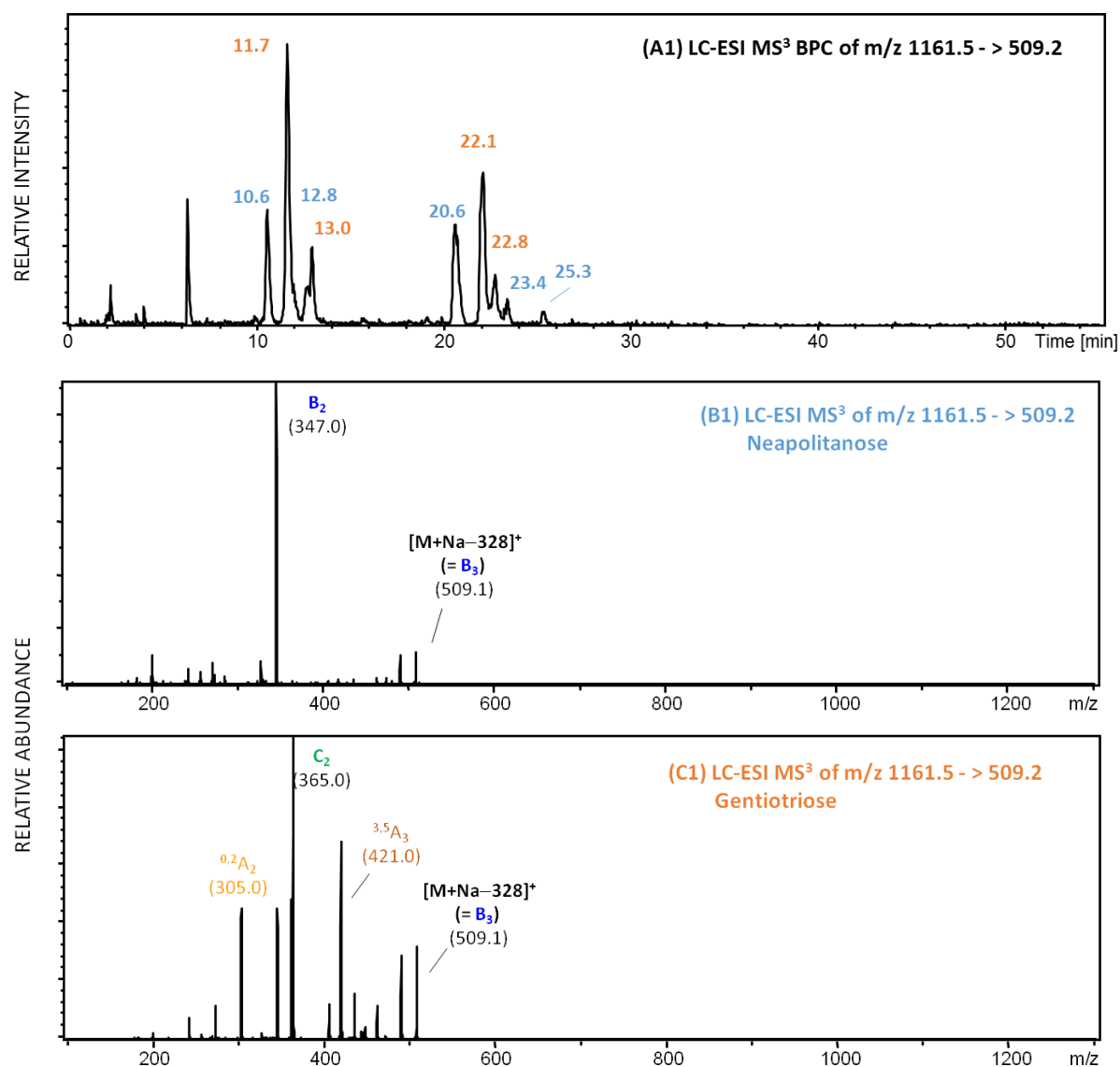


Figure 31: Base peak chromatogram of m/z 1161.5 -> 509.2 (A1); LC-ESI MS³ of m/z 1161.5 -> 509.2 showing neapolitanose (B1) and gentiotriose (C1) (the A ions result from cross ring cleavages while the B and C ions result from glycosidic bond cleavages)

The retention times of gentiotriose and neapolitanose are shown in Figure 31 (A1) with neapolitanose eluting at 10.6, 12.8, 20.6, 23.4 and 25.3 minutes and gentiotriose eluting at 11.7, 13, 22.1 and 22.8 minutes. In Figure 31 (B1) and Figure 31 (C1) LC-ESI MS³ of m/z

1161.5 \rightarrow 509.2 is shown. In case of neapolitanose there is only one abundant fragment ion B_2 at m/z 347.0 (theoretical m/z 347.1, $\Delta m = 0.1$) corresponding to 2 glucose units. In case of gentiotriose beside the fragment ion C_2 at m/z 365.0 (theoretical m/z 365.1, $\Delta m = 0.1$) corresponding to 2 glucose units two A fragment ions are also visible which arise as a result from cross ring cleavages.

3.1.1.2 Norcrocetin structures

Beside the already known aglycon crocetin (a C_{20} apocarotenoid), a new chain-shortened aglycon, which we call norcrocetin (a C_{17} apocarotenoid) was discovered (Figure 32). These two crocetins are the result of the activity of two different carotenoid cleavage dioxygenase enzymes which are present in saffron stigmas.

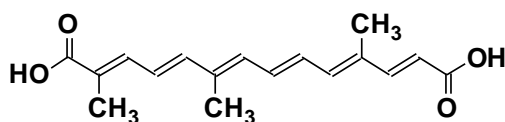


Figure 32: Chemical structure of norcrocetin, a C_{17} aglycon

During the experiment 4 crocin derivatives (glycosylated) of norcrocetin, whereas one crocin had two isomers, could be detected by LC-ESI MS and verified with MS^2 and MS^3 measurements (Table 14). Further crocin derivatives of norcrocetin could not be detected probably because of the low abundance. Addition of formic acid to the mobile phase did not improve the detection of other crocin derivatives of norcrocetin.

Compound name	Number of glucose units	[M+Na] ⁺ m/z found / calculated / Δm
mono-glucosyl-norcrocetin	1	473.20 / 473. 21 / 0.01
bis-glucosyl-norcrocetin	2	635.30 / 635.26 / 0.04
gentiobiosyl -norcrocetin	2	635.30 / 635.26 / 0.04
gentiobiosyl-glucosyl-norcrocetin	3	797.20 / 797. 32 / 0.12
bis-gentiobiosyl-norcrocetin	4	959.40 / 959.37 / 0.03

Table 14: List of crocin derivatives with the new aglycon norcrocetin

It was observed that the chain shortening of the aglycon influenced the retention time. If the aglycon is shortened by 3 carbon atom, like in case of norcrocetin, the retention time is shifted by roughly 5 minutes to earlier elution time.

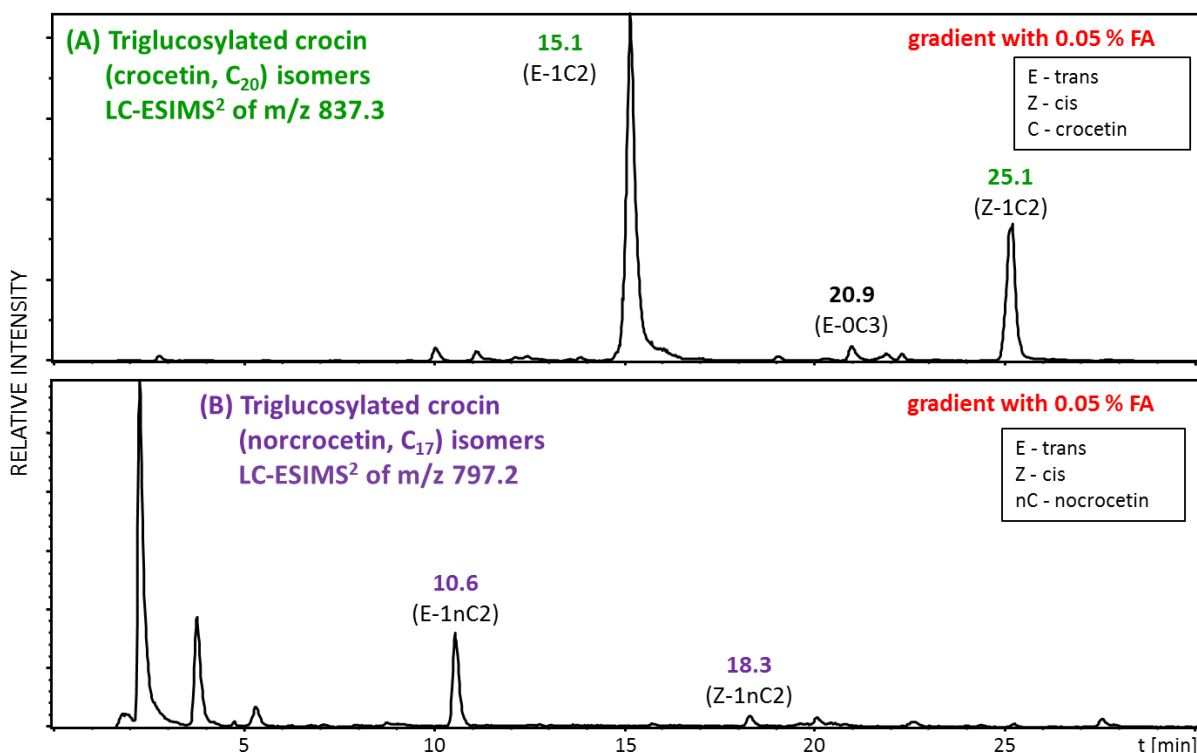


Figure 33: Base peak chromatograms showing the Influence on the retention behavior of crocins depending on the chain length of the aglycon (C₂₀ versus C₁₇); C stands for crocetin and nC for norcrocetin; E stands for trans, Z for cis and the numbers represent the number of glucose units, example: E-1C2 represents trans crocetin with 1 glucose units on one side and 2 glucose units on the other side of the crocetin , Z-1nC2 represents cis norcrocetin with one glucose unit on one side and 2 glucose units on the other side of the norcrocetin

Figure 33 shows the example of the time shift in the case of triglycosylated crocetin with crocetin C_{20} and triglycosylated crocetin with norcrocetin C_{17} . It is clear that the trans and cis crocins are eluting much earlier when C_{17} is present than in the case of crocetin C_{20} .

The MS^2 spectrum of crocins with three glucose units confirms the existence of this shortened aglycon (Figure 34). The CID spectra in panel A and B show almost identical fragmentations, spaced by a mass difference of 40 Da in all product ions in the panel B including the sodiated product ion aglycon with m/z 311 (theoretical m/z 311.13, $\Delta m = 0.13$). Both spectra show the product ion $[M+Na-92]^+$ which indicates the loss of 92 Da, which arises from the in-chain rearrangement of the aglycon.

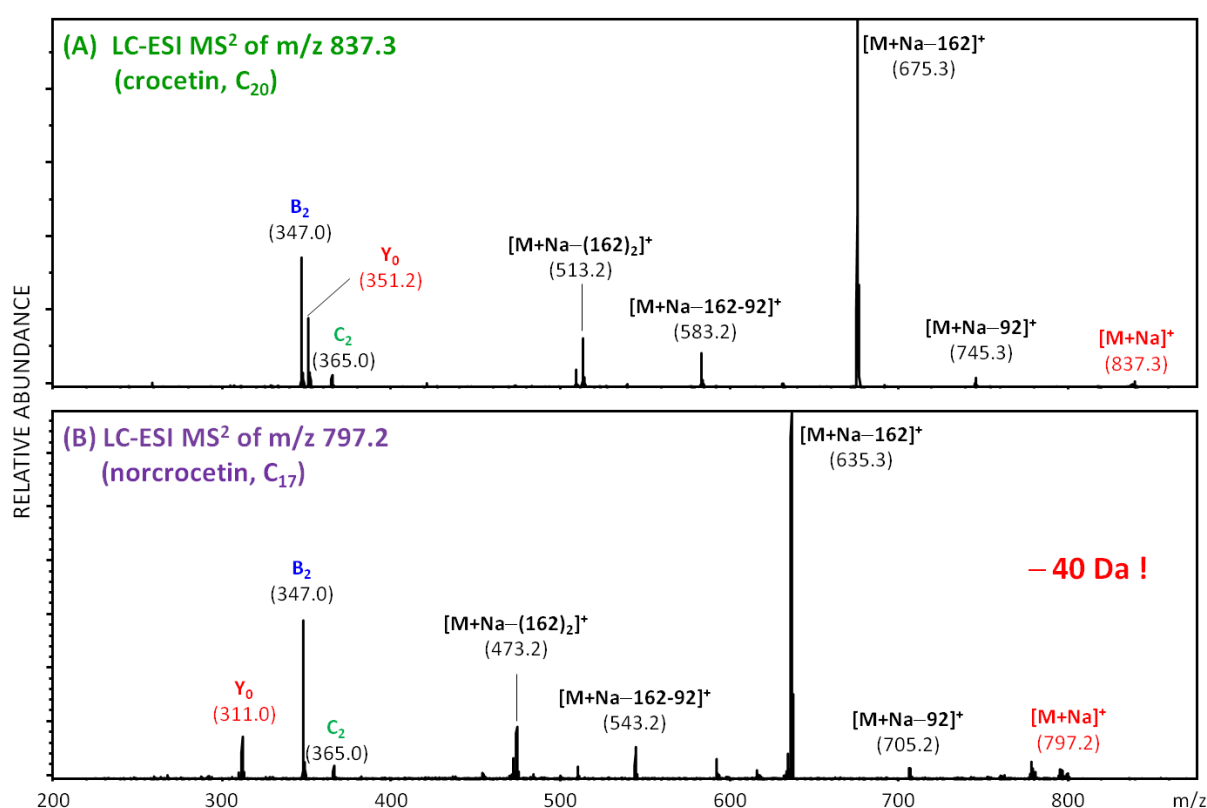


Figure 34: LC-ESI MS^2 mass spectrum of triglycosylated crocetin m/z 837.3 (theoretical m/z 837.32, $\Delta m = 0.02$) with $R_t = 15.1$ min (A) and triglycosylated norcrocetin m/z 797.2 with $R_t = 15.1$ min 10.6 min (B)

Further evidence of the existence of norcrocetin are product ions, which are except for the mass difference of 40 Da identical with those when crocetin aglycon is present. The fragment ions are shown in Table 15.

LC-ESI MS ² of m/z 837.30 (crocetin, C ₂₀)		LC-ESI MS ² of m/z 797.20 (norcrocetin, C ₁₇)	
m/z found / calculated / Δm	Fragment ion	Compound name	m/z found / calculated / Δm
745.29 / 745.25 / 0.04	[M+Na-92] ⁺	92 Da neutral loss	705.23 / 705.25 / 0.02
675.27 / 675.26 / 0.01	[M+Na-162] ⁺	Loss of one glucose unit	635.30 / 635.26 / 0.04
583.27 / 583.20 / 0.07	[M+Na-162-92] ⁺	92 Da neutral loss	543.19 / 543.20 / 0.01
513.20 / 513.21 / 0.01	[M+Na-(162) ₂] ⁺	Loss of second glucose unit	473.20 / 473.21 / 0.01
365.04 / 365.10 / 0.06	C ₂	Sodiated gentiobiose	365.04 / 365.11 / 0.07
347.04 / 347.10 / 0.06	B ₂	Sodiated dehydrated gentiobiose	347.04 / 347.09 / 0.05
351.19 / 351.16 / 0.03	Y ₀	Sodiated aglycon	311.05 / 311.13 / 0.08

Table 15: List of fragment ions from precursor ion m/z 837.30 (theoretical m/z 837.32, Δm = 0.02) and m/z 797.20 (theoretical m/z 797.32, Δm = 0.12))

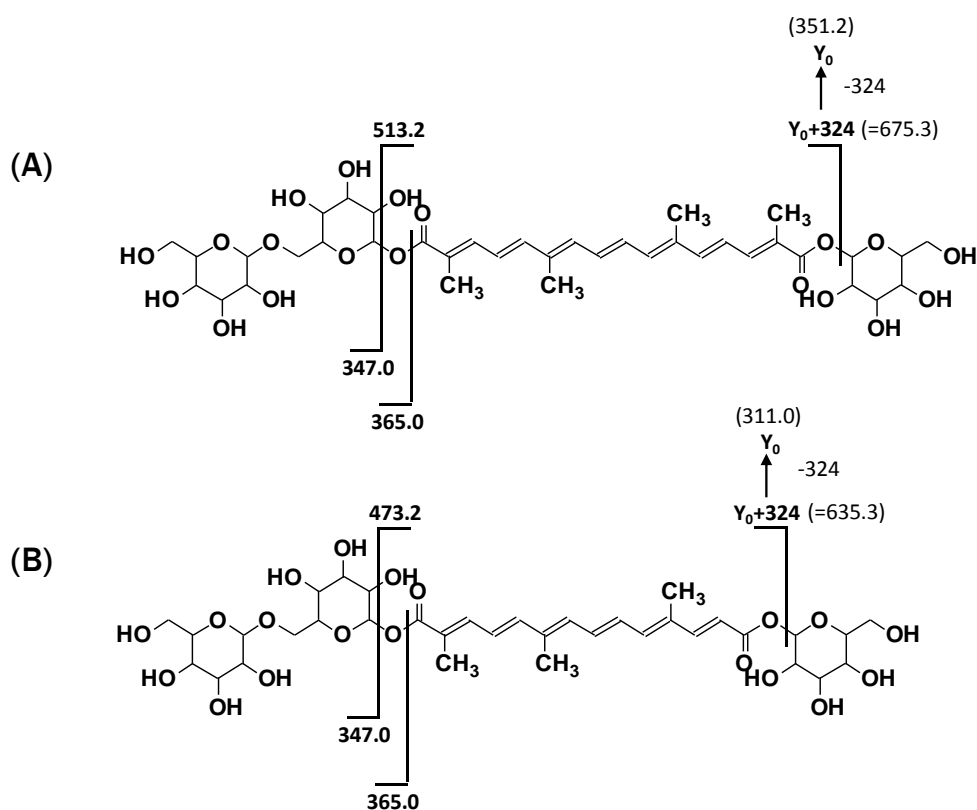


Figure 35: Fragmentation pattern of [M+Na]⁺ = 837.3 by LC-ESI MS² (A) and fragmentation pattern of [M+Na]⁺ = 797.2 by LC-ESI MS² (B)

Fragmentation pattern of triglucosylated norcrocetin occurs the same way as when triglucosylated crocetin is present (Figure 35). The only difference that can be observed is the mass difference of 40 Da.

3.1.2 Highly glycosylated crocetin

Addition of formic acid to the mobile phase allowed the detection of highly glycosylated crocins. The detection was possible only in the case of the crocetin C₂₀ aglycon, while the maximum number of detectable glucose units attached to norcrocetin was limited to 4.

The experiment showed that crocetin could be glycosylated with up to 11 glucose units. Crocetin ester glycosides containing from 7 up to 11 glucose units had two characteristics in common: they were all monosubstituted and they all eluted at the same time on the LC column used for these experiments (see Experimental section) (Figure 36).

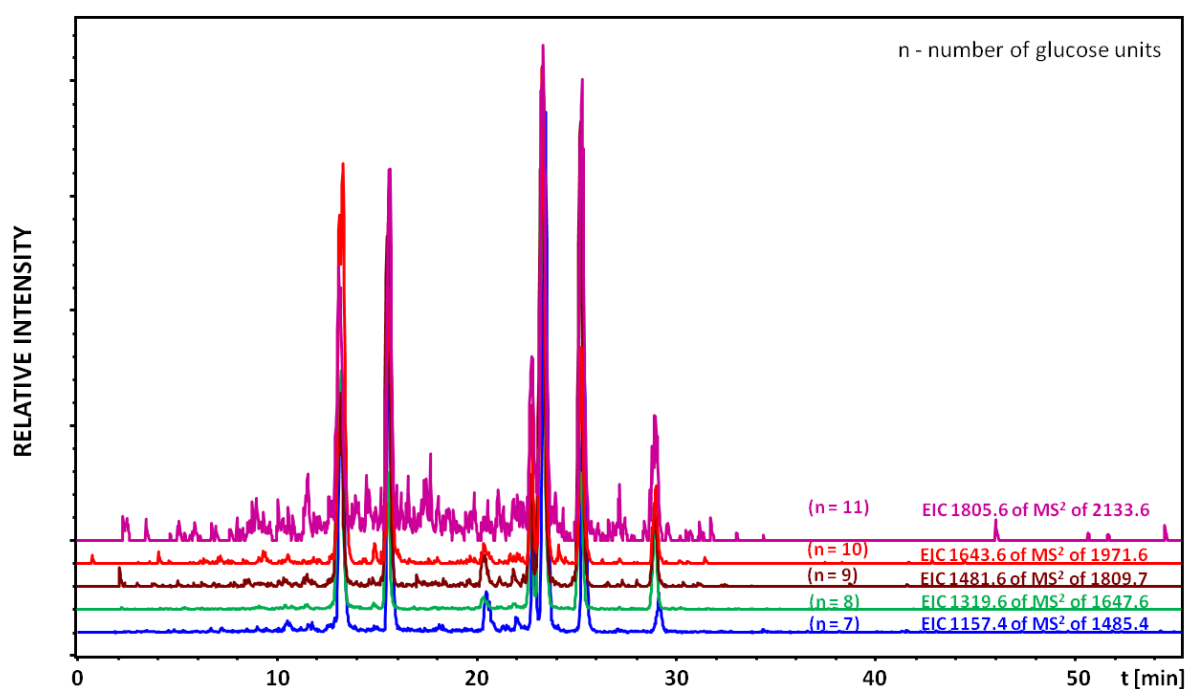


Figure 36: Extracted ion chromatogram of mono-glycosylated crocetin differing in chain length from 7 up to 11 glucose units

A large number of peaks in the extracted ion chromatogram is most likely because of the aglycon trans-cis isomerization. This means that when the aglycon is located on the end of the glucose chain the isomerization could maybe occur much easier as when the aglycon is glycosylated on both sides.

Mass spectrum of the monosubstituted crocetin ester glycoside with 11 glucose units corresponding to m/z 2133.7 (theoretical m/z 2133.74, $\Delta m = 0.04$) is shown in Figure 37. The characteristically C_7H_8 hydrocarbon loss coming from in chain rearrangement of the aglycon is present at m/z 2041.7.

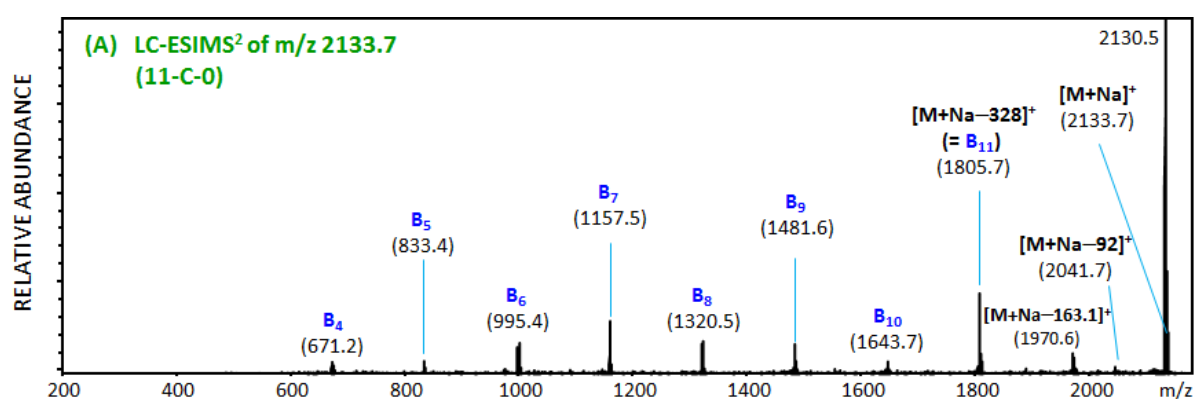


Figure 37: LC-ESI MS^2 mass spectrum of m/z 2133.7 (theoretical m/z 2133.74, $\Delta m = 0.04$) (where B represents the glucose and the subscript represents the number of the glucose units)

The loss of 328 (theoretical m/z 328.17, $\Delta m = 0.17$) Da at m/z 1805.7 (theoretical m/z 1805.57, $\Delta m = 0.13$) corresponds to the loss of the aglycon, meaning that a chain of 11 glucose units as fragment ion B_{11} remains. This indicates that the aglycon is located on the end of the glucose chain. Other fragment ions named B_4 - B_{10} probably originate from the in source fragmentation of B_{11} , but because of the extremely small abundance of m/z 2133.7, MS^3 experiments could not be performed. MS^2 and MS^3 spectra of product ions m/z 1971.7 (theoretical m/z 1971.69, $\Delta m = 0.01$), m/z 1809.6 (theoretical m/z 1809.63, $\Delta m = 0.03$), m/z 1647.6 (theoretical m/z 1647.58, $\Delta m = 0.02$), and m/z 1485.5 (theoretical m/z 1485.53, $\Delta m = 0.03$) corresponding to crocetins glycosylated with 10, 9, 8 and 7 glucose unit respectively, can be found in the chapter 10 Appendix.

Unfortunately the intensity of these highly glycosylated crocetins is rather low and their detection in the full scan by LC-ESI-MS was not possible because other more abundant components are probably obscuring them.

Nevertheless the first evidence for their existence is the compatibility with the calculated molecular masses. The second is the presence of the 92 Da loss which represents the in chain rearrangement of the aglycon and the third evidence is the neutral loss of 328 Da, which is the loss of the aglycon, and also the characteristic carbohydrate fragmentations are present.

3.1.3 Summary

With the addition of formic acid to the LC mobile phase, new crocetin glycosides were identified. Crocetin glycosides with seven up to eleven glucose units were all found as mono-substituted derivatives. Starting with the crocetin glycoside with 7 glucose units roughly no change in the retention time was observed. Besides the already known C₂₀ aglycon crocetin, a new C₁₇ apocarotenoid aglycon, which we call norcrocetin, was found in 4 different crocetin glycosides whereas crocin with 3 glucose units had 2 isomers. It was observed that the retention time for all 4 crocetin glycosides shifts towards lower elution time when norcrocetin is present.

Norcrocetin aglycon		
Number of glucose units	LC-ESI MS ² [M+Na] ⁺ found m/z	LC-ESI MS ³ [M+Na] ⁺ found m/z
1	473.2	473.2->311.1
2	635.3	635.3->311.1
3	797.2	The measurements were not performed
4	959.5	The measurements were not performed

Table 16: List of performed MS² and MS³ measurements of crocins with norcrocetin aglycon

Norcrocetin aglycon			
Precursor Ion m/z	Fragmentation pattern m/z	Retention time (min)	Glycosylation pattern
473.2	381.1, 311.1	12.7	Glu-C ₁₇
635.3	473.2, 311.1 543.2, 347	12.7 16.5	Glu-C ₁₇ -Glu Glu-Glu-C ₁₇
797.2	705.2, 635.3, 347	10.6	Glu-Glu-C ₁₇ -Glu
959.5	867.3, 635.3, 543.1, 347.1, 311	8.1	Glu-Glu-C ₁₇ -Glu-Glu

Table 17: Fragmentation pattern of crocins with norcrocetin aglycon

Table 16 shows performed MS² and MS³ measurements of crocins containing the norcrocetin C₁₇ aglycon and in Table 17 the corresponding fragmentation pattern is shown. All CID spectra can be found in the chapter 10 Appendix.

Table 18 shows performed MS² and MS³ measurements of crocins containing the crocetin C₂₀ aglycon with acid free mobile phase and mobile phase with 0.05% of FA. In Table 19 the corresponding fragmentation pattern is shown. All mass spectra can be found in the chapter 10 Appendix.

Crocetin aglycon		
Number of glucose units	LC-ESI MS ² [M+Na] ⁺ m/z	LC-ESI MS ³ [M+Na] ⁺ m/z
Mobile phase H ₂ O/MeOH		
1	513.2	513.2->351.1
2	675.5	The measurements were not performed
3	837.3	837.3->509.2
4	999.5	999.5->509.2 999->347
Mobile phase H ₂ O/MeOH + 0,05 % FA		
1	513.2	The measurements were not performed
2	675.5	The measurements were not performed
3	837.3	837.3->509.2
4	999.5	999.5->509.2
5	1161.5	1161.5->509.2 1161.5->671.3 1161.5->833.3
6	1323.5	1323.5->509.2 1323.5->671.3 1323.5->833.3 1323.5->995.4
7	1485.5	1485.5->1157.4
8	1647.6	1647.6->1319.5
9	1809.6	1809.6->1481.5
10	1971.7	1971.6->1643.6

Table 18: List of performed MS² and MS³ measurements of crocins with crocetin aglycon

Crocetin aglycon			
Precursor Ion m/z	Fragmentation pattern m/z	Retention time (min)	Glycosylation pattern
513.2	351.1	15.2	Glu-C ₂₀
675.5	513.2, 421.1, 351.1 583.2, 365, 347	17.7 12.8	Glu-C ₂₀ -Glu Glu-Glu-C ₂₀
837.3	745.3, 675.3, 583.2, 513.2, 347.1 745.3, 509.1, 347.1	15.1 20.9	Glu-Glu-C ₂₀ -Glu Glu-Glu-Glu-C ₂₀
999.5	509, 351 907.2, 837.3, 671.3, 509.2, 347 907.3, 675.3, 583.2, 347	14.0 15.6 12.7	Glu-Glu-Glu-C ₂₀ -Glu Glu-Glu-Glu-Glu-C ₂₀ Glu-Glu-C ₂₀ -Glu-Glu
1161.5	1069.3, 837.3, 675.3, 509.2, 351, 347.1 1069.3, 837.3, 745.3, 675.3, 583.3, 509.2, 347.1 1069.3, 999.5, 671.3 1069.3, 999.5, 833.3, 671.3, 509.2	10,0 11,1 14,1 15,2	Glu-Glu-C ₂₀ -Glu-Glu-Glu (NP) Glu-Glu-C ₂₀ -Glu-Glu-Glu (GT) Glu-C ₂₀ -Glu-Glu-Glu-Glu Glu-Glu-Glu-Glu-Glu-C ₂₀
1323.5	1231.4, 1161.5, 999.4, 907.3, 837.4, 671.3, 509.2 1231.4, 1161.5, 995.4, 833.3, 671.3, 509.2	10,4 12,6	Glu-Glu-C ₂₀ -Glu-Glu-Glu-Glu Glu-Glu-Glu-Glu-Glu-Glu-C ₂₀
1485.5	1393.6, 1157.4, 999.5, 833.4, 675.3	13,1	(Glu) ₇ -C ₂₀
1647.6	1555.7, 1319.6, 995.4, 833.4, 671.3	13,1	(Glu) ₈ -C ₂₀
1809.6	1717.8, 1481.7, 1319.5, 1157.5, 995.4, 833.4, 671.3	13,1	(Glu) ₉ -C ₂₀
1971.7	1879.7, 1879.8, 1643.8, 1481.5, 1319.5, 1157.5, 995.4, 833.4, 671.3	13,1	(Glu) ₁₀ -C ₂₀
2133.7	2041.7, 1970.6, 1805.7, 1643.7, 1481, 6, 1319.5, 1157.5, 995.4, 833.4, 671.2	13,1	(Glu) ₁₁ -C ₂₀

Table 19: Fragmentation pattern of crocins with crocetin aglycon

3.2 Imaging MALDI MS

Imaging data are acquired using two different instruments the UltrafleXtreme and the Axima TOF² which were described in detail in the chapter 2.2.

Two different matrices were used, DHB and THAP (for more details see chapter 2.2.1). For DHB matrix solution a mixture of MeOH and H₂O as matrix solvents was used while for the THAP matrix solution pure MeOH was used.

Saffron stigmas were put on the ITO slides which were coated with a conductive tape for adhesion of the stigmas. The slides were then stored overnight in a desiccator for better drying. The first IMS experiments were performed on stigmas that were not stored in a desiccator but no useful results could be obtained. Matrix solutions with different concentrations were prepared and satisfying (almost homogenous surface coverage) coverage of the stigmas was found. For the spraying process the whole matrix solution was used but it is not possible to define the exact amount of the matrix which was deposited on the sample (e.g. amount per mm²) because of the dispersion during the spraying process. Because the stigmas do not have a complete smooth surface total homogeny coverage could never be achieved.

Figure 38 shows saffron stigmas covered with DHB matrix solutions of different concentrations while Figure 38 shows stigmas covered with THAP matrix solutions of different concentrations.

An imaging experiment of the conductive tape on the Axima TOF² instrument was also performed in order to ensure authenticity of the m/z values corresponding to crocetin glycosides. During the measurement two unidentified peaks at m/z 473.2 and m/z 606.2 were observed but because of the low intensity no image could be generated.

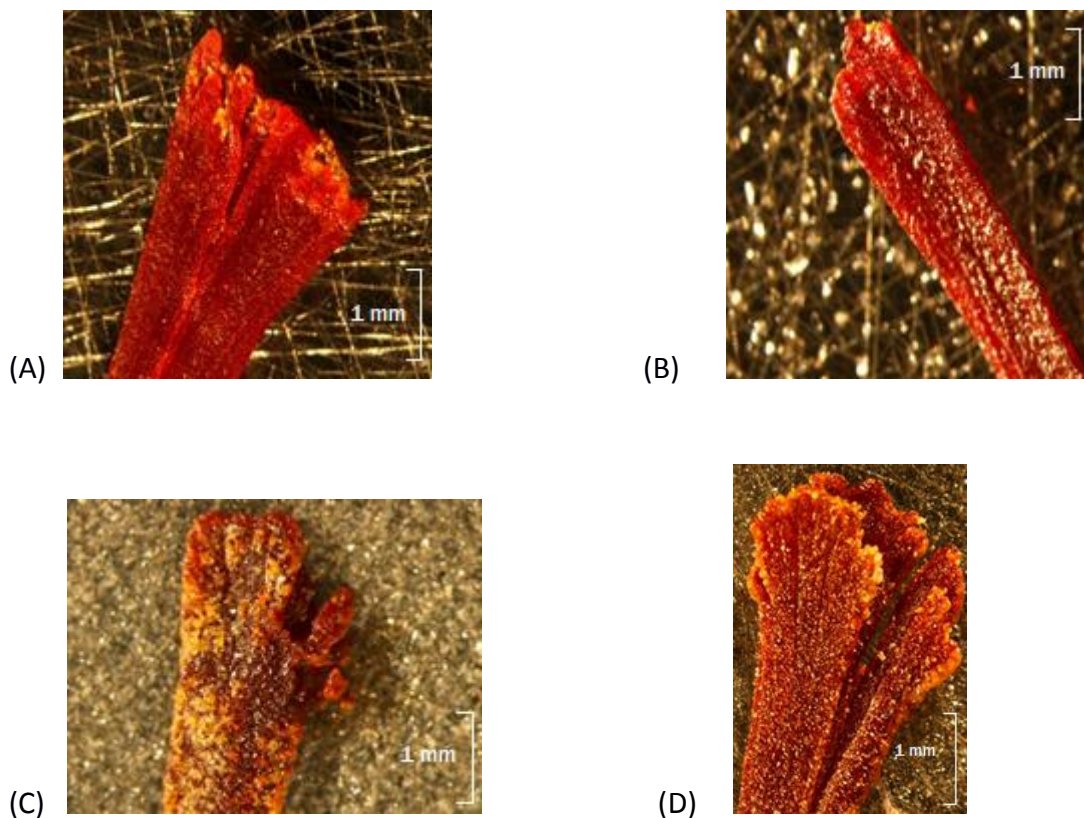


Figure 38: Saffron stigmas covered with different matrix solutions: (A) 40 mg/ml in H₂O:MeOH (1:1, v/v) doped with NaCl, spray volume 2 ml, (B) 40 mg/ml in H₂O:MeOH (1:1, v/v) doped with NaCl, spray volume 10 ml, (C) 200 mg/ml in H₂O:MeOH (1:1, v/v) doped with NaCl, spray volume 5 ml, (D) 200 mg/ml in H₂O:MeOH (1:4, v/v) doped with NaCl, spray volume 5 ml

As can be seen in Figure 38 the most homogenous coverage of the stigma was achieved when preparation D was used. Matrix solutions with preparation A and B produced none or very little matrix crystals while the concentration C had too high concentration of water which lead to transfer of analytes from their original positioning the stigmas i.e. diffusion of analytes.

The best homogenous coverage of the stigmas, when THAP matrix is used, is achieved with preparation C (Figure 39). In other cases it was observed that the THAP matrix tends to stick mostly to the edges of the saffron stigmas.

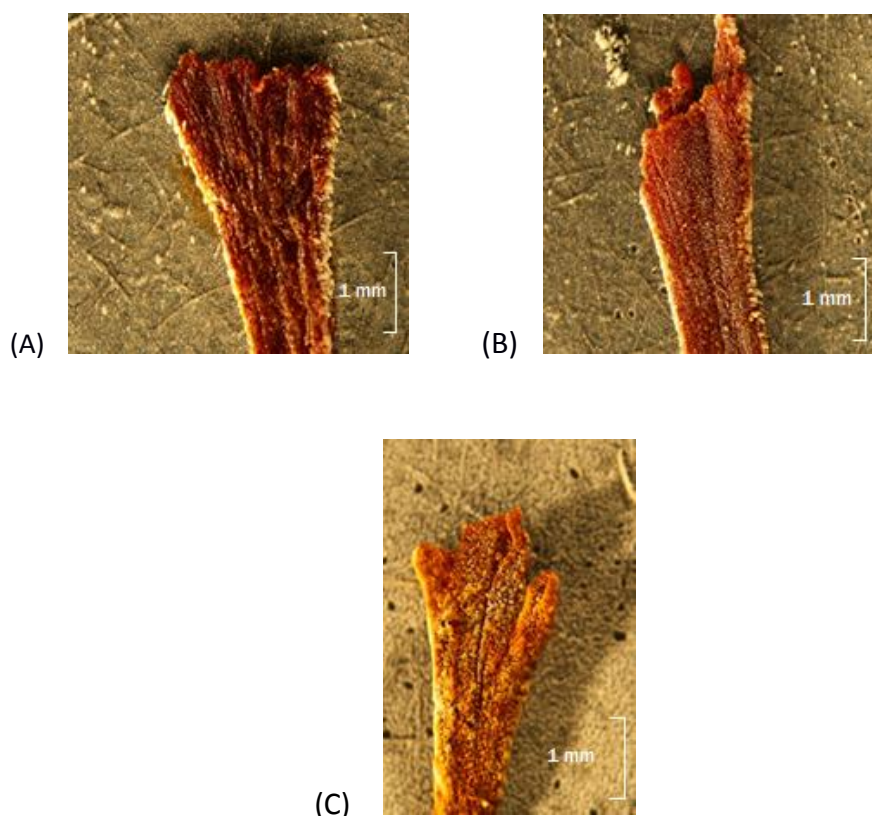


Figure 39: Saffron stigmas covered with different matrix solutions: (A) 40 mg THAP in MeOH doped with NaCl, spray volume 2 ml, (B) 64 mg THAP in MeOH doped with NaCl, spray volume 2.5 ml, (C) 50 mg THAP in MeOH doped with NaCl, spray volume 5 ml

3.2.1 UltrafleXtreme

The total ion current (TIC) normalization is one of the more common types of global normalizations in MALDI-MS. This type of data processing considers the sum of all intensities in the spectrum divided by the number of data points assuming that all spectra have a similar area (large extent of chemical noise plus small extent by peak intensities). This average value is used for normalization. Therefore this method is not affected by moderate peak intensity variations in the data set and artifacts may only be created by peaks with unusually large areas or by low spectral noise [47]. In order to generate images with desired glycosylated crocetins, the m/z values representing those glycosylated crocetins were selected from the average mass spectrum. The imaging was performed at 41 μm pixel size.

As mentioned earlier, two different matrices were used for the imaging experiment. The results obtained using DHB matrix with the matrix preparation D (see Figure 38) are shown in Figures 40 - 42.

Three stigmas A, B, C are investigated for the comparison. The different colors represent different m/z values. The green color in the images of Figure 40, Figure 41 and Figure 42 represents crocins with four glucose units. The yellow color represents crocins with three glucose units and the red color represents crocins with two glucose units. The m/z values are listed in the Table 20. The m/z range was set to $\pm 0.25\%$ for each m/z value. It gives the number of Da to the left and to the right side of the center mass window selection with which the mass filter works.

	Crocins with four glucose units	Crocins with three glucose units	Crocins with two glucose units
	m/z found / calculated / Δm	m/z found / calculated / Δm	m/z found / calculated / Δm
Stigma A	1003.59 (± 2.5 Da) / 999.37 / 4.22	841.06 (± 2.1 Da) / 837.32 / 3.74	679.53 (± 1.7 Da) / 675.26 / 4.27
Stigma B	1000.89 (± 2.5 Da) / 999.37 / 1.52	838.87 (± 2.1 Da) / 837.32 / 1.55	675.76 (± 1.7 Da) / 675.26 / 0.50
Stigma C	1002.21 (± 2.5 Da) / 999.37 / 2.84	840.16 (± 2.1 Da) / 837.32 / 2.84	678.12 (± 1.7 Da) / 675.26 / 2.86

Table 20: m/z values of different crocetin glycosides obtained with UltrafleXtreme and DHB matrix solution

It was observed that the location of crocetin glycosides on the stigmas surface changed from stigma to stigma. In some cases crocins were scattered all over the surface while in other they were centered in the middle or near the corners. The chosen method of matrix application and different heights of the surfaces of the stigmas (for more information see chapter 3.3) are probably the reason for that. But it seems that the crocins with three glucose units (yellow color in the Figure 40-42) in this imaging experiment are found in larger areas on the surface of the stigmas as dominating species than other crocins. This does not match the results that were obtained with LC-ESI MS where the most abundant crocin was the one with four glucose units with m/z 999.4 (theoretical m/z 999.37, $\Delta m = 0.03$). More results can be found in the chapter 10 Appendix.

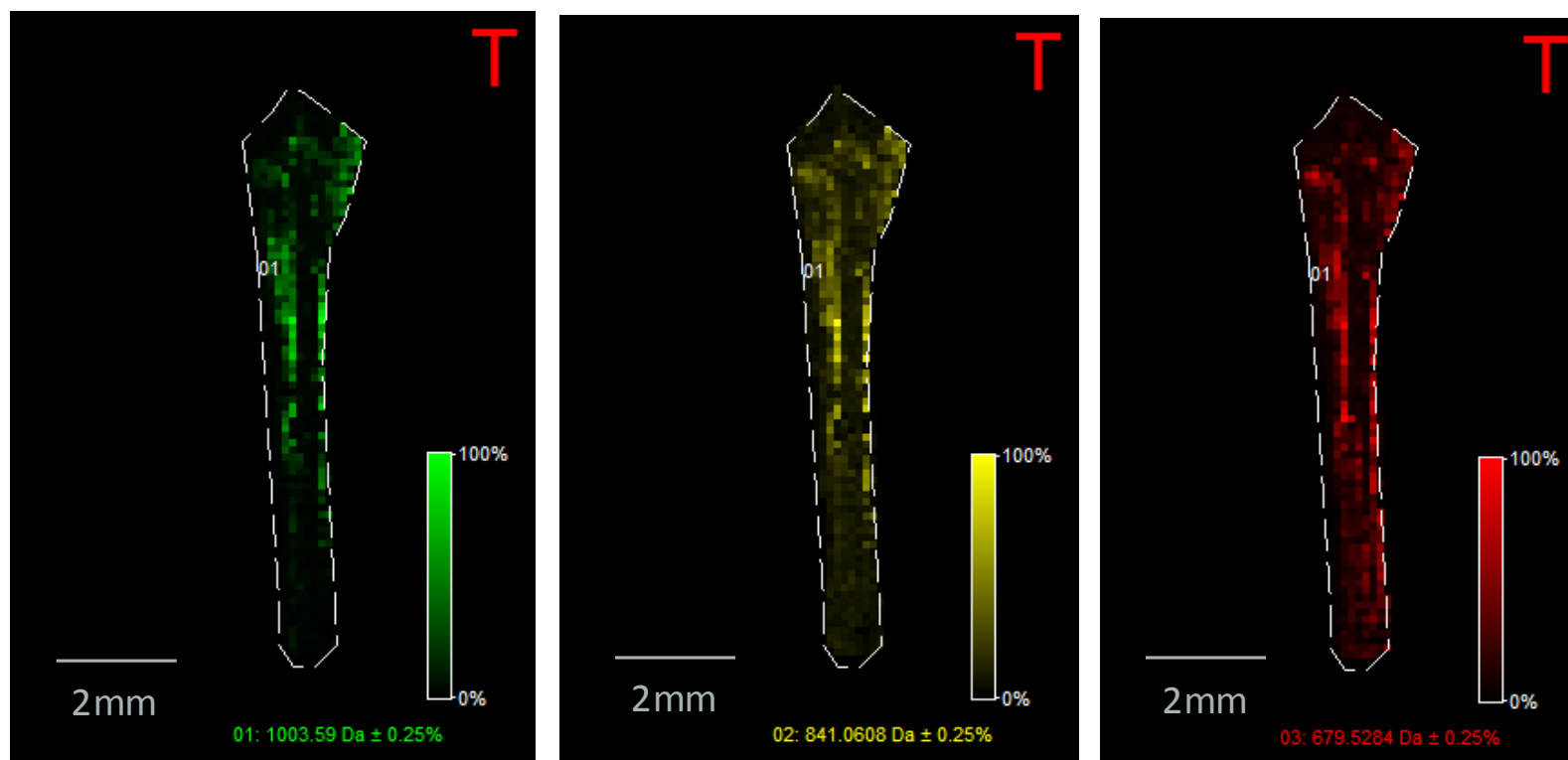


Figure 40: Imaging experiment with the UltrafleXtreme using DHB matrix showing stigma A with different m/z values (the white broken line shows the imaged area)

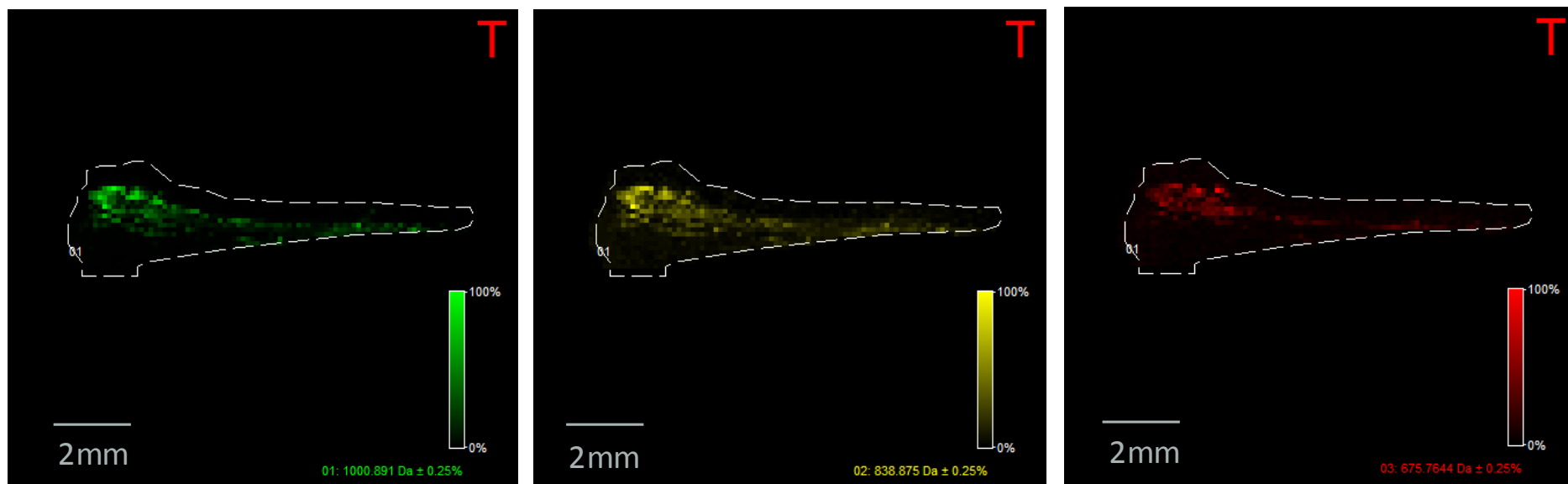


Figure 41: Imaging experiment with the UltrafleXtreme using DHB matrix showing stigma B with different m/z values

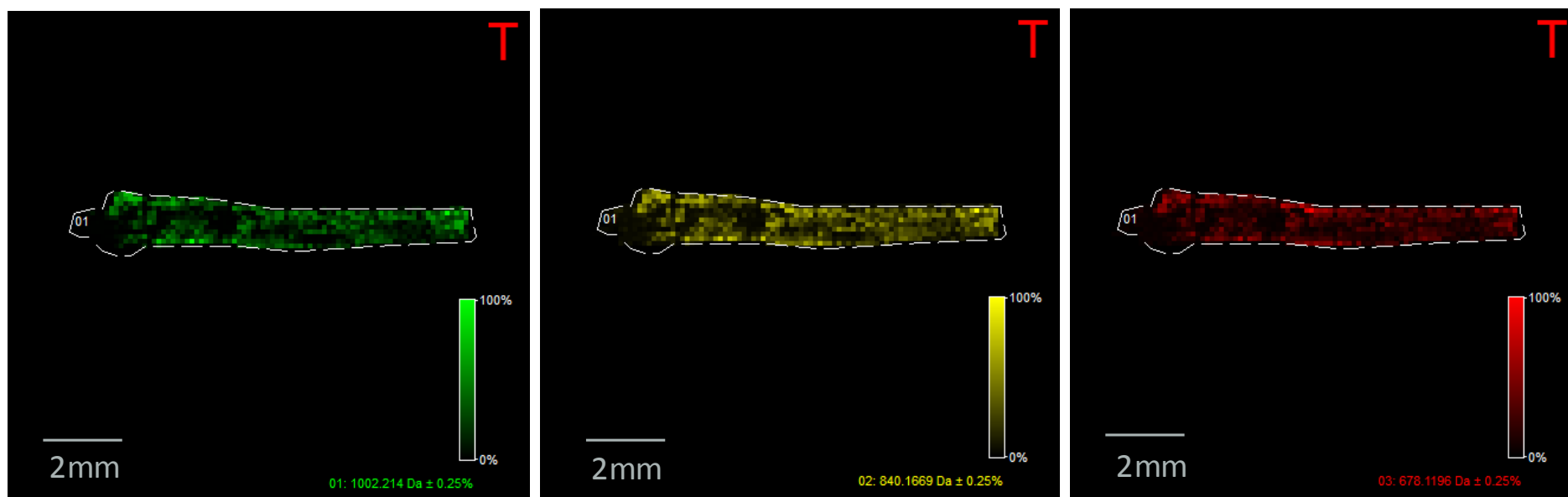


Figure 42: Imaging experiment with the UltrafleXtreme using DHB matrix showing stigma C with different m/z values

Besides the DHB matrix, the THAP matrix was also used for the experiment. Unfortunately, the results were not as satisfying as with the DHB matrix because no homogeneous coverage could be achieved. A large number of measurements delivered no results and if there were results they almost always resulted from the transfer of analytes from their original position due to dissolution in the matrix solvent.

In Figure 43 and Figure 44 two saffron stigmas are shown. The different colors of the stigma A represent different m/z values. The green color represents crocins with four glucose units and the yellow color represents crocins with three glucose units. The corresponding m/z values are listed in the Table 21. The m/z range was set to $\pm 0.25\%$ for each m/z value. It gives the number of Da to the left and to the right side of the center mass with which the mass filter works. No other usable results were obtained using the THAP matrix.

	Crocins with four glucose units	Crocins with three glucose units
	m/z found / calculated / Δm	m/z found / calculated / Δm
Stigma A	1001.93 (± 2.5 Da) / 999.37 / 2.56	840.79 (± 2.1 Da) / 837.32 / 3.47
Stigma B	1002.23 (± 2.5 Da) / 999.37 / 2.86	No results were found

Table 21: m/z values of different crocetin glycosides obtained with UltrafleXtreme and THAP matrix solution

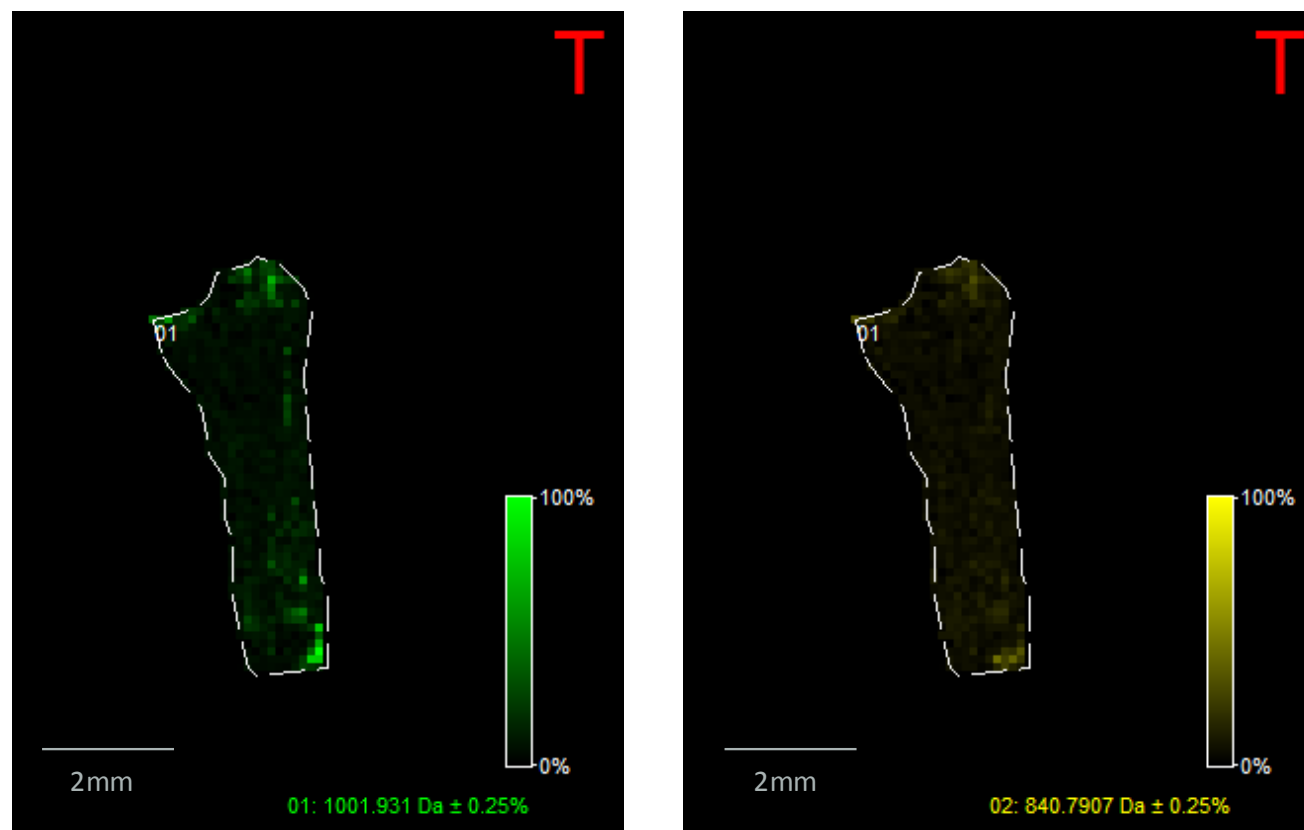


Figure 43: Imaging experiment with the UltrafleXtreme using THAP matrix showing stigma A with different m/z values

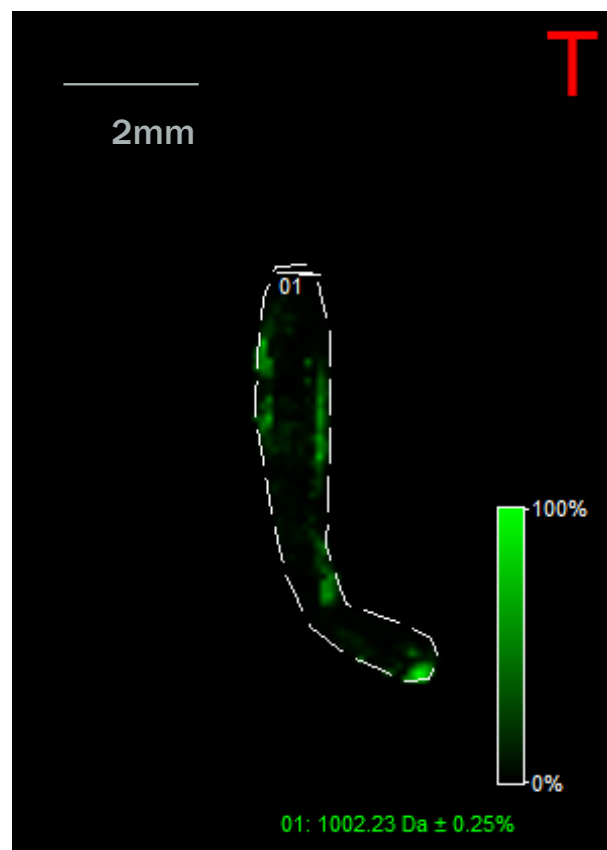


Figure 44: Imaging experiment with the UltrafleXtreme using THAP matrix showing crocins with four glucose units of the stigma B

3.2.2 Axima TOF²

The data acquired with Axima TOF² were exported to an open source program called Biomap which allows visualization and analysis of obtained data. Because the imaging experiment was done in several steps, the final pictures were stitched together to give a better overview of the crocin distribution. The imaging was performed at 40 μm pixel size. Equally to UltrafleXtreme measurements, two different matrices were used. The results obtained when DHB matrix was used are shown in Figure 45 - 50. In Figure 45 the distribution of crocins with 4 glucose units of the stigma A is shown. In Figure 46 the distribution of crocins with 3 glucose units and in Figure 47 distribution of crocins with two glucose units of the stigma A are shown. The corresponding m/z values can be found in Table 22.

	Crocins with four glucose units	Crocins with three glucose units	Crocins with two glucose units
	m/z found / calculated / Δm	m/z found / calculated / Δm	m/z found / calculated / Δm
Stigma A	1002.71 / 999.37 / 3.34	839.6 / 837.32 / 2.28	676.9 / 675.26 / 1.64
Stigma B	1002.6 / 999.37 / 3.23	840.1 / 837.32 / 2.78	676.5 / 675.26 / 1.24

Table 22: m/z values of different crocetin glycosides obtained with Axima TOF² and DHB matrix solution

For the stigma A it can be concluded that this particular stigma contains more crocins with 4 glucose units than crocins with three or two glucose units. This is opposite to the results that were obtained with UltrafleXtreme (crocins with three glucose units were the most present, followed by crocins with 4 and with two glucose units) but matching with the result obtained with LC-ESI MS (crocins with 4 glucose units were the most present, followed by crocins with three and two glucose units).

In Figure 47 the distribution of crocins with 4 glucose units of the stigma B is shown. In Figure 48 the distribution of crocins with 3 glucose units and in Figure 49 distribution of crocins with two glucose units of the stigma B are shown. The corresponding m/z values can be found in Table 22. According to the images obtained with Axima TOF² it can be said that the location of crocins with the same number of glucose units is different for every tested stigma.

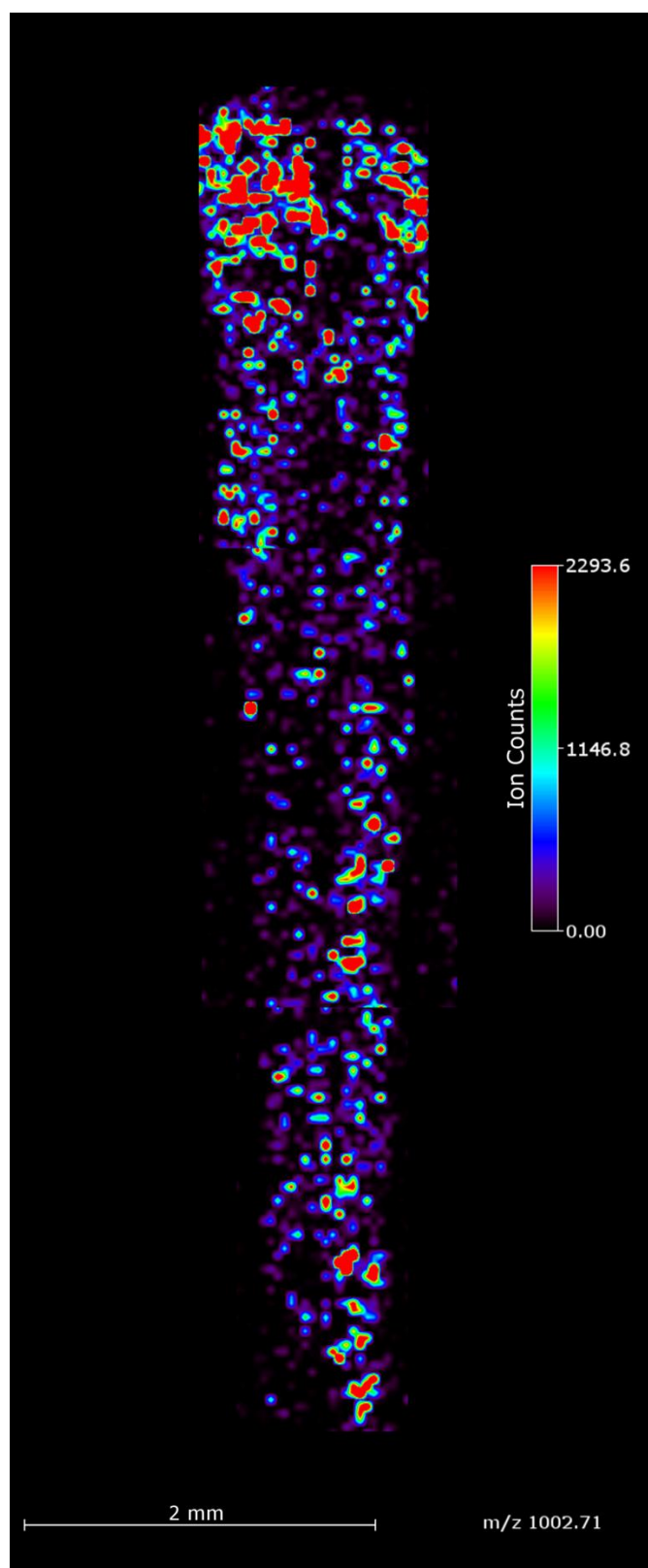


Figure 45: Imaging experiments with the AXIMA TOF² using DHB matrix showing distribution of crocins with four glucose units of stigma A

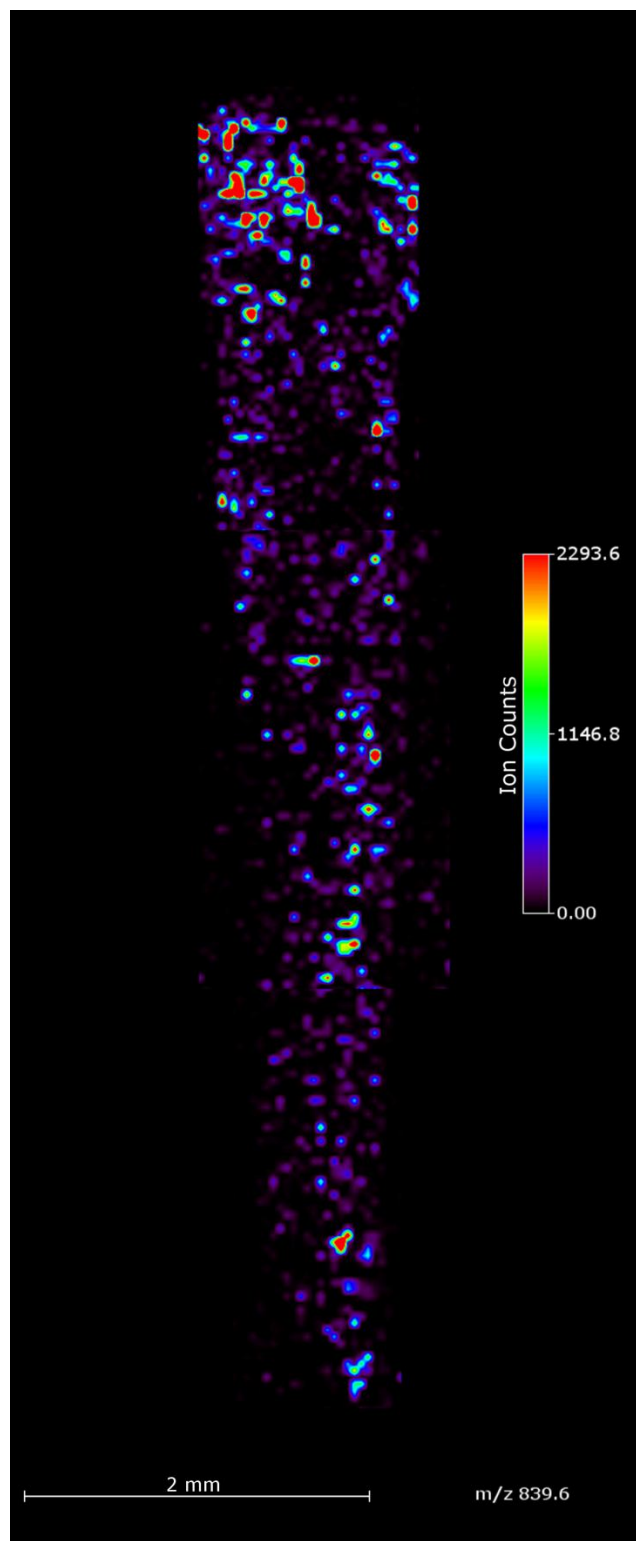


Figure 46: Imaging experiments with the AXIMA TOF² using DHB matrix showing distribution of crocins with three glucose units of stigma A

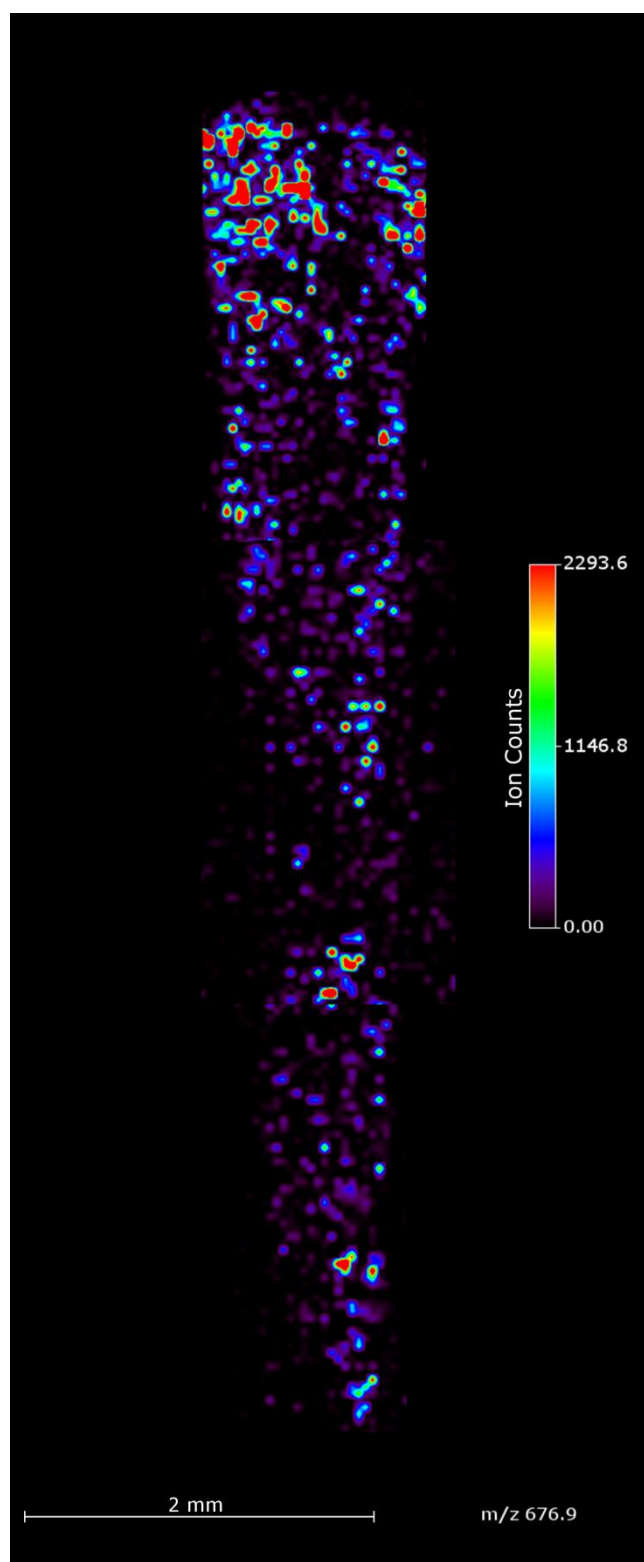


Figure 47: Imaging experiments with the AXIMA TOF² using DHB matrix showing distribution of crocins with two glucose units of stigma A

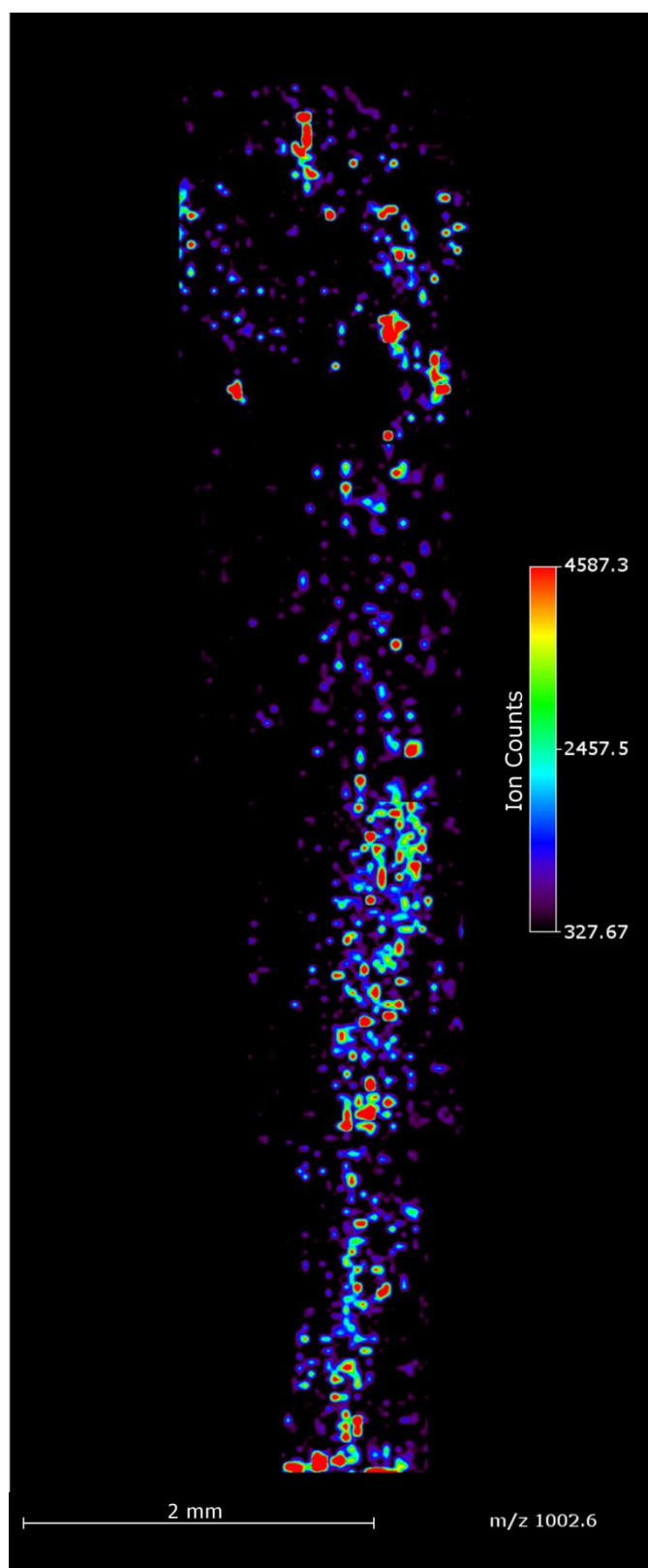


Figure 48: Imaging experiments with the AXIMA TOF² using DHB matrix showing distribution of crocins with four glucose units of stigma B

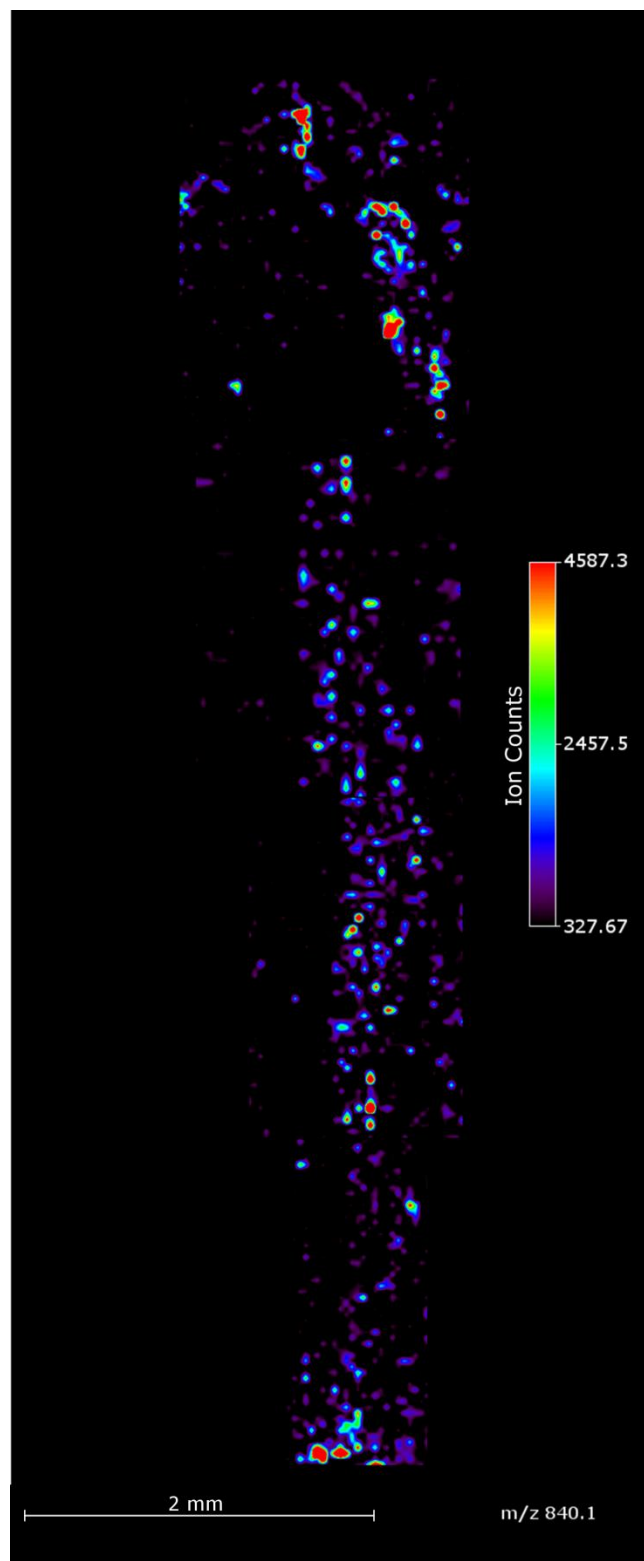


Figure 49: Imaging experiments with the AXIMA TOF² using DHB matrix showing distribution of crocins with three glucose units of stigma B

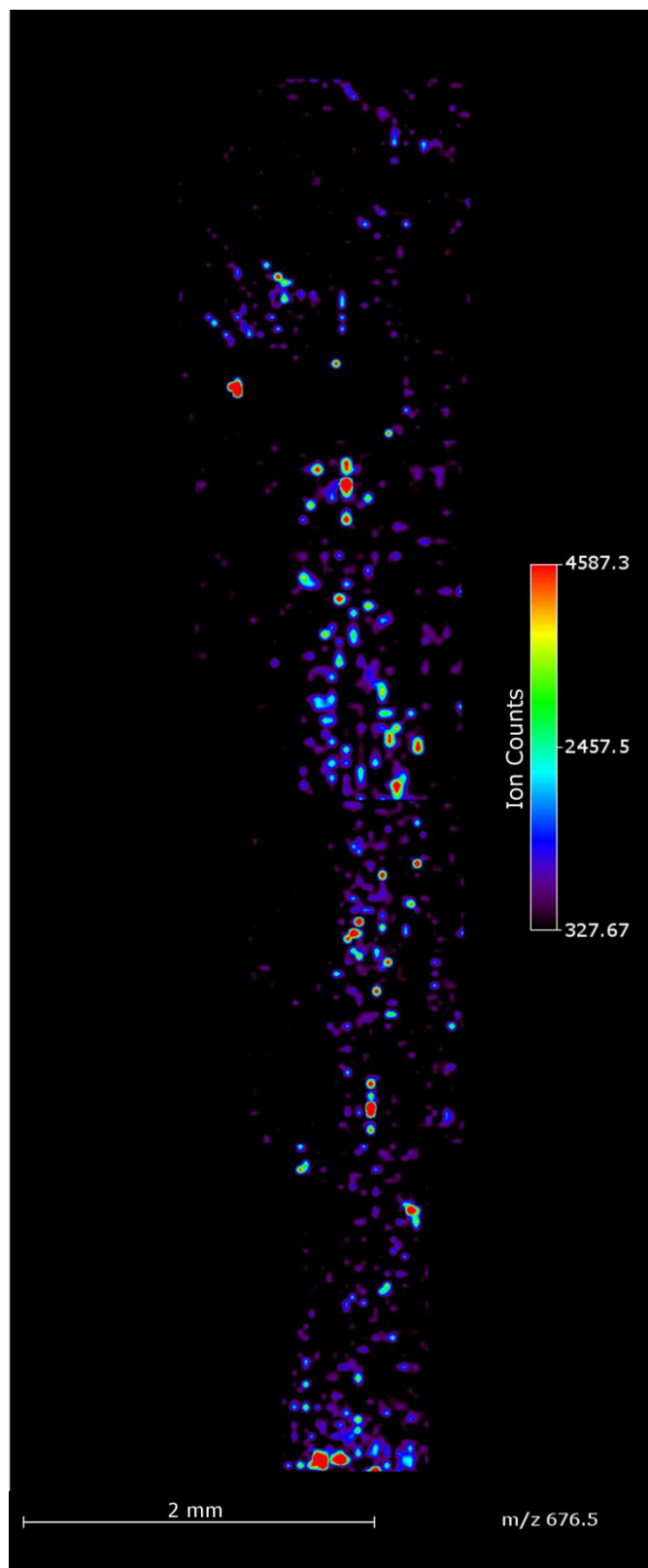


Figure 50: Imaging experiments with the AXIMA TOF² using DHB matrix showing distribution of crocins with two glucose units of stigma B

From approximately 15 stigmas used for Axima TOF² IMS experiment with DHB matrix only three produced usable images. Imaging results of the third stigma can be found in Chapter 10 Appendix.

The same experiment was performed using THAP matrix. In Figure 51 m/z values corresponding to crocins with 4 glucose units of stigma A and in the Figure 52 of stigma B are shown. The m/z values corresponding to crocins with three and two glucose units could not be detected when THAP matrix solution was used. Found and calculated m/z values are shown in Table 23.

Crocins with four glucose units	
m/z found / calculated / Δm	
Stigma A	999.5 / 999.37 / 0.13
Stigma B	1003 / 999.37 / 3.63

Table 23: m/z values of crocins with 4 glucose of stigma A and B obtained with Axima TOF² and THAP matrix solution

It can be seen that most crocins are located on the edges of the stigmas. The reason for that is probably because the THAP matrix tended to concentrate on the sharper edges of the stigmas during the matrix application. Nevertheless the AXIMA TOF² delivered slightly better results when THAP matrix was applied compared to data generated on the UltrafleXtreme. Also the shift in mass with AXIMA TOF² was lower for some stigmas than it was in UltrafleXtreme where shift of up to 4 Da could be observed.

For Axima TOF² IMS experiment with THAP matrix approximately 15 stigmas were used but only three could be used to generate images (IMS result from the third stigma can be found in the Chapter 10 Appendix).

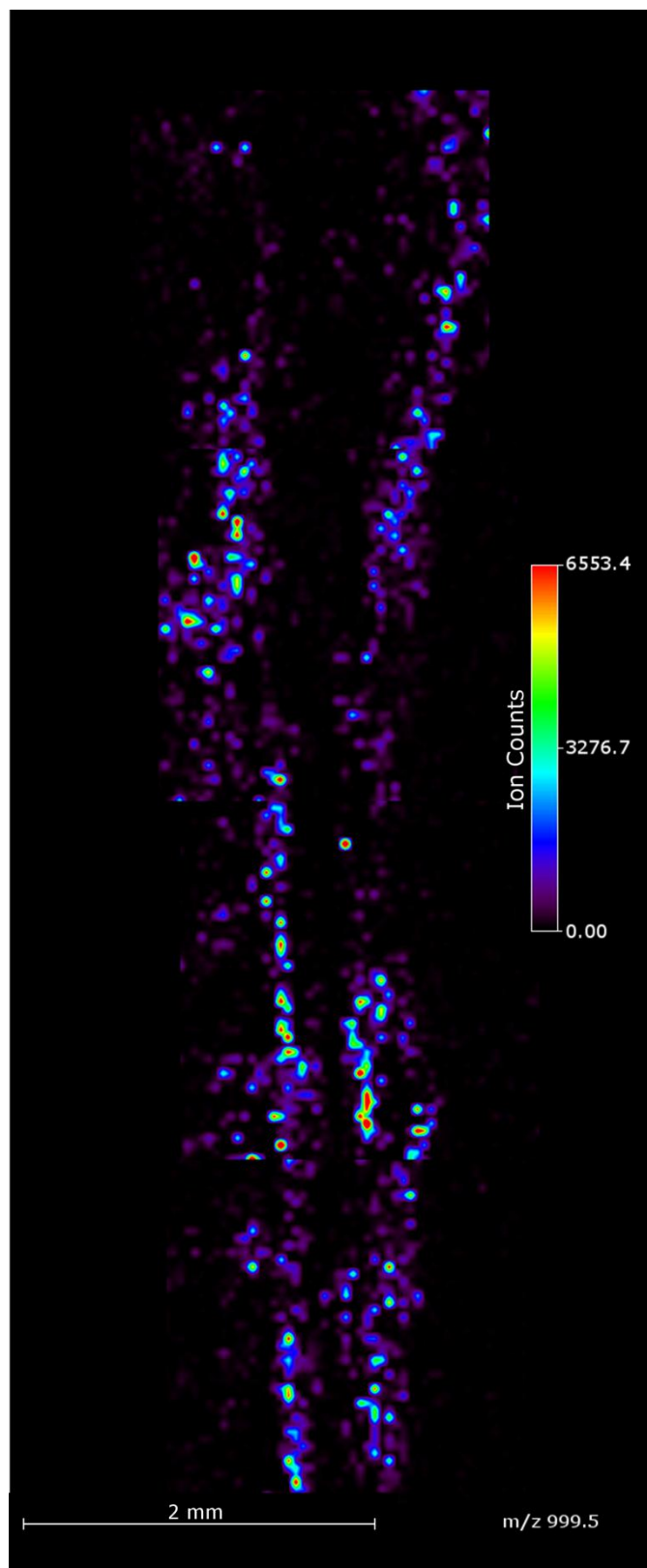


Figure 51: Imaging experiments with the AXIMA TOF² using THAP matrix showing distribution of crocins with four glucose units of stigma A

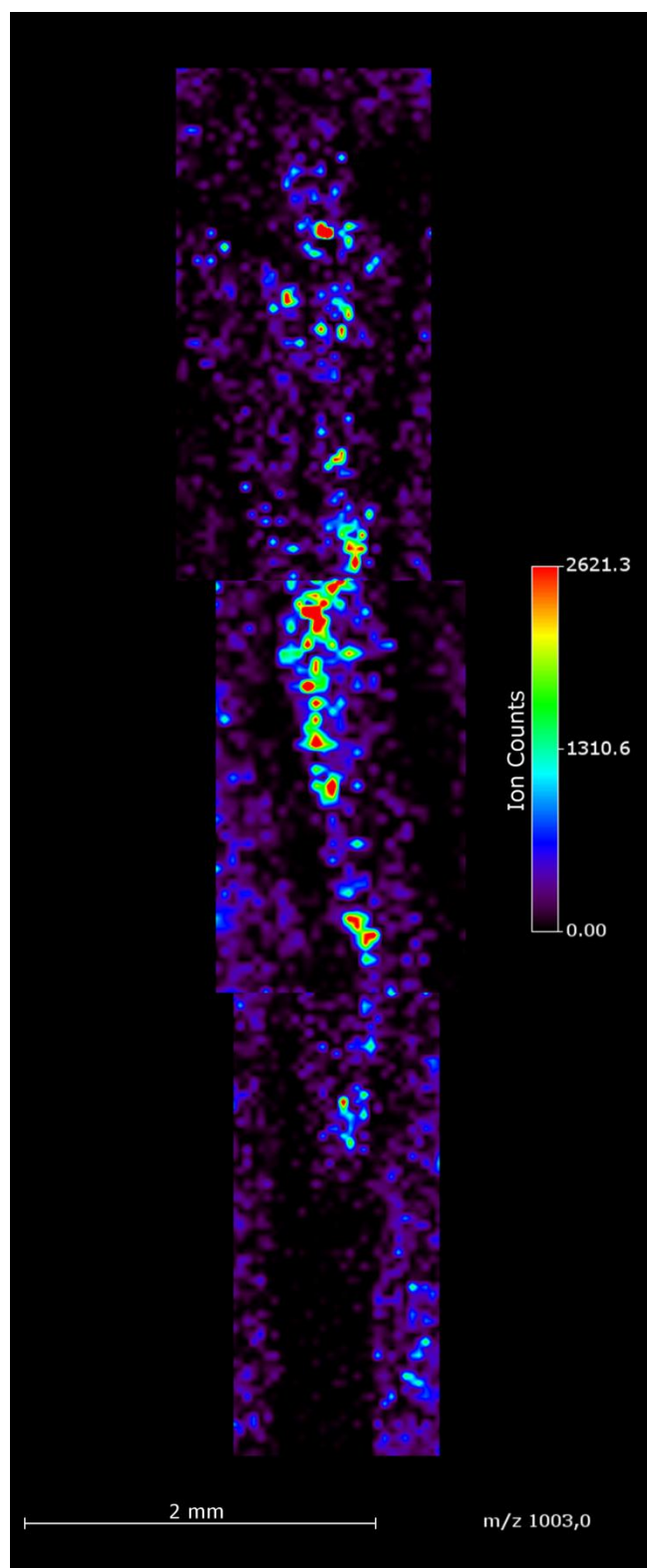


Figure 52: Imaging experiments with the AXIMA TOF² using THAP matrix showing distribution of crocins with four glucose units of stigma B

3.3 Electron Microscopy

There were three questions that needed to be answered with EM measurements:

- a) The first question was to see if any changes happened on the surface of the stigma parts that were held at roughing vacuum (roughly 10^{-2} mbar) as obtained for 24 hours compared to those that were storage under atmospheric pressure.
- b) The second question was to see what happens on the surface of the stigmas when different matrices are used.
- c) The third question was to see how a single stigma reacts to two different matrices, by cutting it in half and applying one matrix to one part and the other matrix on the other part.

The images in Figure 53 show parts of two stigmas (1 and 2) stored under different conditions. Part 1 of each stigma was stored under atmospheric pressure whereas the part 2 was stored under vacuum. It can be seen that the measured stigmas have an irregular and uneven surface with a lot of fractures but other than that no difference between the stigmas stored in vacuum and those under the atmospheric pressure could be observed.

For the second (b) question the stigmas were covered with DHB (stigma 3 and 4) and THAP (stigma 5 and 6) matrix solution. The same matrices were used in the case (c) for the stigma 7. For (b) the stigmas were stored under the atmospheric pressure before the matrix solution was applied whereas for (c) they were stored 24 hours in the vacuum (roughly 10^{-2} mbar). The EM images of experiment (b) can be seen in the Figure 54 and of experiment (c) in the Figure 55.

The pictures of the stigmas 3 and 4 in the Figure 54 show slightly better surface coverage with the DHB matrix solution than when the THAP matrix was used (stigma 5 and 7). THAP matrix formed island like parts whereas in the DHB case the deposited matrix parts were more connected or differently described overlapping flat sheets.

The comparison of the Figures 54 and 55 gives the impression that the stigma in Figure 55, which was stored in vacuum before the matrix solution was applied, has better coverage of the surface with both matrices than the stigmas in the Figure 54.

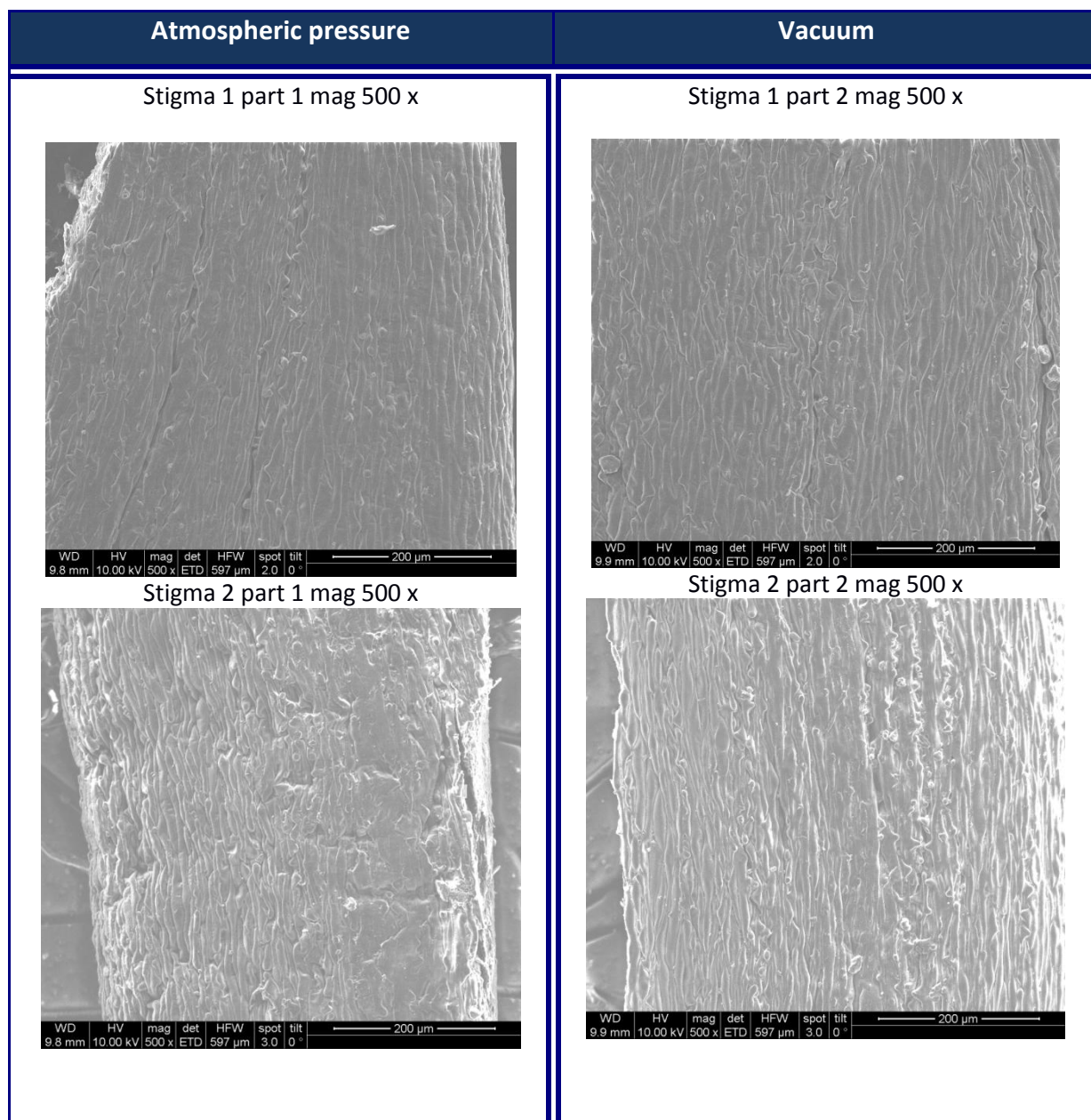


Figure 53: Electron Microscopy images of two saffron stigmas (stigma 1 and stigma 2) which were prepared according to the first approach: the left part was stored under atmospheric pressure and the right part in vacuum

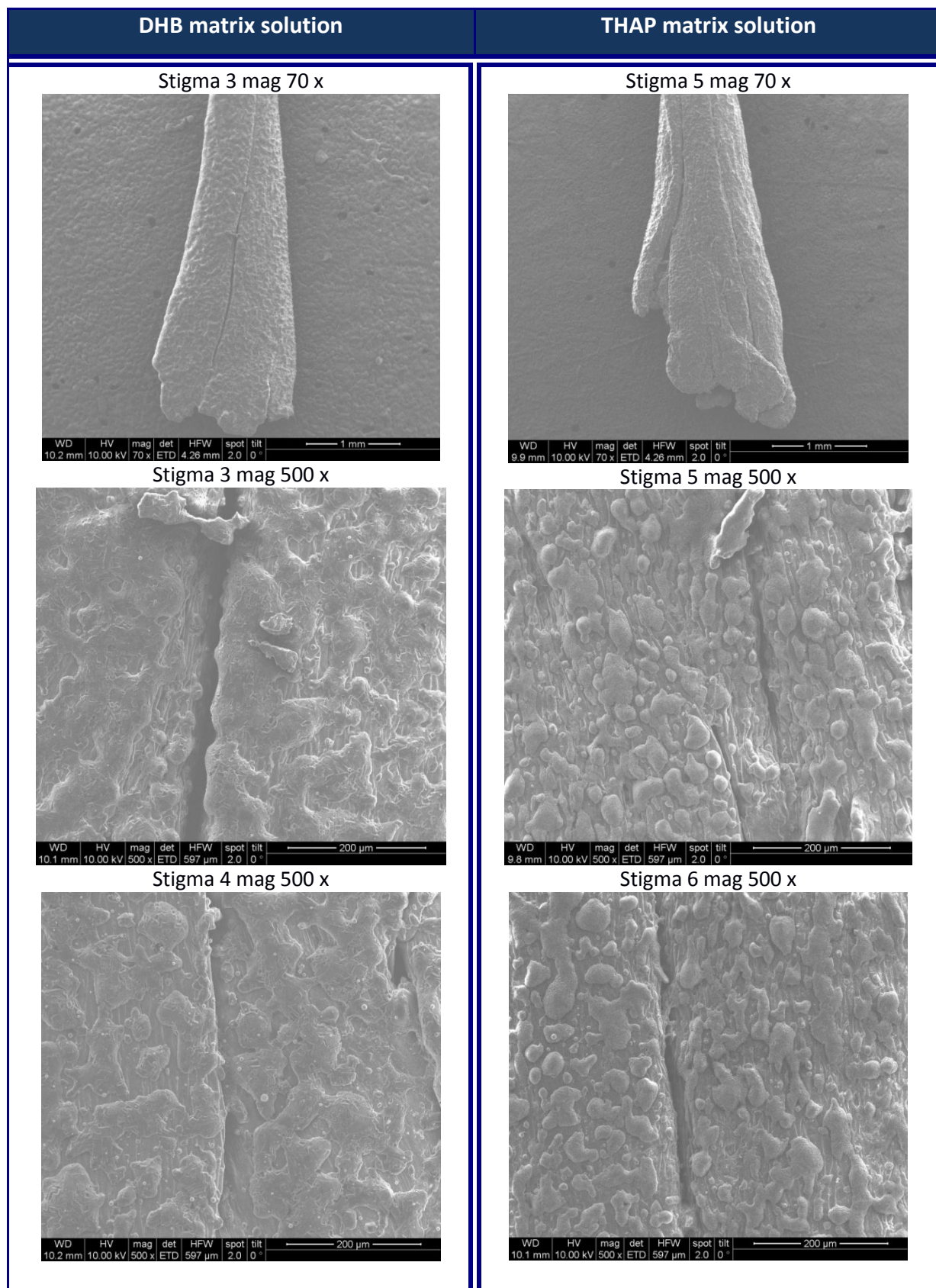


Figure 54: Electron Microscopy images of four saffron stigmas prepared according to second approach: stigmas 3 and 4 were sprayed with DHB and 5 and 6 with THAP matrix solution; the stigmas were stored under atmospheric pressure

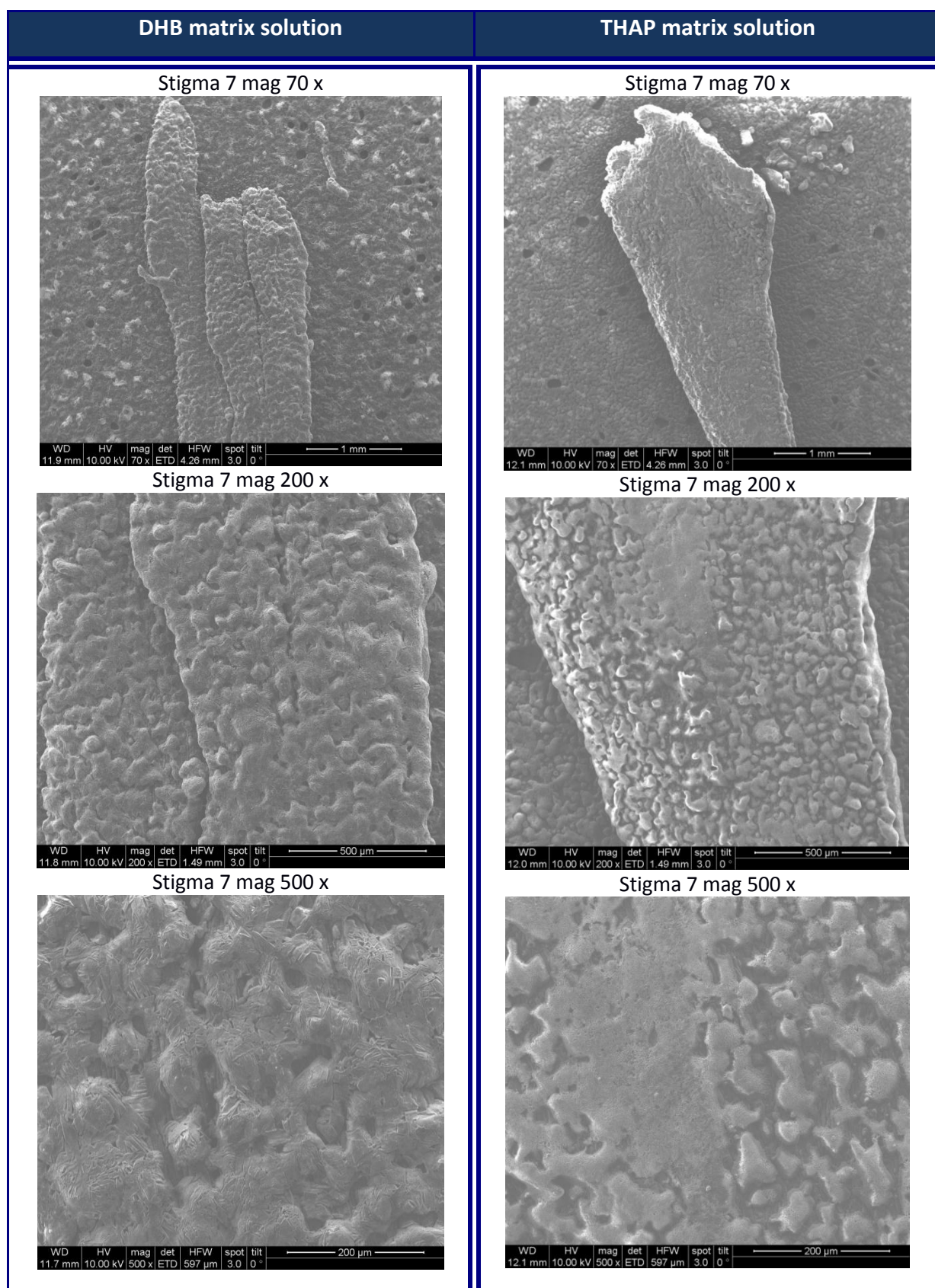


Figure 55: Electron Microscopy images of one saffron stigma (stigma 7), prepared according to third approach: left part was sprayed with DHB and the right with THAP matrix solution; the stigma was stored under vacuum before matrix application

The problem with the saffron stigmas is the uneven surface which looks different when different stigma parts are used for the EM measurement. Because of that it cannot be concluded that the distribution of matrix solution is always better when the stigmas are stored in vacuum before the matrix application, it could be that the measured part was better covered and others were not. Nevertheless the IMS measurements of the stigmas showed that good results could be obtained for the stigmas that were stored in the vacuum before the matrix was applied, whereas other stigmas delivered no results.

More results from the experiment (a) and (b) can be found in the Chapter 10 Appendix.

4. Conclusion

This work showed that the chemical composition of crocins from the saffron stigmas is much more complex than previously determined by ESI-MS. The addition of formic acid to the HPLC mobile phase led to discovery of new crocetin glycosides due to improved chromatographic resolution.

Until recently it was assumed that crocetin could be glycosylated with a maximum of five glucose units, but in this work new crocetin glycosides with up to eleven glucose units were found. The detection of crocetin glycosides containing 7-11 glucose units was possible only after the addition of the formic acid to the mobile phase of the HPLC by positive ion ESI-MS. Furthermore it was of interest that these crocins were present only as mono-substituted derivatives, i.e. one free -COOH moiety was present.

New discovery was also a large number of structural isomers of already known crocins. The difference between gentiotriose and neapolitanose could also be observed using MS³ measurements (see Chapter 10 Appendix).

The second major discovery was an until now unknown aglycon which was found in 5 different crocetin glycosides. This new chain-shortened C₁₇ apocarotenoid aglycon was termed “norcrocetin”. This could be identified by CID (MS²) and full scan MS. A detection of a 40 Da shift of the sodiated molecule and a number of structure characteristic fragment ions were observed.

In the second part of this work a first attempt to locate the crocins on the surface of dried saffron stigmas was made by positive ion MALDI-MS. For that purpose two different matrix solutions using DHB and THAP matrix were used with spray deposition and the experiments were performed on two different instruments, from different vendors (different λ , pulse rate and resolving power). The only crocetin glycosides that could be detected in imaging experiment were those with two (found m/z 675.3, theoretical m/z 675.26, $\Delta m = 0.04$), three (found m/z 837.3, theoretical m/z 837.32, $\Delta m = 0.02$), and four (found m/z 999.4, theoretical m/z 999.37, $\Delta m = 0.03$), glucose unit. Other glycosides could not be detected

because of the very low abundances of these species at the surface of the investigated stigmas.

It could be shown that the choice of matrix had a large influence on the IMS results. On the stigmas surface which were covered with the matrix solution containing THAP matrix almost no crocins were detectable when the UltrafleXtreme was used. The Axima TOF² delivered better but not satisfying results. Far better results with both instruments were obtained in the case of the DHB matrix and therefore this matrix is the MALDI matrix of choice with the applied deposition technique.

Nevertheless the location of crocetin glycosides was different on every stigma (15 successful MS images were generated under identical experimental conditions) regardless of the matrix that was used and because of this a general fixed location of crocins could not be determined. This might indicate that there is no special localization of certain crocin molecules, i.e. a homogenous crocin distribution is given at the stigma surface.

The reason for that might be also that the used method for matrix application did not allow a very homogenous coverage of the surface. Besides the matrix application method the surface of the stigmas also plays an enormous role in the imaging results. The uneven surfaces of the stigmas lead to inhomogeneous matrix coverage. This was confirmed during the EM measurements which showed that the deposition of matrix solution formed a large number of small island like parts leaving the in between surface free of matrix solution. As expected the deposited DHB matrix solution covered the stigma surface slightly better than the THAP matrix solution.

Unfortunately the EM measurements did not show any significant difference on the stigmas surface between the stigmas that were stored under vacuum and those stored under atmospheric pressure prior to matrix application. This discovery did not help to understand why the IMS measurements yielded results only in the cases where saffron stigmas were stored under vacuum for 24 hours prior to the matrix application.

Crocus sativus L. dried stigmas used for the measurements in this work were produced in two different countries: India and Greece. Kashmiri Saffron from India was chosen for the

imaging experiments because it has a more flat surface than the Greece one which was used for ESI measurements.

These were the first imaging experiments performed on saffron stigmas and can be considered as a starting point for further investigations using different matrix application systems as for example sublimation of DHB or different matrices as cinnamonic acid derivatives.

5. References

- [1] A. O. Stella, Z. T. Maria; Saffron quality: effect of agricultural practices, processing and storage; *Production Practices and Quality Assessment of Food Crops* 1, 209-260 (2004)
- [2] E. Pittenauer, N. S. Koulakiotis, A. Tsarbopoulos, G. Allmaier; In-chain neutral hydrocarbon loss from crocin apocarotenoid ester glycosides and the crocetin aglycon (*Crocus sativus* L.) by ESI-MS⁽ⁿ⁾ (n=2, 3); *Journal of Mass Spectrometry* 48, 1299-1307 (2013)
- [3] L. Cossignani, E. Urbani, M. S. Simonetti, A. Maurizi, C. Chiesi, F. Blasi; Characterisation of secondary metabolites in saffron from central Italy (Cascia, Umbria); *Food Chemistry* 143, 446-451 (2014)
- [4] D.C. Katariya, N. Nilakshi, G. R. Vijay, M. M. Abhayankar; Detailed profile of *Crocus sativus*; *International Journal of Pharma and Bio Sciences* 2, 530-540 (2011)
- [5] F. Hadizadeh, S. A. Mohajeri, M. Seifi; Extraction and purification of crocin from saffron stigmas employing a simple and efficient crystallization method; *Pakistan Journal of Biological Sciences* 13, 691-698 (2010)
- [6] L. Maggi, M. Carmona, A. M. Sanchez, G. L. Alonso; Saffron flavor: compounds involved, biogenesis and human Perception; *Functional Plant Science and Biotechnology* 4, 44-55 (2010)
- [7] A. V. Negueruela; Saffron; K.V. Peter (Ed.); *Handbook of herbs and spices*; Woodhead Publishing, Cambridge, England, 276-286 (2001)
- [8] R. K. Singla, G. B. Varadaraj; Crocin: an overview; *Indo Global Journal of Pharmaceutical Sciences* 1, 281-286 (2011)
- [9] "Mass Spectrometry Strategies for Structural Analysis of Carbohydrates and Glycoconjugates; Tandem Mass Spectrometry-Molecular Characterization"; Retrieved 18.06.2015 <http://www.intechopen.com/books/tandem-mass-spectrometry-molecular-characterization/mass-spectrometry-strategies-for-structural-analysis-of-carbohydrates-and-glycoconjugates>
- [10] B. Domon, C. E. Costello; A systematic nomenclature for carbohydrate fragmentations in FAB-MS/MS spectra of glycoconjugates; *Glycoconjugate Journal* 5, 397-409 (1988)

- [11] S. Akhondzadeh, N. Tahmacebi-Pour, A.A Noorbala, H. Amini, H. Fallah-Pour, A.H. Jamshidi, M. Khani; *Crocus sativus* L. in the treatment of mild to moderate depression: a double-blind, randomized and placebo-controlled trial; *Phytother Research* 19, 148-51 (2005)
- [12] G. G. William, G. Reed, A. Ray, S. Anant, A. Dhar; Crocetin: an agent derived from saffron for prevention and therapy for cancer; *Current Pharmaceutical Biotechnology* 13, 173-179 (2012)
- [13] R. N. Rambaran, L. C. Serpell; Amyloid fibrils: abnormal protein assembly; *Prion* 2, 112-117 (2008)
- [14] A. Ghahghaei, S. Z. Bathaie, E. Bahraminejad; Mechanism of the effect of crocin on aggregation and deposition of A β 1-40 fibrils in Alzheimer's disease; *International Journal of Peptide Research and Therapeutics* 18, 347-351 (2012)
- [15] Talaga Group; "Single molecule fluorescence and protein conformational dynamics"; Retrieved 23.12.2014 from <http://talaga.rutgers.edu/research/amyloid.php>
- [16] R. Soares, C. Francoa, E. Piresa, M. Ventosaa, R. Palhinhasa, K. Kocia, A. Martinho de Almeidaa, A. V. Coelho; Mass spectrometry and animal science: Protein identification strategies and particularities of farm animal species, *Journal of Proteomics* 75, 4190-4206 (2012)
- [17] F. Hillenkamp, M. Karas; The MALDI process and method; F. Hillenkamp, J. Peter-Katalinic (Ed.); *MALDI MS: a practical guide to Instrumentation, methods and applications*; Wiley-VCH, Weinheim, Germany, 1-21 (2007)
- [18] S.S. Rubakhin, J.C. Jurchen, E.B. Monroe, J.V. Sweedler; Imaging mass spectrometry: fundamentals and applications to drug discovery; *Drug Discovery Today* 10, 823-837 (2006)
- [19] A. R. Moraga, O. Ahrazem, J. L. Rambla, A. Granell, L. G. Gomez; Crocins with high levels of sugar conjugation contribute to the yellow colours of early-spring flowering crocus tepals; *PLoS One* 8, e71946 (2013)
- [20] Á. Somogyi; Mass spectrometry instrumentation and techniques; K. Vékey, A. Telekes, A. Vertes (Ed.); *Medical applications of mass spectrometry*; Elsevier, Amsterdam, Netherlands, 111-115 (2008)
- [21] F. Lottspeich, J. W. Engels; *Bioanalytik*; Springer Spektrum, Berlin, Heidelberg, Germany, 330-367 (2012)

- [22] M. Wilm; Principles of electrospray ionization; *Molecular & Cellular Proteomics* 10, 1-8 (2011)
- [23] "Summary of the characteristics of different mass analyzers"; Retrieved 23.12.2014 from <http://www.research.uky.edu/core/massspec/jeolanalyzers.pdf>
- [24] E. de Hoffmann, V. Stroobant; *Mass Spectrometry: principles and applications*; Wiley, Chichester, England, 85-199 (2007)
- [25] J. T. Watson and O. D. Sparkman; *Introduction to mass spectrometry instrumentation, applications and strategies for data interpretation*; Chichester, England, Wiley, 73-74 (2007)
- [26] G. Hopfgartner; Overview of the various types of mass spectrometers that are used in drug discovery and drug development; W. A. Korfmacher (Ed.); *Mass spectrometry for drug discovery and drug development*; Wiley, New Jersey, USA, 1-28 (2013)
- [27] M.E. Bier; Coupling ESI and MALDI sources to the quadrupole mass filter, quadrupole ion trap, linear quadrupole ion trap, and orbitrap mass analyzers; C. B. Richard; *Electrospray and MALDI mass spectrometry: Fundamentals, instrumentation, practicalities, and biological applications*; Wiley, New Jersey, USA, 265-331 (2010)
- [28] G. Hart-Smith, S. J. Blanksby; *Mass Analysis*; B. K. Christopher, T. Gruending, J. Falkenhagen, S. Weidner (Ed.); *Mass spectrometry in polymer chemistry*; Wiley-VCH, Weinheim, Germany, 17-31 (2012)
- [29] R. Nieckarz; *Modern mass spectrometry and coupling techniques*; Retrieved 23.12.2014 from http://www.analytik.ethz.ch/vorlesungen/modernMS/Analytische_Chemie_III_Nieckarz_Oct_2010.pdf
- [30] J.Grassl, N. L. Taylor, A. H. Millar; Matrix-assisted laser desorption/ionization mass spectrometry imaging and its development for plant protein imaging; *Plant Methods* 7, 1-11 (2011)
- [31] N. Zaima; Application of matrix-assisted laser desorption/ionization imaging mass spectrometry; Retrieved 23.12.2014 from <http://www.intechopen.com/books/pharmacology/application-of-matrix-assisted-laser-desorption-ionization-imaging-mass-spectrometry-for-pharmacolog>
- [32] "Basics of LC/MS"; Retrieved 23.12.2014 from <http://ccc.chem.pitt.edu/wipf/Agilent%20LC-MS%20primer.pdf>

- [33] "The theory of HPLC"; Retrieved 23.12.2014 from <http://www.chromacademy.com/>
- [34] M. C. McMaster; LC/MS: a practical user's guide; Wiley-Interscience, New Jersey, USA, 1-71 (2005)
- [35] "Electron Multipliers for Mass Spectrometry"; Retrieved 23.12.2014 from <https://www.chromspec.com/pdf/e/rk123.pdf>
- [36] "New drug could improve the learning ability of individuals with Down syndrome"; Retrieved 23.12.2014 from <http://www.gate2biotech.com/new-drug-could-improve-the-learning-ability-of-individuals-with-down-syndrome-1/>
- [37] "Time-of-Flight Mass Analyzers"; Retrieved 29.01.2015 from http://courses.chem.indiana.edu/c613/Time-of-Flight_Mass_Analyzers.ppt
- [38] "BioMap"; Retrieved 29.01.2015 from http://www.maldi-msi.org/index.php?option=com_content&task=view&id=14&Itemid=39
- [39] P. B. O'Connor, F. Hillenkamp; MALDI Mass Spectrometry Instrumentation; F. Hillenkamp, J. Peter-Katalinic (Ed.); MALDI MS: a practical guide to Instrumentation, methods and applications; Wiley-VCH, Weinheim, Germany, 49-51 (2007)
- [40] N. S. Koulakiotis, E. Pittenauer, M. Halabalaki, A. Tsarbopoulos, G. Allmaier; Comparison of different tandem mass spectrometric techniques (ESI-IT, ESI- and IP-MALDI-QRTOF and vMALDI-TOF/RTOF) for the analysis of crocins and picrocrocin from the stigmas of *Crocus sativus* L.; Rapid Communications in Mass Spectrometry 26, 670-678 (2012)
- [41] J. T. Watson and O. D. Sparkman; Introduction to mass spectrometry instrumentation, applications and strategies for data interpretation; Wiley, Chichester, England, 177-180 (2007)
- [42] C. M. Mahoney, S. M. Weidner; Surface Analysis and Imaging Techniques; B. K. Christopher, T. Gruending, J. Falkenhagen, S. Weidner (Ed.); Mass spectrometry in polymer chemistry; Wiley-VCH, Weinheim, Germany, 175-208 (2012)
- [43] C. Dass; Fundamentals of Contemporary Mass Spectrometry; Wiley, New Jersey, USA, 67-146 (2007)
- [44] "What is electron microscopy?"; Retrieved 10.06.2015 from https://www.jic.ac.uk/microscopy/intro_EM.html
- [45] "Scanning Electron Microscope"; Retrieved 10.06.2015 from <https://www.purdue.edu/ehps/rem/rs/sem.htm>

- [46] "Electron microscopes"; Retrieved 10.06.2015 from <http://www.explainthatstuff.com/electronmicroscopes.html>
- [47] Bruker Daltonik; Fleximaging 3.0 user manual; Bruker Daltonik, Bremen Germany, 280-285 (2011)
- [48] "Lambley nursery"; Retrieved 05.12.2015 from <http://lambley.com.au/plant/crocus-sativus>

6. Equipment / Instruments / Materials

Ultrasonic cleaner by VWR (Vienna, Austria)

Laboratory centrifuge Mini Star Silverline by VWR (Vienna, Austria)

Bruker Esquire 3000^{plus} 3D-quadrupole ion trap by Bruker Daltonics (Bremen, Germany)

HPLC Hitachi LaChrom Elite (Tokyo, Japan)

Reversed phase XTerra MS C₈ column by Waters (Eschborn, Germany)

UtrafleXtreme TOF/RTOF mass spectrometer by Bruker Daltonik (Bremen, Germany)

Axima TOF² TOF/RTOF mass spectrometer by Shimadzu Kratos Analytical, (Manchester, UK)

Simplicity water purification system by Milipore (Molsheim, France)

Labor vacuum system ILMVAC (Ilmenau, Germany)

ITO glass slides by Delta Technologies (Loveland, Colorado, USA)

MTP slide adapter II by Bruker Daltonik (Bremen, Germany)

Airbrush system by Sparmax (Taiwan)

Saffron (Greece)

Kashmiri Saffron (India)

DHB by Sigma-Aldrich (Steinheim, Germany)

THAP by Sigma-Aldrich (Steinheim, Germany)

Sodium chloride by Merck (Darmstadt, Germany)

Methanol by Merck (Darmstadt, Germany)

Formic acid 98-100% by Merck (Darmstadt, Germany)

7. List of Figures

Figure 1: *Crocus sativus* L. – Saffron, drawn after a photograph from [48]

Figure 2: Saffron stigmas

Figure 3: Chemical structure of bis-gentiobiosyl crocetin $C_{44}H_{64}O_{24}$ (Monoisotopic mass: 976.3787 Da)

Figure 4: *Crocus sativus* solution obtained by extracting 10 saffron stigmas in two ml of H_2O

Figure 5: Formation of the amyloid fibrils, lag and growth phase. Adapted from [15, 36]

Figure 6: Scheme of a mass spectrometer

Figure 7: Illustration of desorption/ionization process using MALDI technique

Figure 8: Illustration of electrospray ionization process, ion formation according to ion evaporation model

Figure 9: Ion formation based on charge residue model (CRM)

Figure 10: Ion formation based on ion evaporation model (IEM)

Figure 11: Definition of mass resolution using full width half maximum definition (FWHM), where Δm is full width of the signal at 50% of the maximum height

Figure 12: Illustration of a linear TOF mass analyzer

Figure 13: Illustration of reflectron TOF mass analyzer (RTOF)

Figure 14: Comparison of MALDI mass spectra obtained in linear mode, linear mode with delayed extraction and reflectron mode with delayed extraction. Figure taken from J. T. Watson and O. D. Sparkman [25]

Figure 15: Illustration of the quadrupole ion trap mass analyzer, cross-section view

Figure 16: Illustration of secondary electron multiplier with (A) discrete dynode and (B) continuous dynode

Figure 17: Illustration of {A} microchannel plates and (B) channel

Figure 18: Illustration of MALDI IMS steps.

Figure 19: Illustration of LC-ESI MS

Figure 21: Saffron stigmas; the upper stigma was produced in India and the lower in the Greece

Figure 22: Saffron extract

Figure 23: Illustration of HPLC mobile phase gradient

Figure 24: Segment of the base peak chromatogram of the full scan LC/ESI MS separation of an aqueous extract of saffron by two different elution solvent systems: acid free solvent gradient (blue) and solvent gradient with 0.05% FA (red). Some peaks are labeled and represent known structures: crocin with 5 glucose units (a), crocin with 4 glucose units (b), crocin with three glucose units (c), crocin with two glucose units (d, e). Other peaks represent crocins with low intensity or unknown structures as well as different unknown compound classes

Figure 25: LC-MS² traces (base peak chromatograms) of the precursor ion m/z value 675.3 (theoretical m/z 675.26, $\Delta m = 0.04$) (isomers of crocetin [C] plus two glucose units), (*) represents other isomers of diglycosylated crocetin as well as in-source fragment ions of higher mass crocins. E stands for trans, Z for cis and the numbers represent the number of glucose units, example: E-1C1 represents trans crocetin with 1 glucose on one side and 1 glucose on the other side of the crocetin C, Z-C2 represents cis crocetin with 2 glucose units on one side of the crocetin

Figure 26: CID mass spectra showing mass spectrometric differences between the two isomeric diglycosylated crocetin bis-glucosyl-crocetin ($R_t = 17.5$ min) (A) and monogentiobiosyl crocetin ($R_t = 22.4$ min) (B)

Figure 27: Elution profile of isomeric hexaglucoylated crocetins (MS² of m/z 1323.5 (theoretical m/z 1323.47, $\Delta m = 0.03$)) (acid free gradient versus gradient with 0.05% formic acid). Green colored retention times represent diglucoyl-tetraglucoyl-crocetin isomers while the purple colored retention times represent the mono-hexaglucoyl-crocetin isomers

Figure 28: LC-ESIMS² mass spectrum of m/z 1323.5 (theoretical m/z 1323.47, $\Delta m = 0.03$) (sodiated species of hexaglucoylated crocetin), showing two different isomers: diglucoyl-tetraglucoyl-crocetin (A) and mono-hexaglucoyl-crocetin (B)

Figure 29: CID MS³ spectrum of the first generation product ion 995.4

Figure 30: Fragmentation pattern of $[M+Na]^+ = 1323.5$ by LC-ESI MS² ; (A) showing fragmentation pattern of diglucoyl-tetraglucoyl-crocetin and (B) of mono-hexaglucoyl-crocetin

Figure 31: Base peak chromatogram of m/z 1161.5 \rightarrow 509.2 (A1); LC-ESI MS³ of m/z 1161.5 \rightarrow 509.2 showing neapolitanose (B1) and gentiotriose (C1) (the A ions result from cross ring cleavages while the B and C ions result from glycosidic bond cleavages)

Figure 32: Chemical structure of norcrocetin, a C₁₇ aglycon

Figure 33: Base peak chromatograms showing the Influence on the retention behavior of crocins depending on the chain length of the aglycon (C₂₀ versus C₁₇); C stands for crocetin and nC for norcrocetin; E stands for trans, Z for cis and the numbers represent the number of glucose units, example: E-1C2 represents trans crocin with 1 glucose units on one side and 2 glucose units on the other side of the crocetin, Z-1nC2 represents cis norcrocin with one glucose unit on one side and 2 glucose units on the other side of the norcrocetin

Figure 34: LC-ESI MS² mass spectrum of triglycosylated crocin m/z 837.3 (theoretical m/z 837.32, $\Delta m = 0.02$) with $R_t = 15.1$ min (A) and triglycosylated crocin m/z 797.2 with $R_t = 15.1$ min 10.6 min (B)

Figure 35: Fragmentation pattern of $[M+Na]^+ = 837.3$ by LC-ESI MS² (A) and fragmentation pattern of $[M+Na]^+ = 797.2$ by LC-ESI MS² (B)

Figure 36: Extracted ion chromatogram of mono-glycosylated crocins differing in chain length from 7 up to 11 glucose units

Figure 37: LC-ESI MS² mass spectrum of m/z 2133.7 (theoretical m/z 2133.74, $\Delta m = 0.04$) (where B represents the glucose and the subscript represents the number of the glucose units)

Figure 38: Saffron stigmas covered with different matrix solutions: (A) 40 mg/ml in H₂O:MeOH (1:1, v/v) doped with NaCl, spray volume 2 ml, (B) 40 mg/ml in H₂O:MeOH (1:1, v/v) doped with NaCl, spray volume 10 ml, (C) 200 mg/ml in H₂O:MeOH (1:1, v/v) doped with NaCl, spray volume 5 ml, (D) 200 mg/ml in H₂O:MeOH (1:4, v/v) doped with NaCl, spray volume 5 ml

Figure 39: Saffron stigmas covered with different matrix solutions: (A) 40 mg THAP in MeOH doped with NaCl, spray volume 2 ml, (B) 64 mg THAP in MeOH doped with NaCl, spray volume 2.5 ml, (C) 50 mg THAP in MeOH doped with NaCl, spray volume 5 ml

Figure 40: Imaging experiment with the UltrafleXtreme using DHB matrix showing stigma A with different m/z values

Figure 41: Imaging experiment with the UltrafleXtreme using DHB matrix showing stigma B with different m/z values

Figure 42: Imaging experiment with the UltrafleXtreme using DHB matrix showing stigma C with different m/z values

Figure 43: Imaging experiment with the UltrafleXtreme using THAP matrix showing stigma A with different m/z values

Figure 44: Imaging experiment with the UltrafleXtreme using THAP matrix showing crocins with four glucose units of the stigma B

Figure 45: Imaging experiments with the AXIMA TOF² using DHB matrix showing distribution of crocins with four glucose units of stigma A

Figure 46: Imaging experiments with the AXIMA TOF² using DHB matrix showing distribution of crocins with three glucose units of stigma A

Figure 47: Imaging experiments with the AXIMA TOF² using DHB matrix showing distribution of crocins with two glucose units of stigma A

Figure 48: Imaging experiments with the AXIMA TOF² using DHB matrix showing distribution of crocins with four glucose units of stigma B

Figure 49: Imaging experiments with the AXIMA TOF² using DHB matrix showing distribution of crocins with three glucose units of stigma B

Figure 50: Imaging experiments with the AXIMA TOF² using DHB matrix showing distribution of crocins with two glucose units of stigma B

Figure 51: Imaging experiments with the AXIMA TOF² using THAP matrix showing distribution of crocins with four glucose units of stigma A

Figure 52: Imaging experiments with the AXIMA TOF² using THAP matrix showing distribution of crocins with four glucose units of stigma B

Figure 53: Electron Microscopy images of two saffron stigmas which were prepared according to the first approach: the left part was stored under atmospheric pressure and the right part in vacuum

Figure 54: Electron Microscopy images of four saffron stigmas prepared according to second approach: stigmas 3 and 4 were sprayed with DHB and 5 and 6 with THAP matrix solution; the stigmas were stored under atmospheric pressure

Figure 55: Electron Microscopy images of one saffron stigma (stigma 8), prepared according to third approach: left part was sprayed with DHB and the right with THAP matrix solution; the stigma was stored under vacuum before matrix application

8. List of tables

Table 1: Chemical structure of the most important saffron components

Table 2: Chemical structure of the aglycon and oligosaccharide portions described so far [2]

Table 3: Saffron stigmas origin and their use for the MS measurements in this work

Table 4: HPLC settings used for the separation of saffron solution

Table 5: Values of the gradient flow used in HPLC

Table 6: ESI parameters used for the separation of saffron analytes

Table 7: ESI Manual MSⁿ parameters used for the separation of saffron analytes

Table 8: Calculated monoisotopic mass values of crocetin ester glycosides

Table 9: Composition of matrix solution 1 and 2

Table 10: flexImaging and AutoXecute method settings

Table 11: FlexImaging settings

Table 12: Axima TOF² acquisition-firing window settings. Regular raster defines the regularly spaced distribution of fired shots around the raster center. Raster style determines the direction of the raster

Table 13: Electron microscope settings

Table 14: List of crocin derivatives with the new aglycon norcrocetin

Table 15: List of fragment ions from precursor ion m/z 837.30 and m/z 797.20

Table 16: List of performed MS² and MS³ measurements of crocins with norcrocetin aglycon

Table 17: Fragmentation pattern of crocins with norcrocetin aglycon

Table 18: List of performed MS² and MS³ measurements of crocins with crocetin aglycon

Table 19: Fragmentation pattern of crocins with crocetin aglycon

Table 20: m/z values of different crocetin glycosides obtained with UltrafleXtreme and DHB matrix solution

Table 21: m/z values of different crocetin glycosides obtained with UltrafleXtreme and THAP matrix solution

Table 22: m/z values of different crocetin glycosides obtained with Axima TOF² and DHB matrix solution

Table 23: m/z values of crocins with 4 glucose of stigma A and B obtained with Axima TOF² and THAP matrix solution

9. List of abbreviations

C	Crocetin
CI	Chemical ionization
CID	Collision induced dissociation
DESI	Desorption electrospray ionization
DHB	2,5-dihydroxy benzoic acid
E	Trans
EI	Electron impact
EM	Electron microscope
ESI	Electrospray ionization
FWHM	Full width half maximum
GB	Gentiobiose
HPLC	High-performance liquid chromatography
IMS	Imaging mass spectrometry
ITO	Indium tin oxide
LC	Liquid chromatography
LIT	Linear ion trap
MALDI	Matrix assisted laser desorption/ionization
MS	Mass spectrometry
nC	Norcrocetin
nESI	Nano Electrospray ionization

QIT	Quadrupole ion trap
RP	Reversed phase
R _t	Retention time
RTOF	Reflectron time of flight
SEM	Secondary electron multiplier
THAP	2,4,6-trihydroxyacetophenone
TOF	Time-of-flight
Z	Cis

10. Appendix

10.1 Mass spectra of identified crocins containing crocetin aglycon

In the Figures 56-70 base peak chromatograms (BPC) with corresponding MS² and MS³ spectra of the found crocetin glycosides with the standard C₂₀ crocetin aglycon are given. C represents abbreviation of crocetin and the numbers on the left and right side of C represent the number of glucose units. For better understanding of the BPC and MS spectra, different colors were used to describe different crocin isomers. Peaks which represent the same isomers are labeled with the same color.

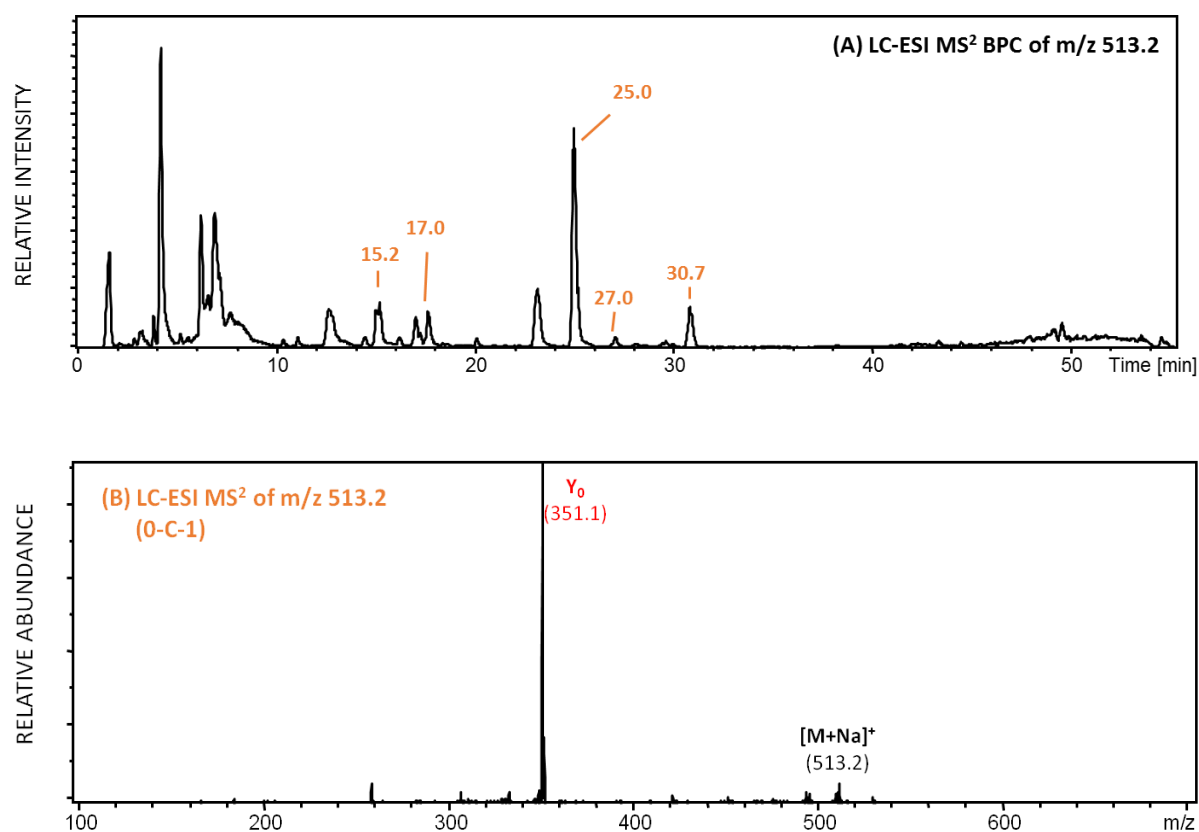


Figure 56: Base peak chromatogram of m/z 513 (theoretical m/z 513.21, $\Delta m = 0.21$) (A); LC-ESI MS² of m/z 513 (theoretical m/z 513.21, $\Delta m = 0.21$) (B)

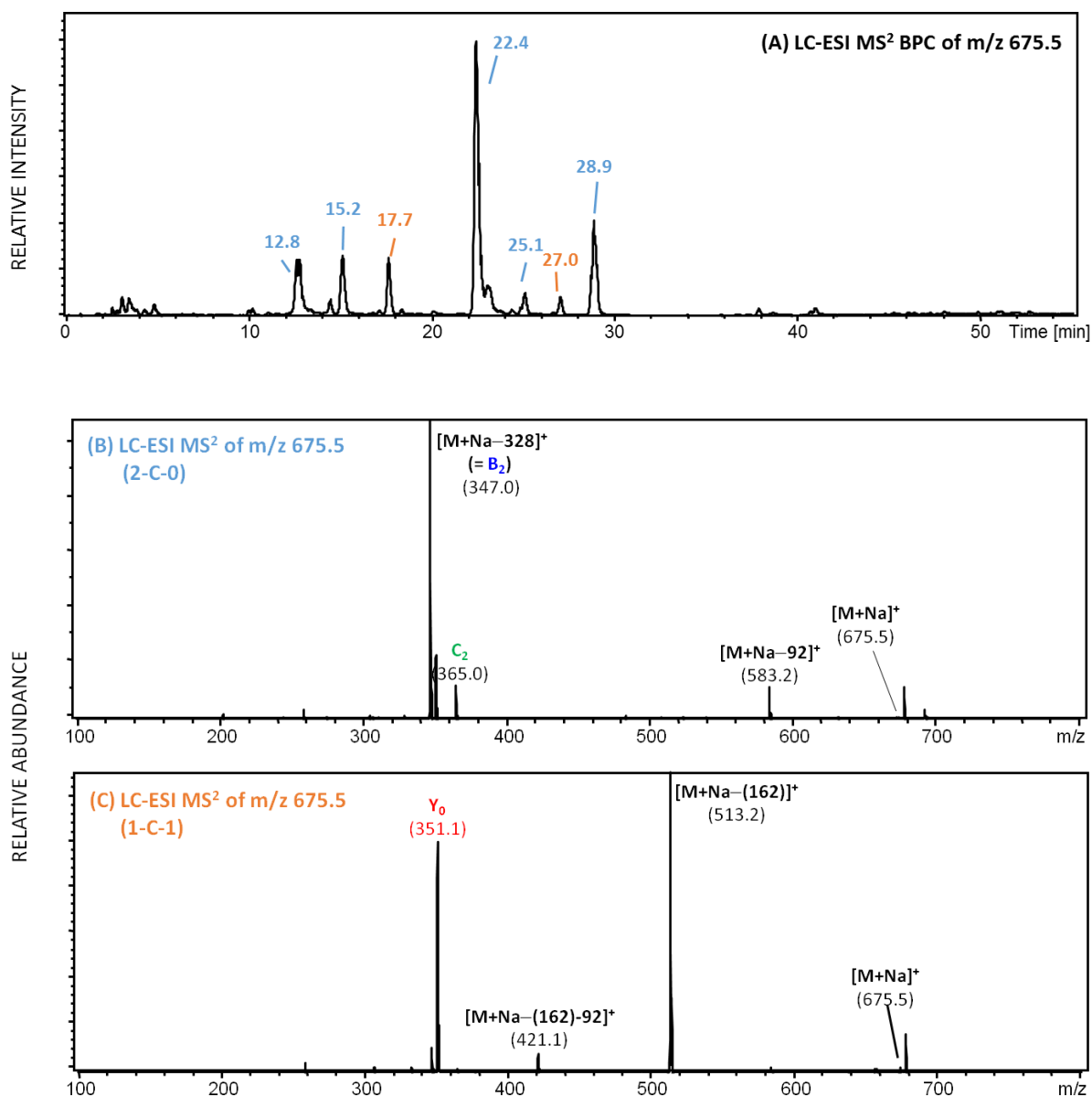


Figure 57: Base peak chromatogram of m/z 675.5 (theoretical m/z 675.26, $\Delta m = 0.24$) (A); LC-ESI MS² of m/z 675.5 (theoretical m/z 675.26, $\Delta m = 0.24$) showing two different isomers (B) and (C)

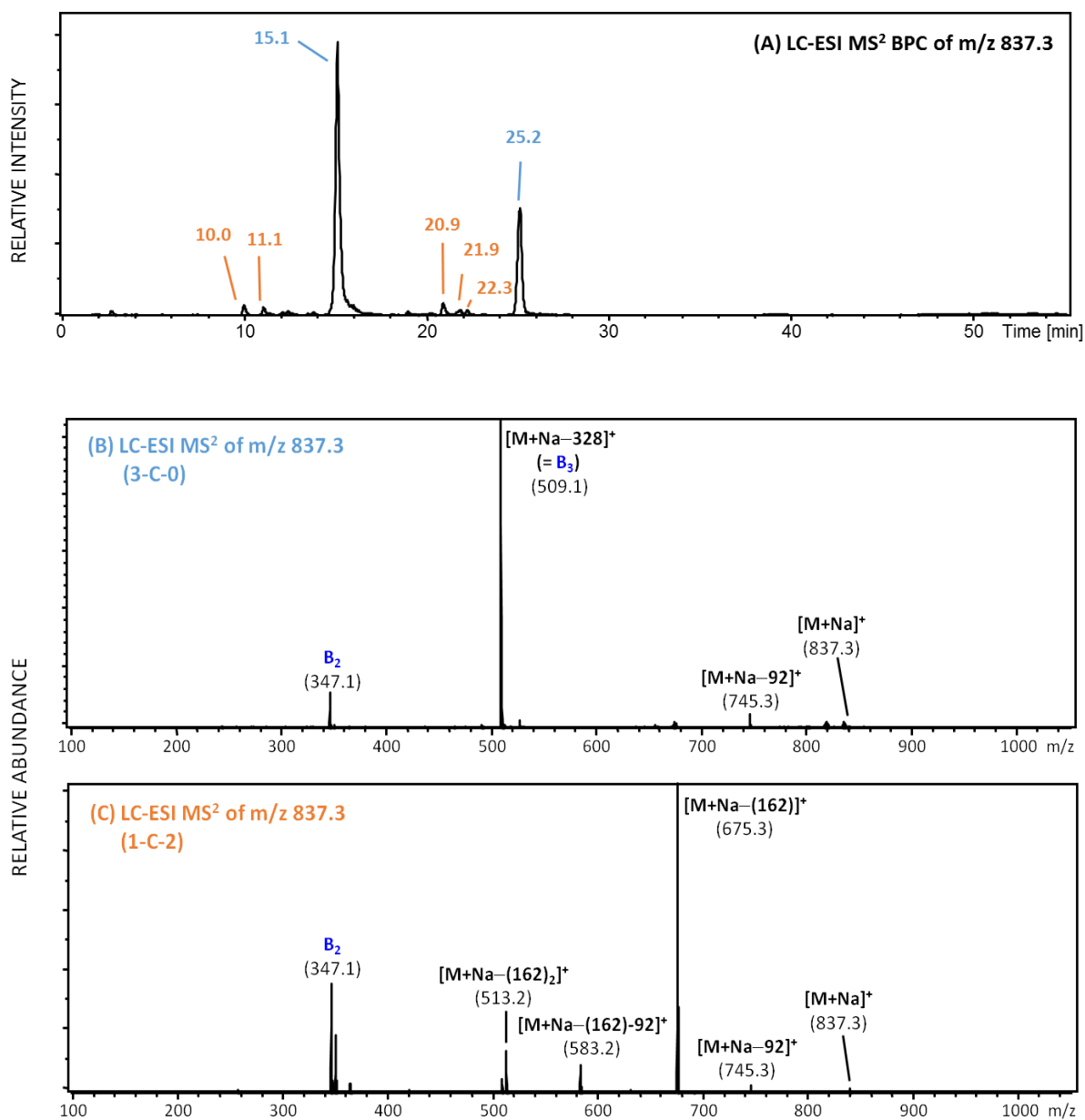


Figure 58: Base peak chromatogram of m/z 837.3 (theoretical m/z 873.32, $\Delta m = 0.02$) (A); LC-ESI MS² of m/z 837.3 (theoretical m/z 573.32, $\Delta m = 0.02$) showing two different isomers (B) and (C)

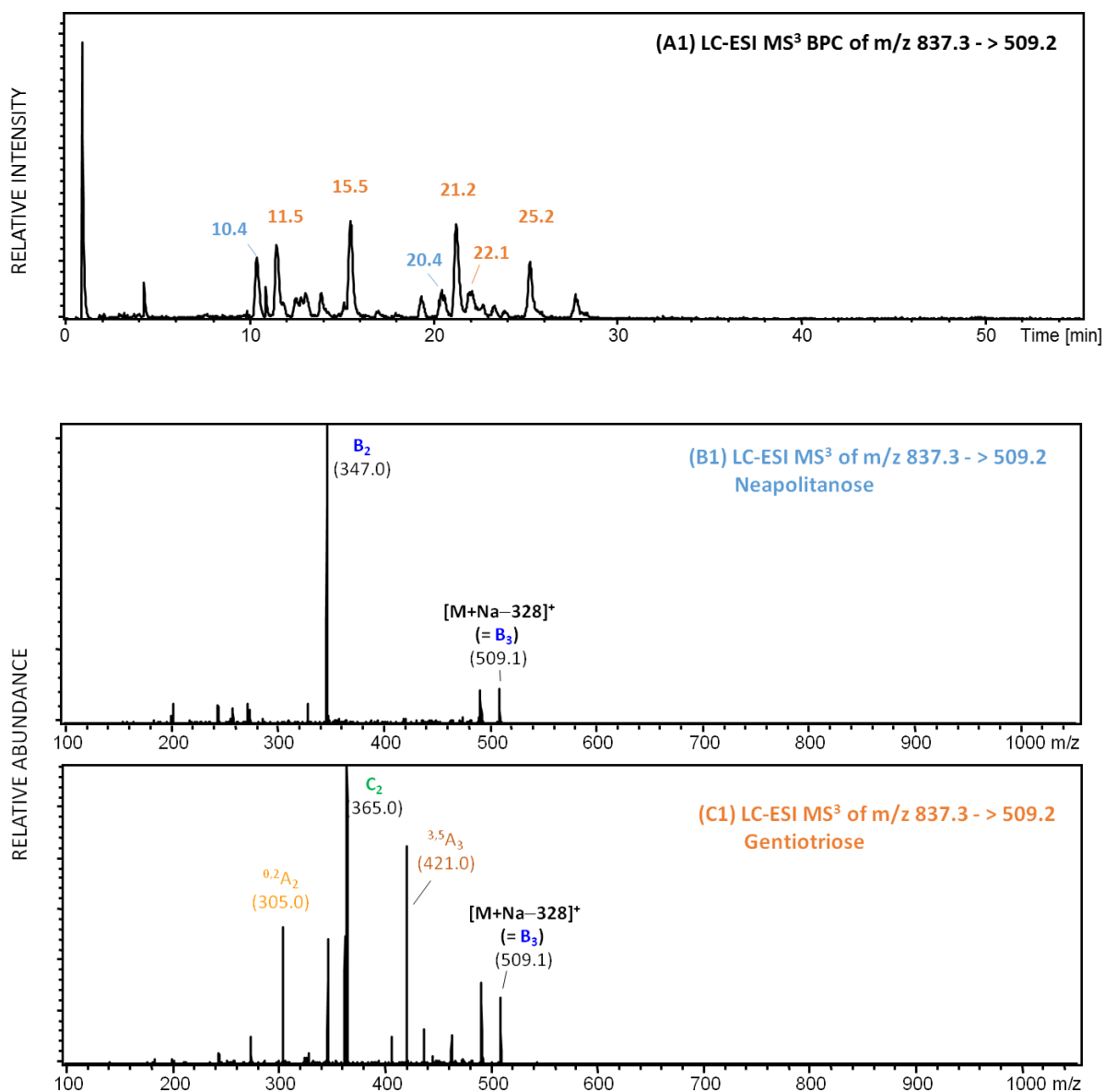


Figure 59: Base peak chromatogram of m/z 837 -> 509 (A1); LC-ESI MS³ of m/z 837 -> 509.2 showing two different isomers (B1) and (C1)

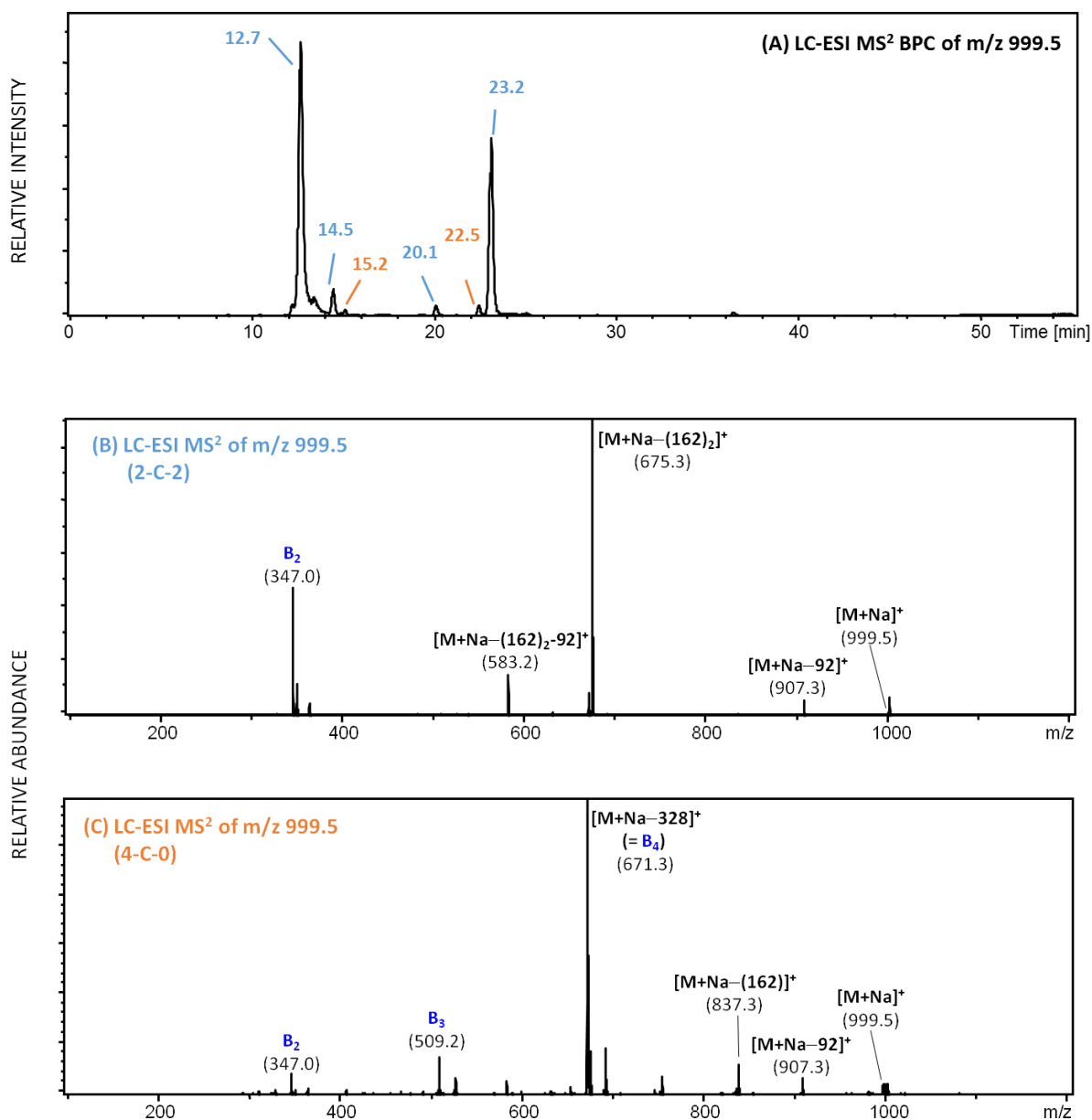


Figure 60: Base peak chromatogram of m/z 999.5 (theoretical m/z 999.37, $\Delta m = 0.13$) (A); LC-ESI MS² of m/z 999.5 (theoretical m/z 999.37, $\Delta m = 0.13$) showing two different isomers (B) and (C)

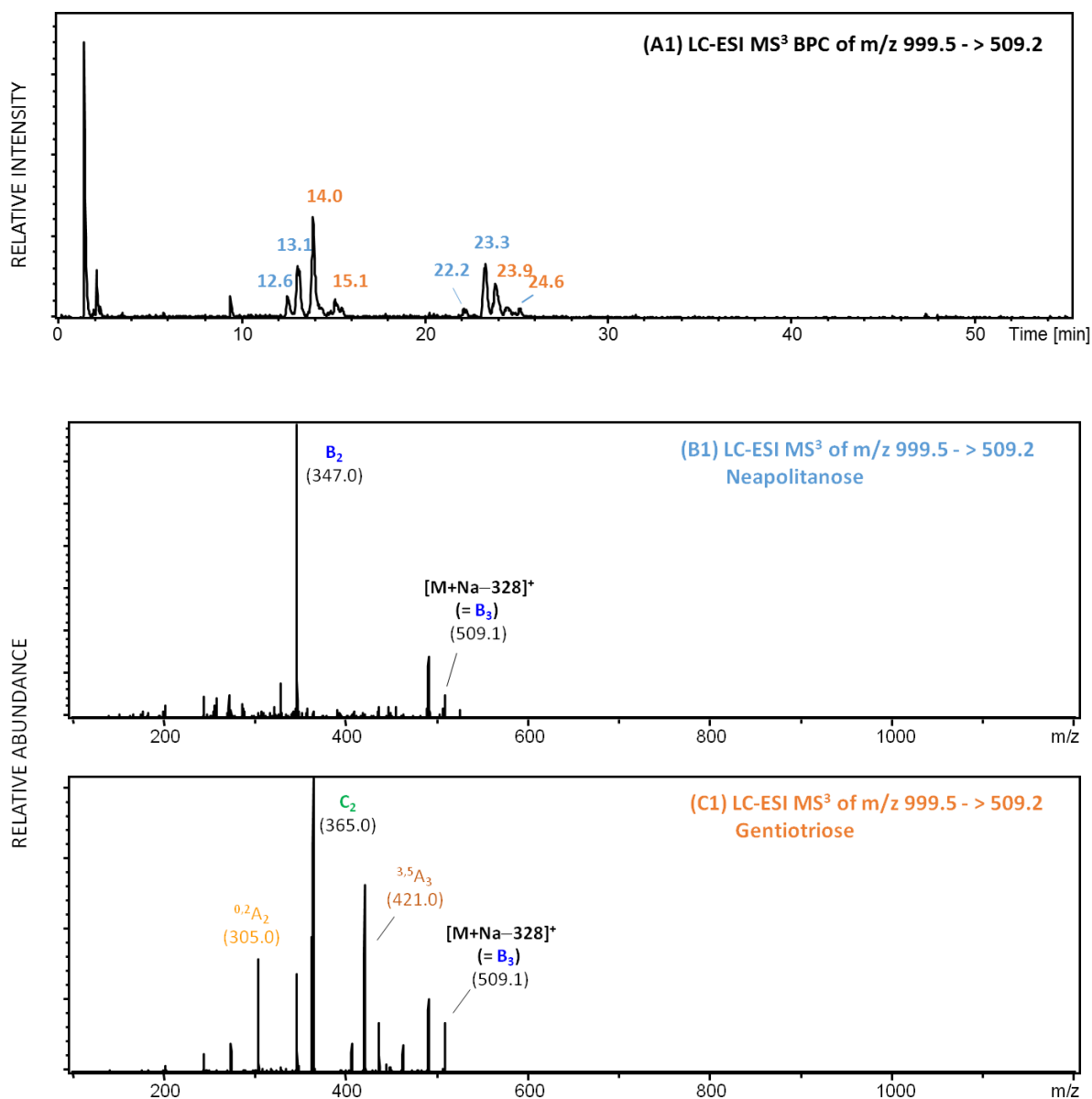


Figure 61: Base peak chromatogram of m/z 999.5 -> 509.2 (A1); LC-ESI MS³ of m/z 999.5 -> 509.2 showing two different isomers (B1) and (C1)

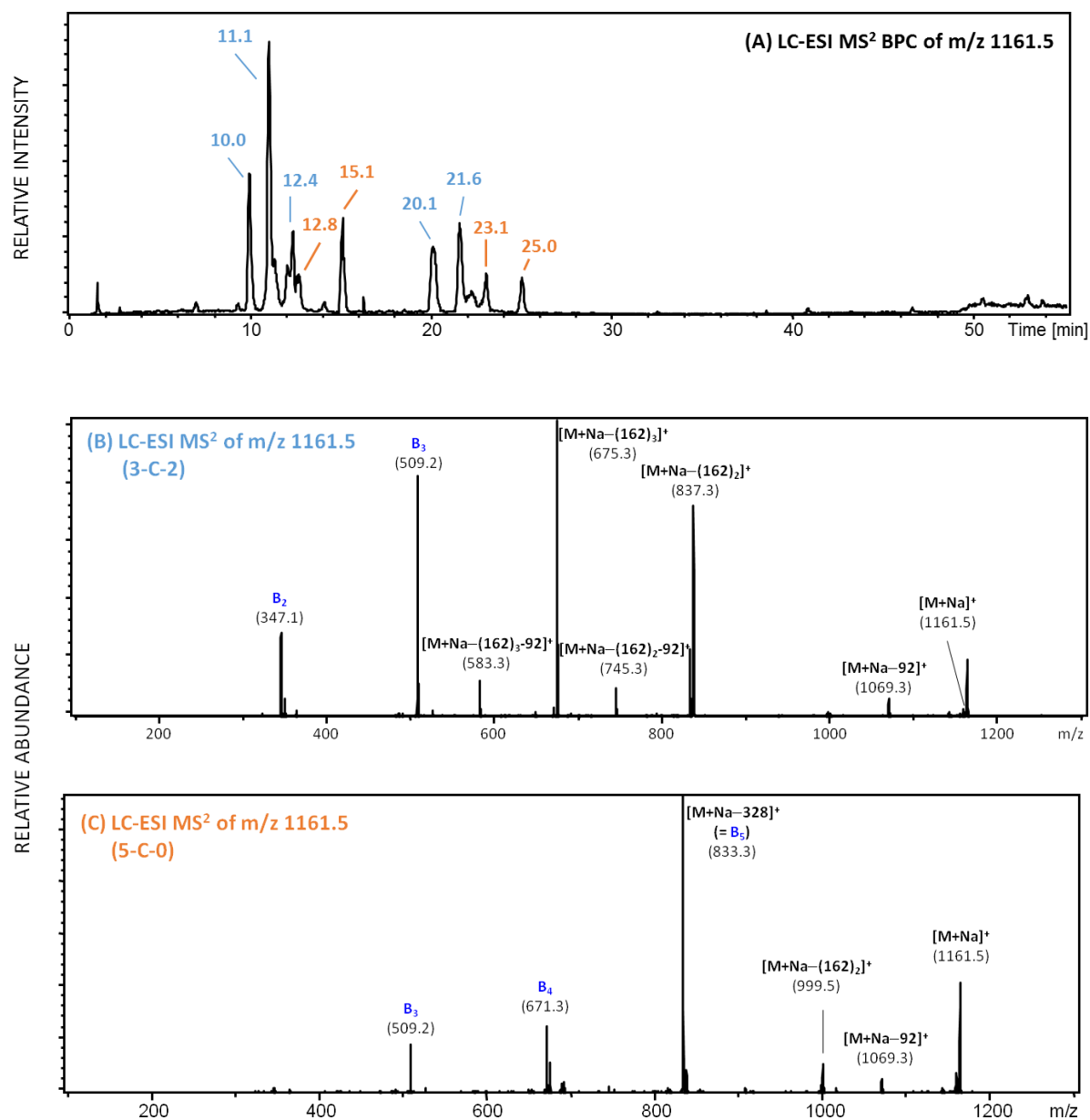


Figure 62: Base peak chromatogram of m/z 1161.5 (theoretical m/z 1161.42, $\Delta m = 0.08$) (A); LC-ESI MS² of m/z 1161.5 (theoretical m/z 1161.42, $\Delta m = 0.08$) showing two different isomers (B) and (C)

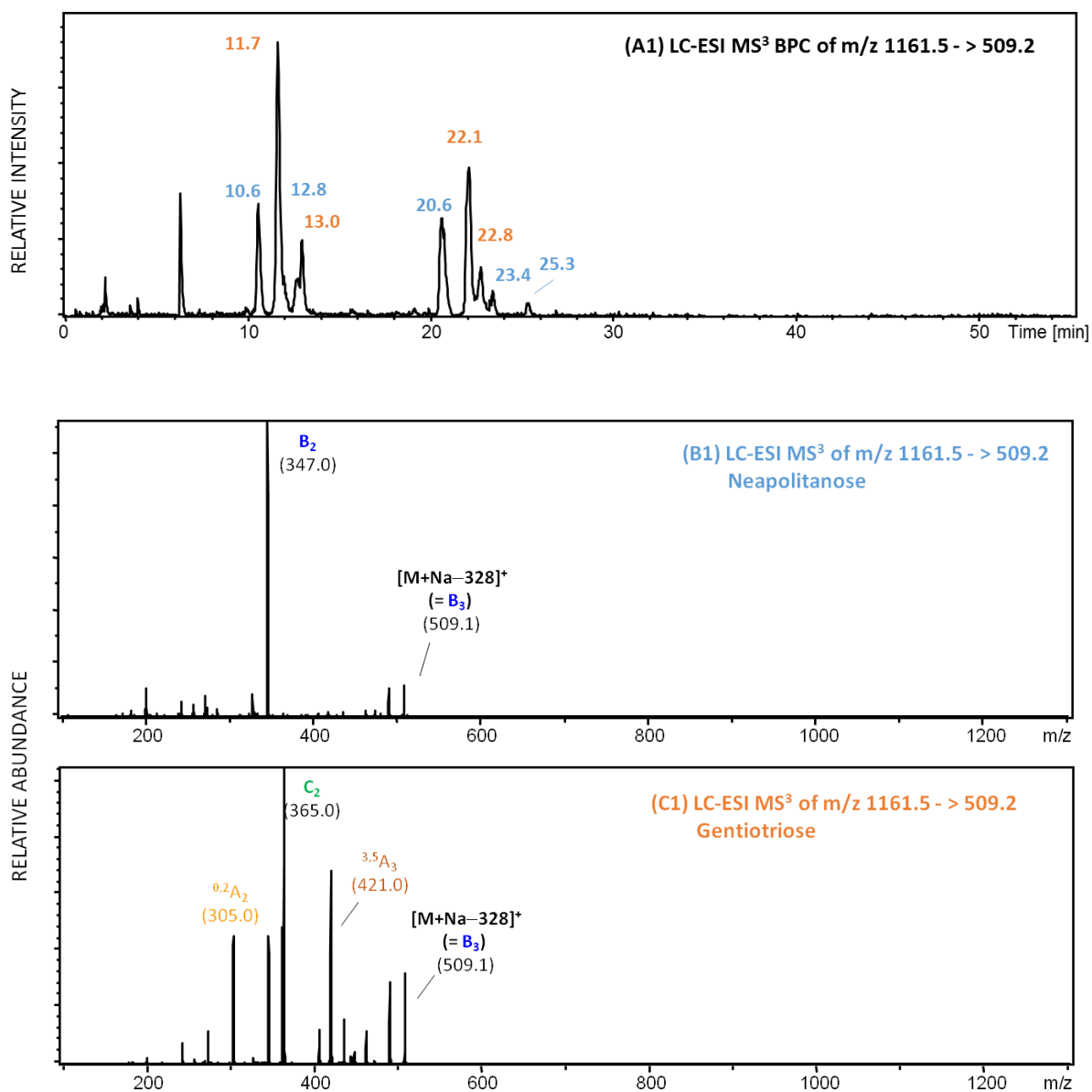


Figure 63: Base peak chromatogram of m/z 1161.5 -> 509.2 (A1); LC-ESI MS³ of m/z 1161.5 -> 509.2 showing two different isomers (B1) and (C1)

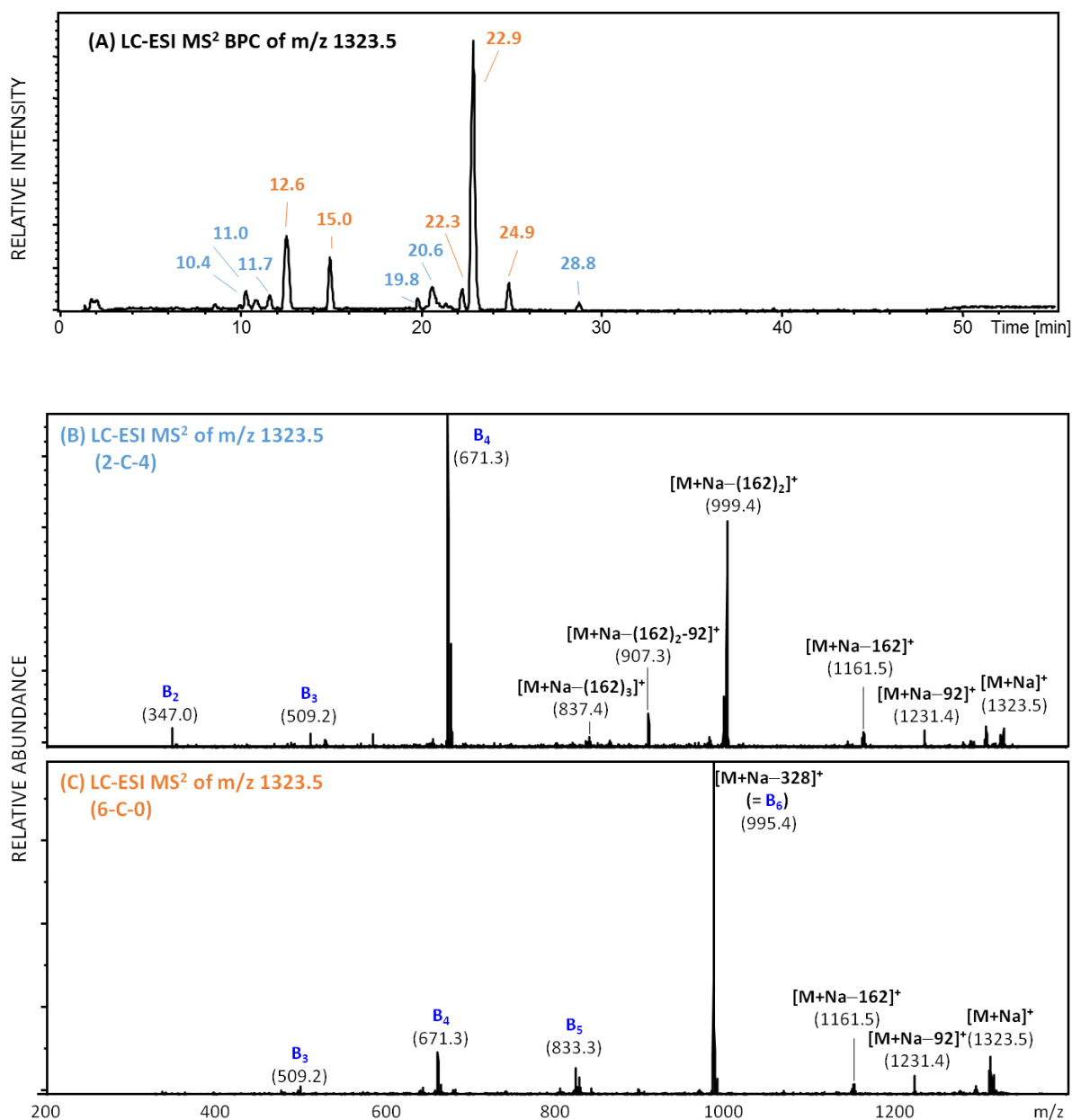


Figure 64: Base peak chromatogram of m/z 1323.5 (theoretical m/z 1323.47, $\Delta m = 0.03$) (A); LC-ESI MS² of m/z 1323.5 (theoretical m/z 1323.47, $\Delta m = 0.03$) showing two different isomers (B) and (C)

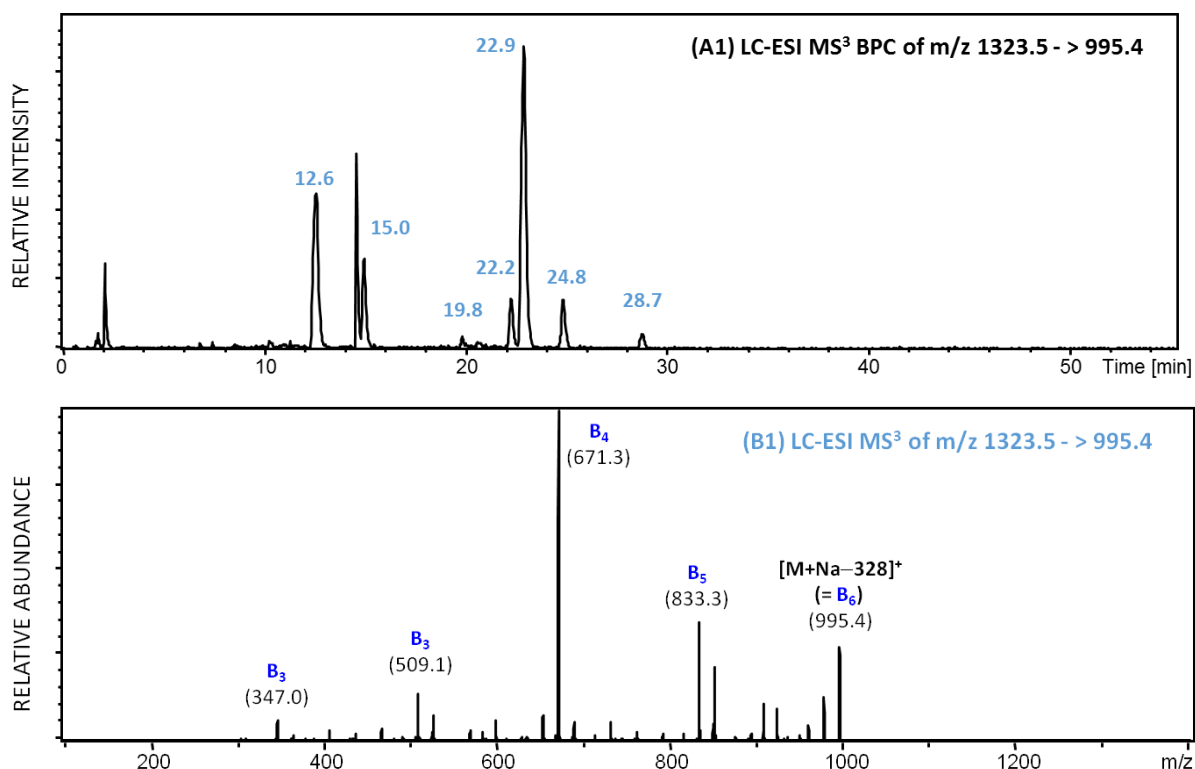


Figure 65: Base peak chromatogram of 1323.5 -> 995.4 (A1); LC-ESI MS³ of m/z 1323.5 -> 995.4 (B1)

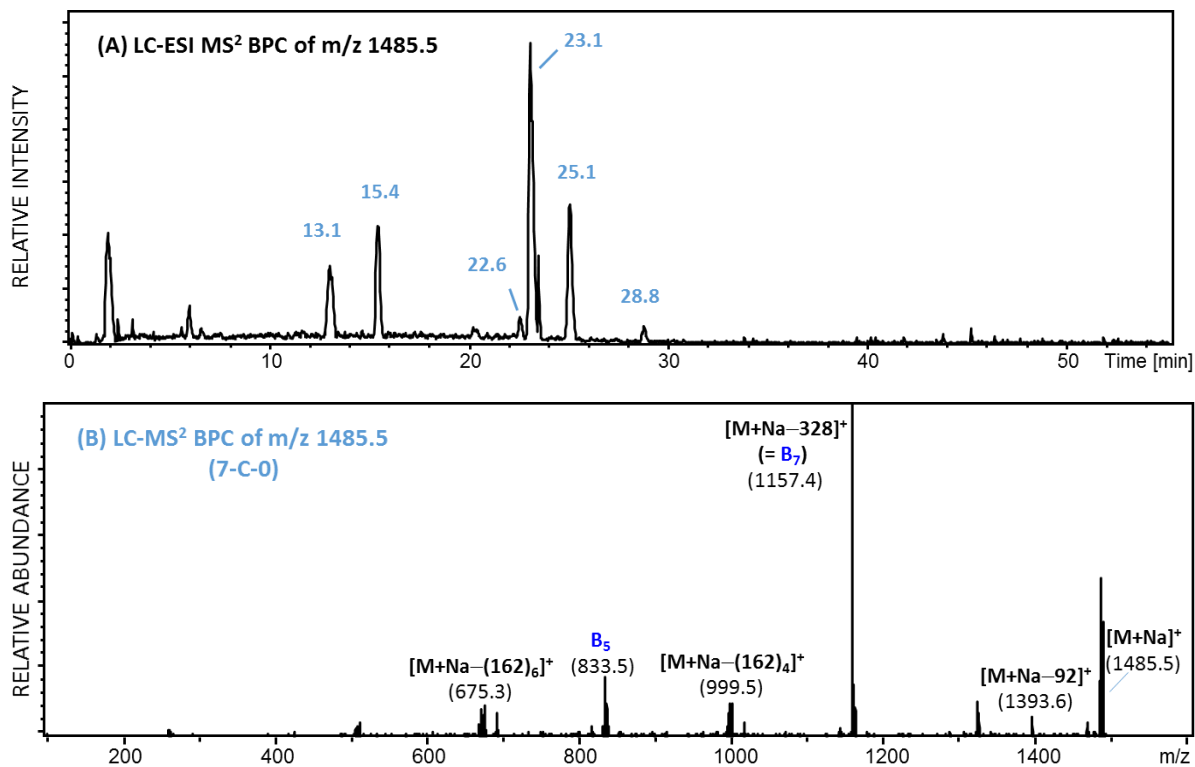


Figure 66: Base peak chromatogram of m/z 1485.5 (theoretical m/z 1485.53, $\Delta m = 0.03$) (A); LC-ESI MS² of m/z 1483.5 (theoretical m/z 1485.53, $\Delta m = 0.03$) (B)

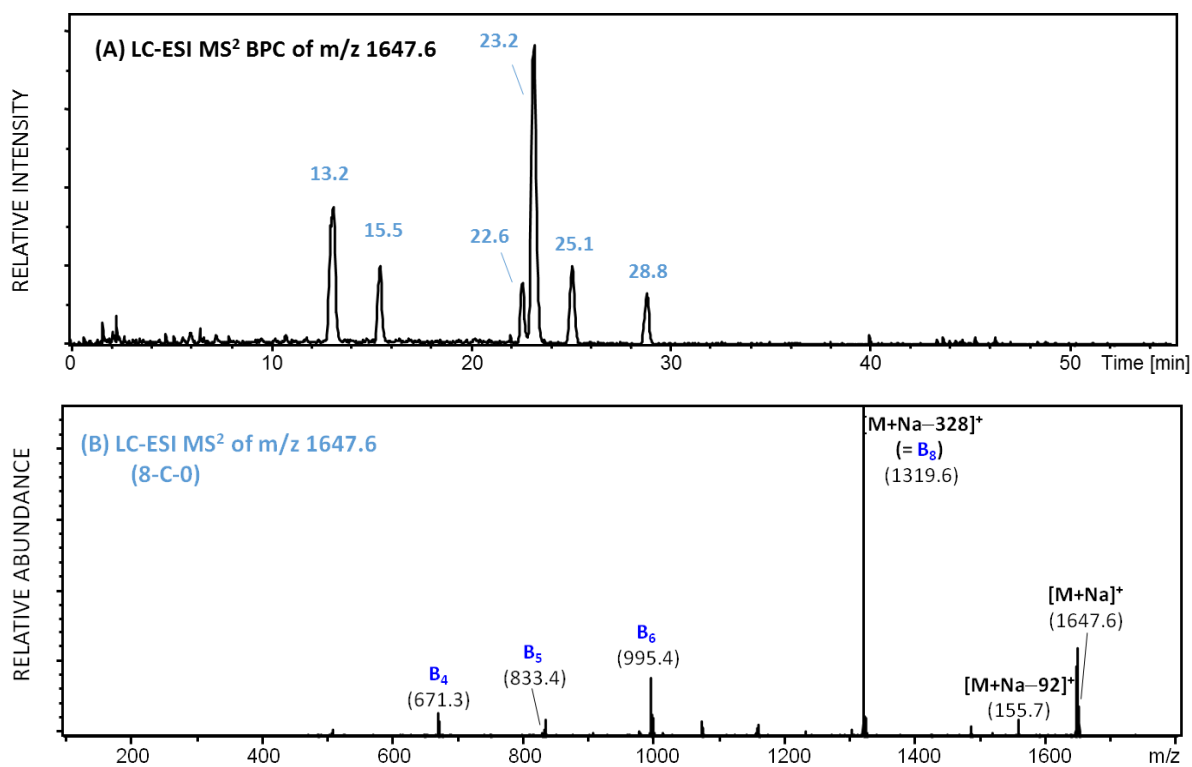


Figure 67: Base peak chromatogram of m/z 1647.6 (theoretical m/z 1647.58, $\Delta m = 0.02$) (A); LC-ESI MS² of m/z 1647.6 (theoretical m/z 1647.58, $\Delta m = 0.02$) (B)

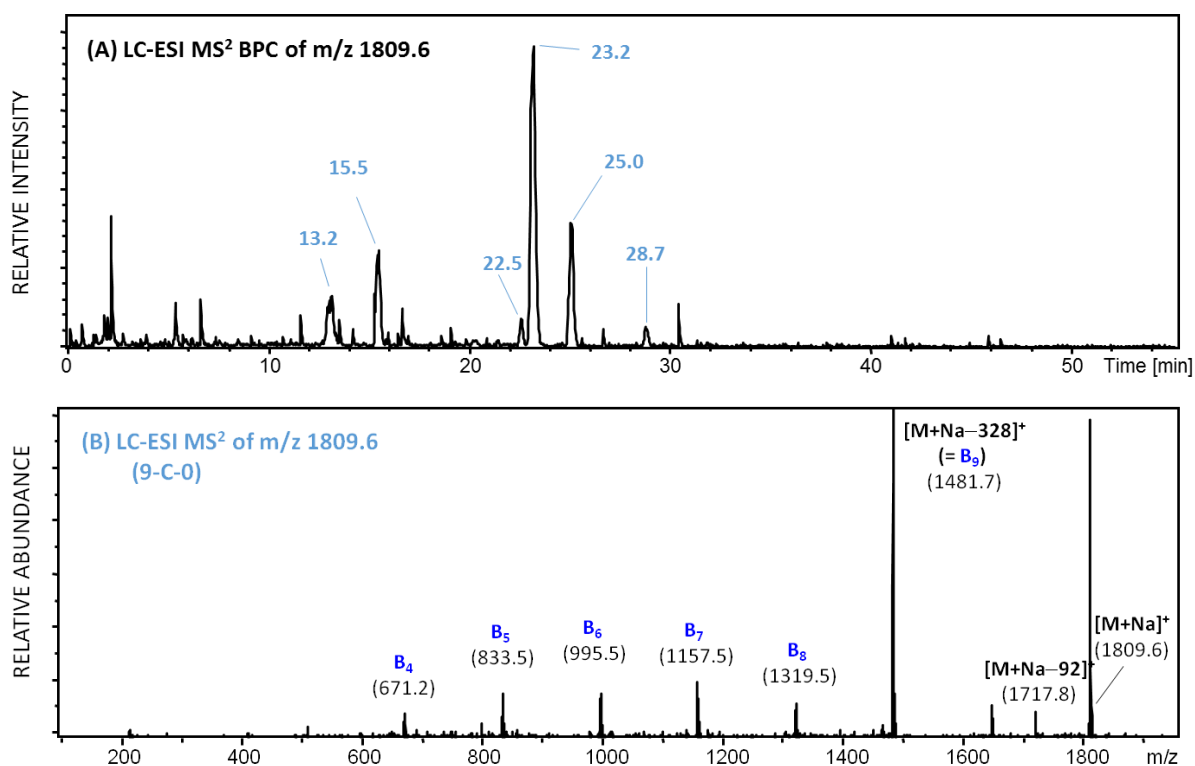


Figure 68: Base peak chromatogram of m/z 1809.6 (theoretical m/z 1809.63, $\Delta m = 0.03$) (A); LC-ESI MS² of m/z 1809.6 (theoretical m/z 1809.63, $\Delta m = 0.03$) (B)

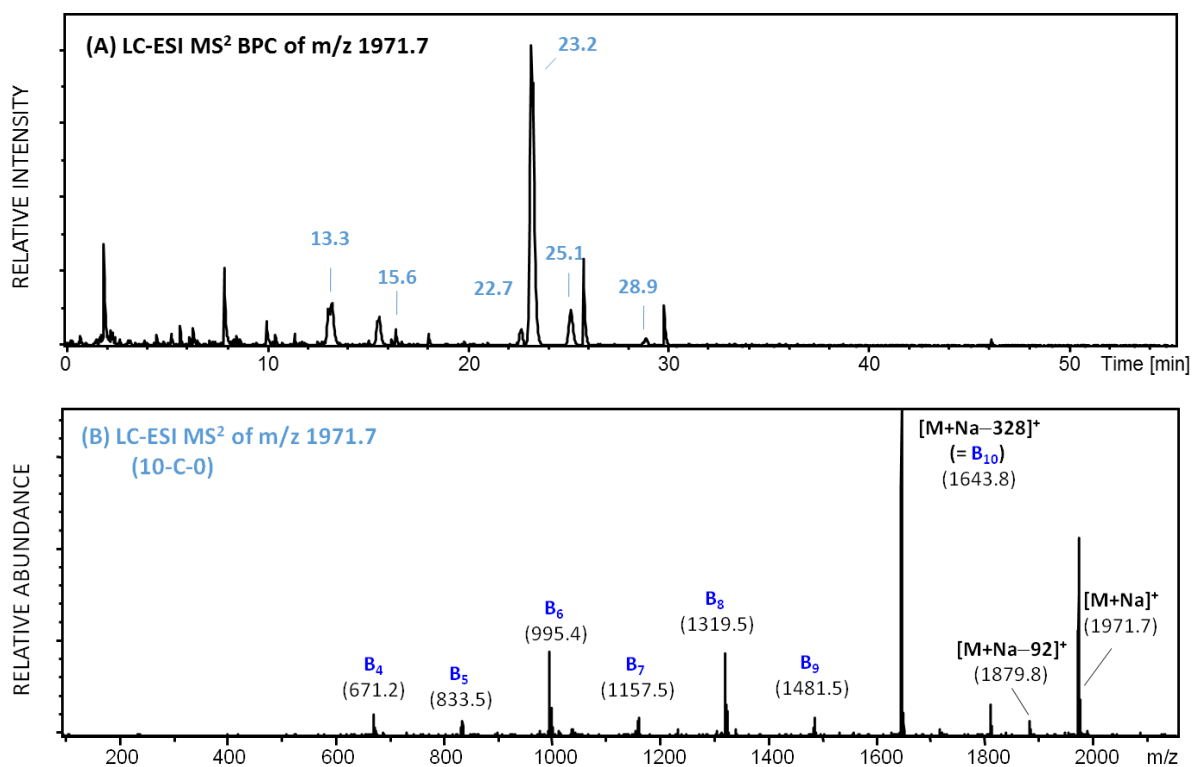


Figure 69: Base peak chromatogram of m/z 1971.7 (theoretical m/z 1971.69, $\Delta m = 0.01$) (A); LC-ESI MS² of m/z 1971.7 (theoretical m/z 1971.69, $\Delta m = 0.01$) (B)

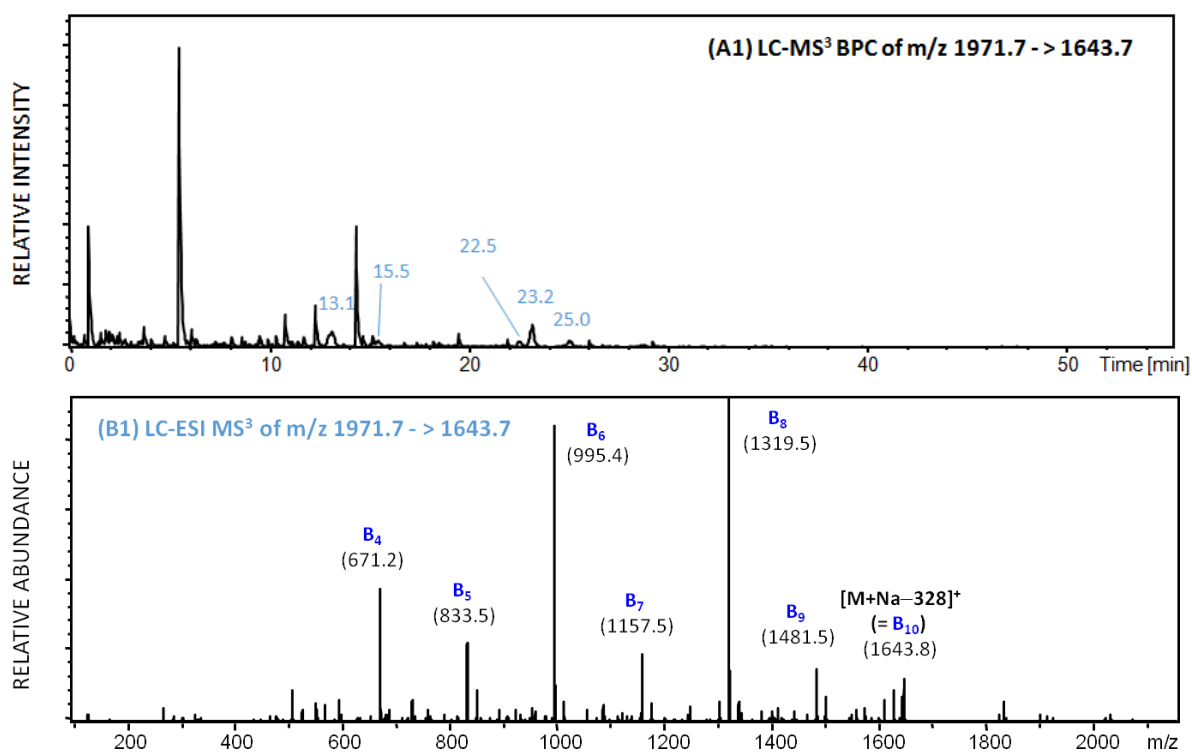


Figure 70: Base peak chromatogram of m/z 1483.5 -> 1643.7 (A1); LC-ESI MS³ of m/z 1483.5 -> 1643.7 (B1)

10.2 Mass spectra of identified crocins containing norcrocin aglycon

In the Figures 71-74 base peak chromatograms (BPC) with corresponding MS² spectra of the found crocetin glycosides with the norcrocin aglycon are given: nC represents abbreviation of norcrocin and the numbers on the left and right side of nC represent the number of glucose units. For better understanding of the BPC and MS spectra, different colors were used to describe different crocin isomers. Peaks which represent the same isomers are labeled with the same color.

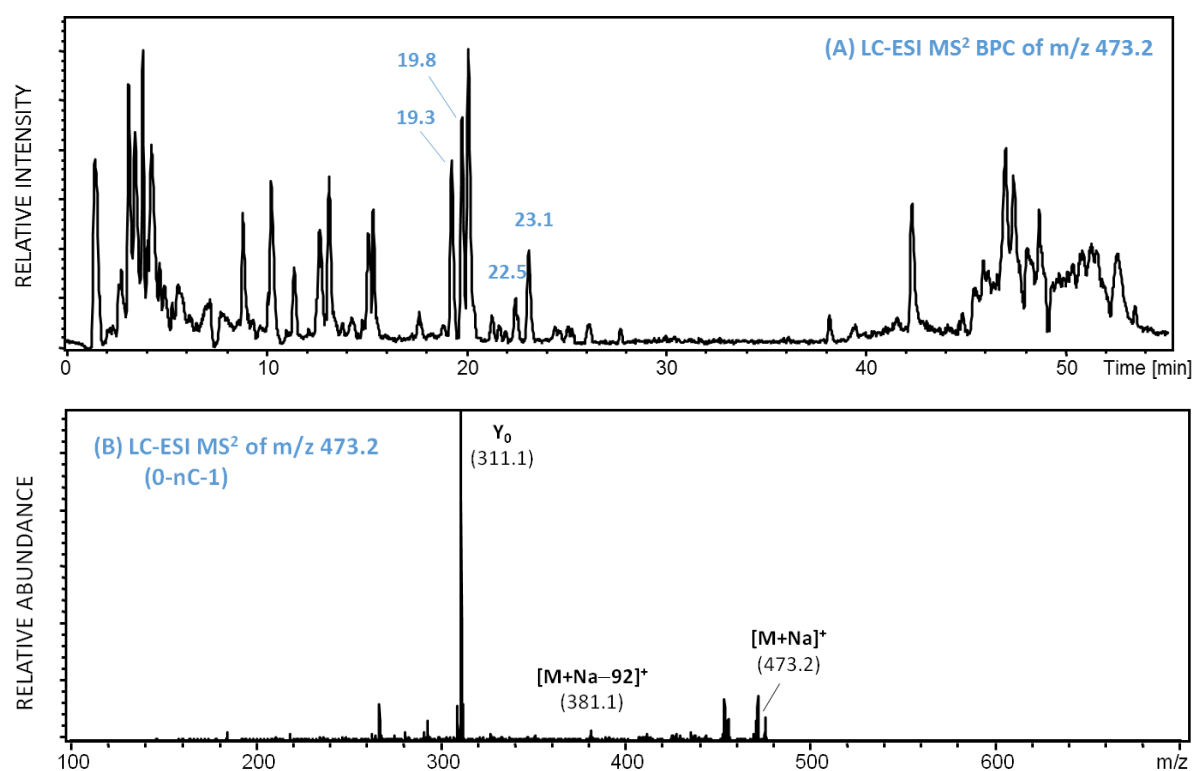


Figure 71: Base peak chromatogram of m/z 473.2 (theoretical m/z 473.21, $\Delta m = 0.01$) (A); LC-ESI MS² m/z 473.2 (theoretical m/z 473.21, $\Delta m = 0.01$) (B)

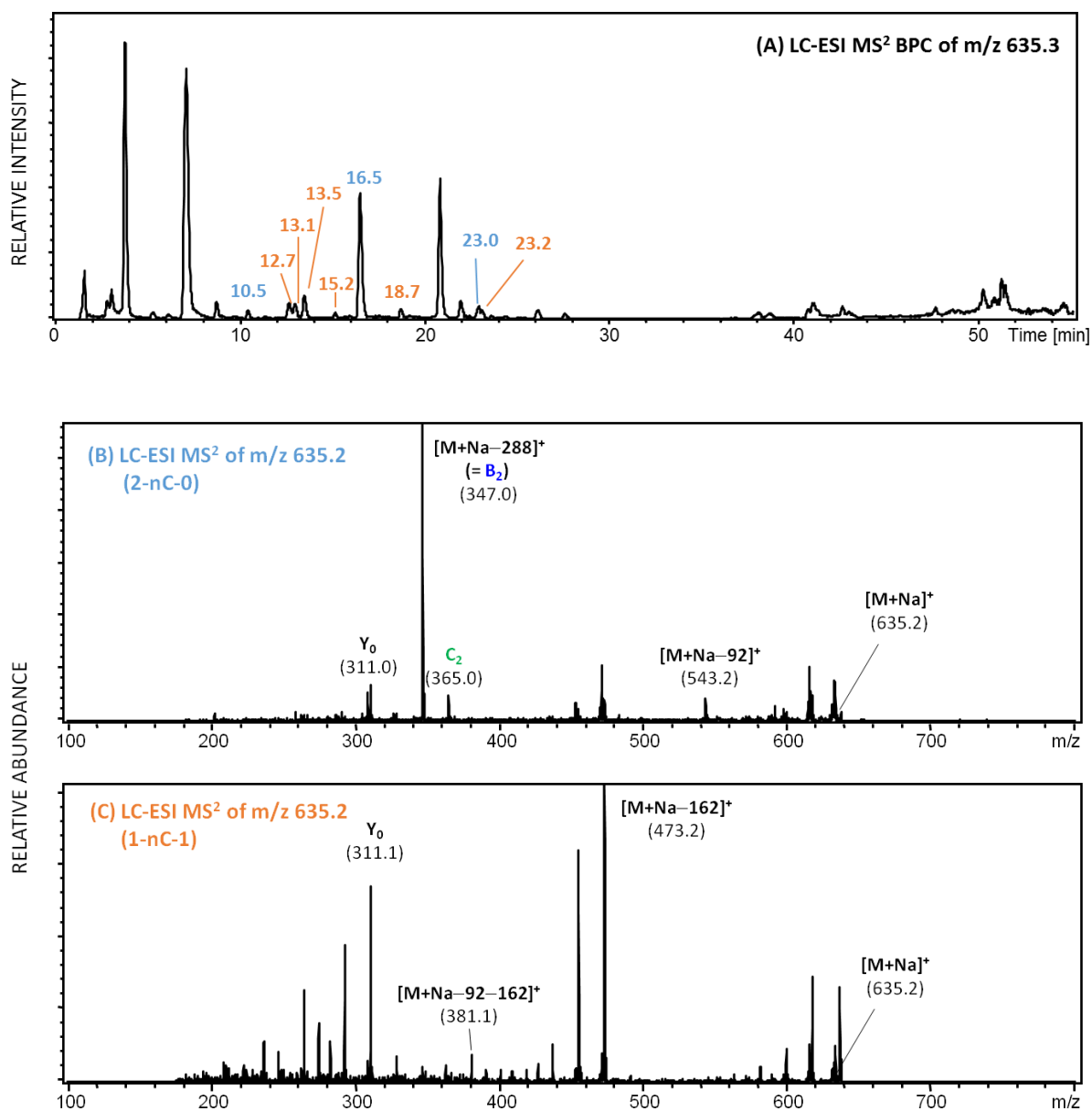


Figure 72: Base peak chromatogram of m/z 635.2 (theoretical m/z 635.26, $\Delta m = 0.06$) (A); LC-ESI MS² of m/z 635.2 (theoretical m/z 635.26, $\Delta m = 0.06$) showing two different isomers (B) and (C)

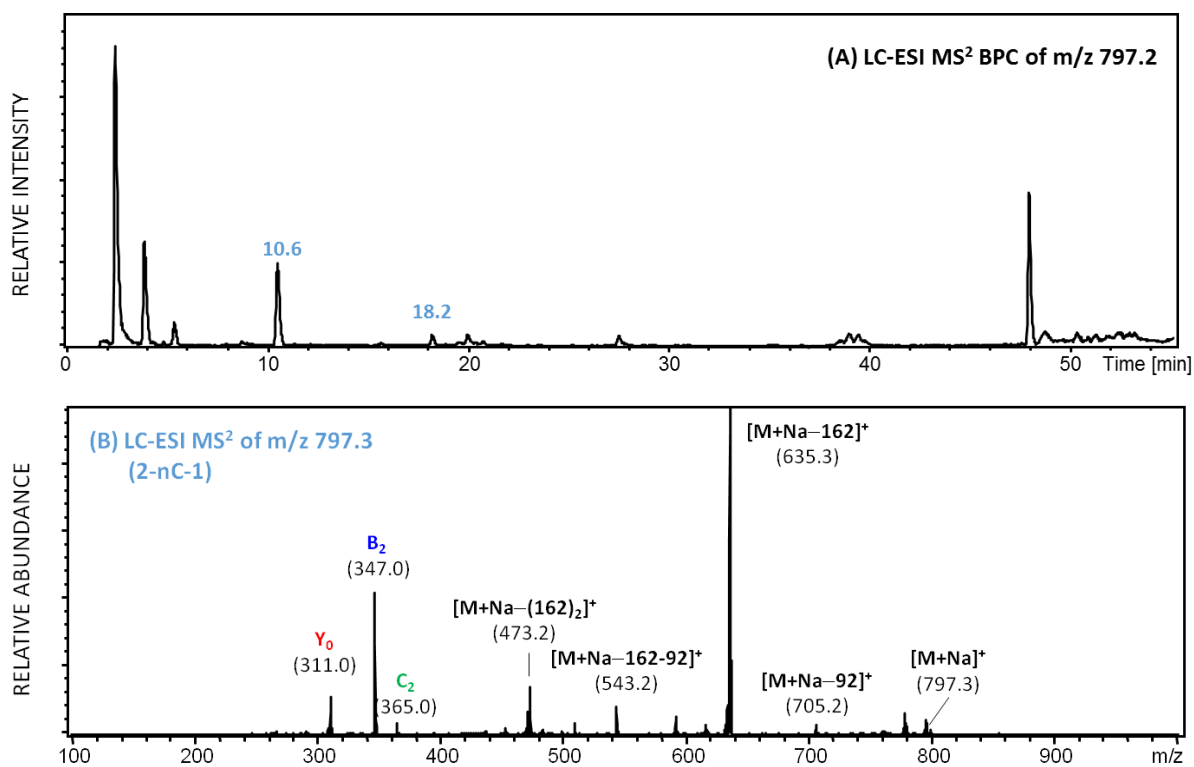


Figure 73: Base peak chromatogram of m/z 797.3 (theoretical m/z 797.32, $\Delta m = 0.02$) (A); LC-ESI MS² of m/z 797.3 (theoretical m/z 797.32, $\Delta m = 0.02$)

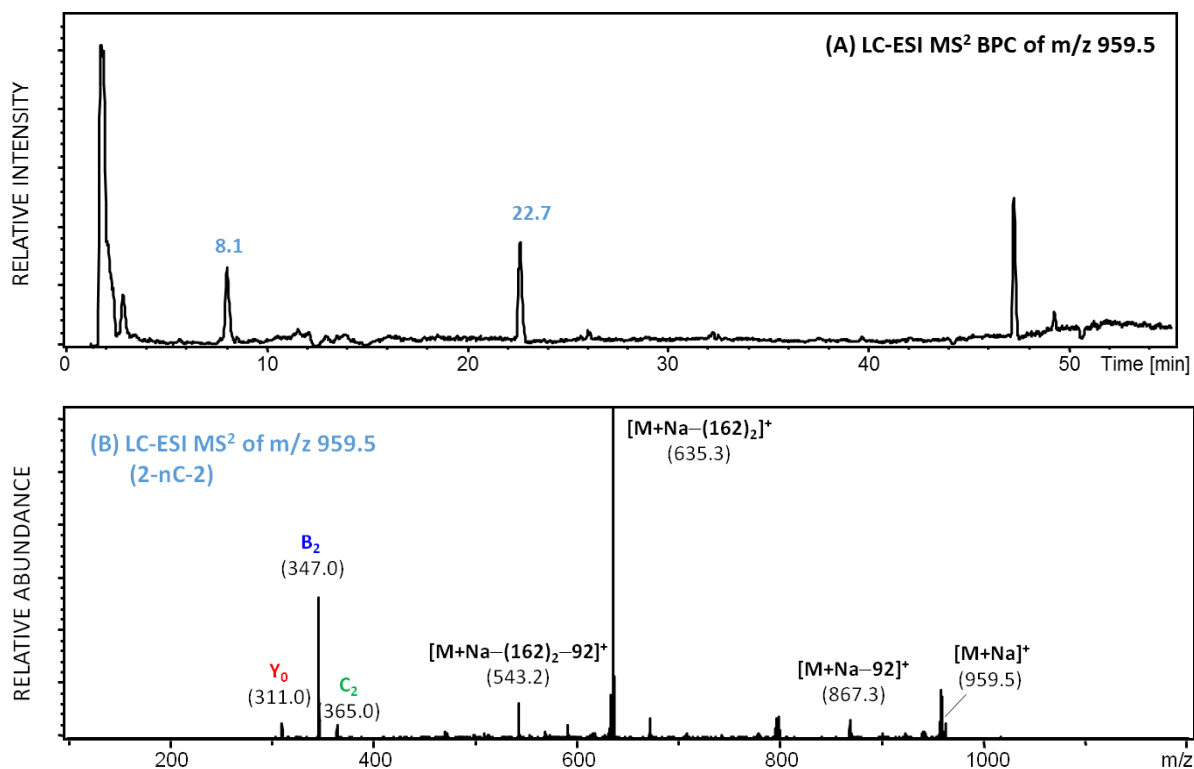


Figure 74: Base peak chromatogram of m/z 959.5 (theoretical m/z 959.37, $\Delta m = 0.13$) (A); LC-ESI MS² of m/z 959.5 (theoretical m/z 959.37, $\Delta m = 0.13$) (B)

10.3 Axima TOF² and UltrafleXtreme IMS results

In the Figure 75-77 imaging results using Axima TOF² instrument and DHB matrix solution are shown, where as in the Figure 78-79 imaging results using THAP matrix solution are shown.

In the Figure 80 the result of IMS experiment with UltrafleXtreme instrument and DHB matrix solution is shown.

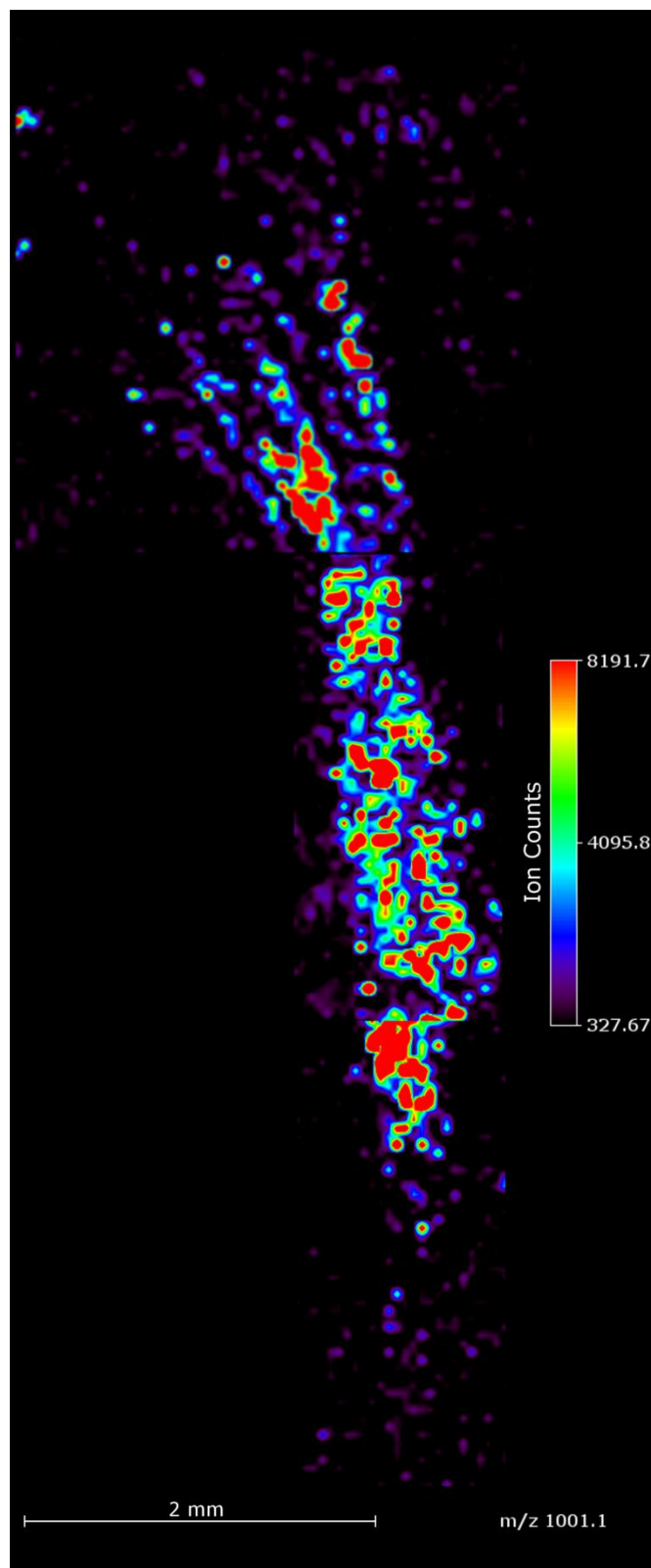


Figure 75: Imaging experiments with the AXIMA TOF² using DHB matrix showing distribution of crocins with four glucose units of stigma A

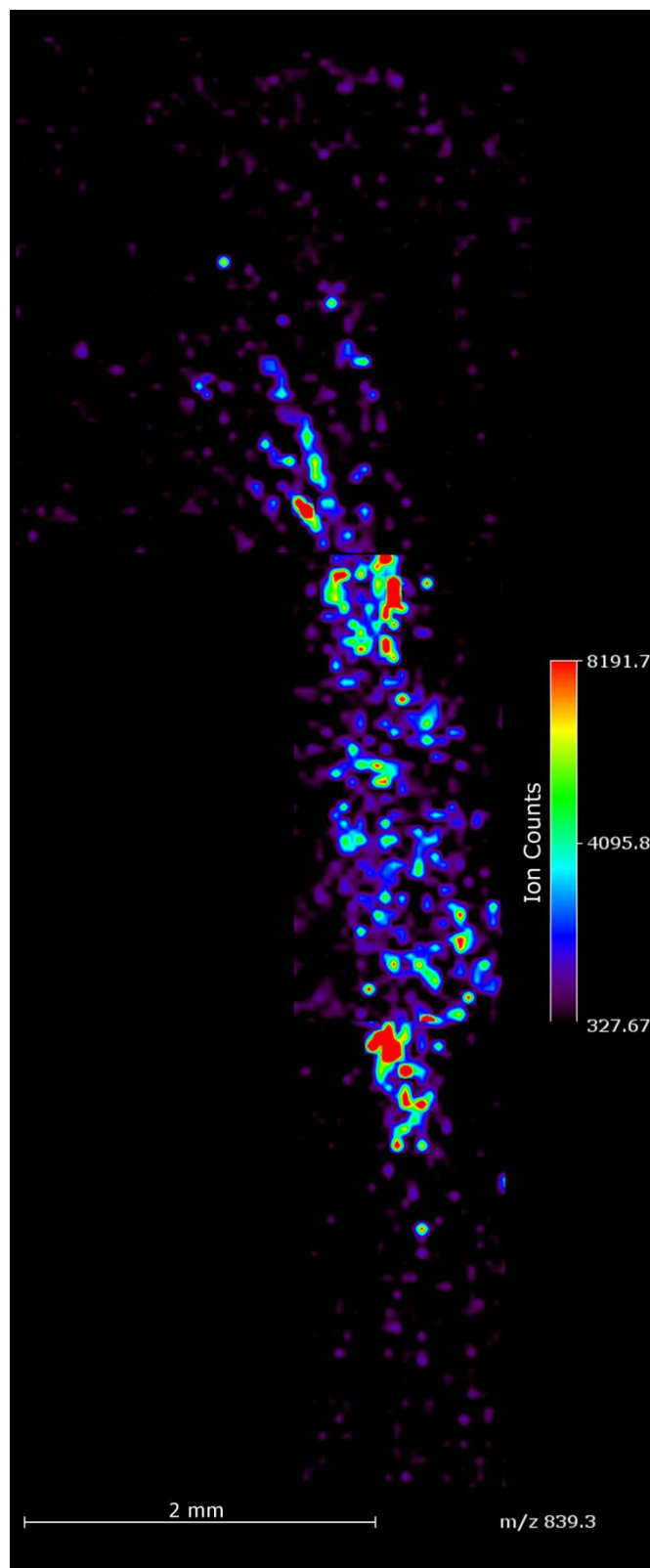


Figure 76: Imaging experiments with the AXIMA TOF² using DHB matrix showing distribution of crocins with three glucose units of stigma A

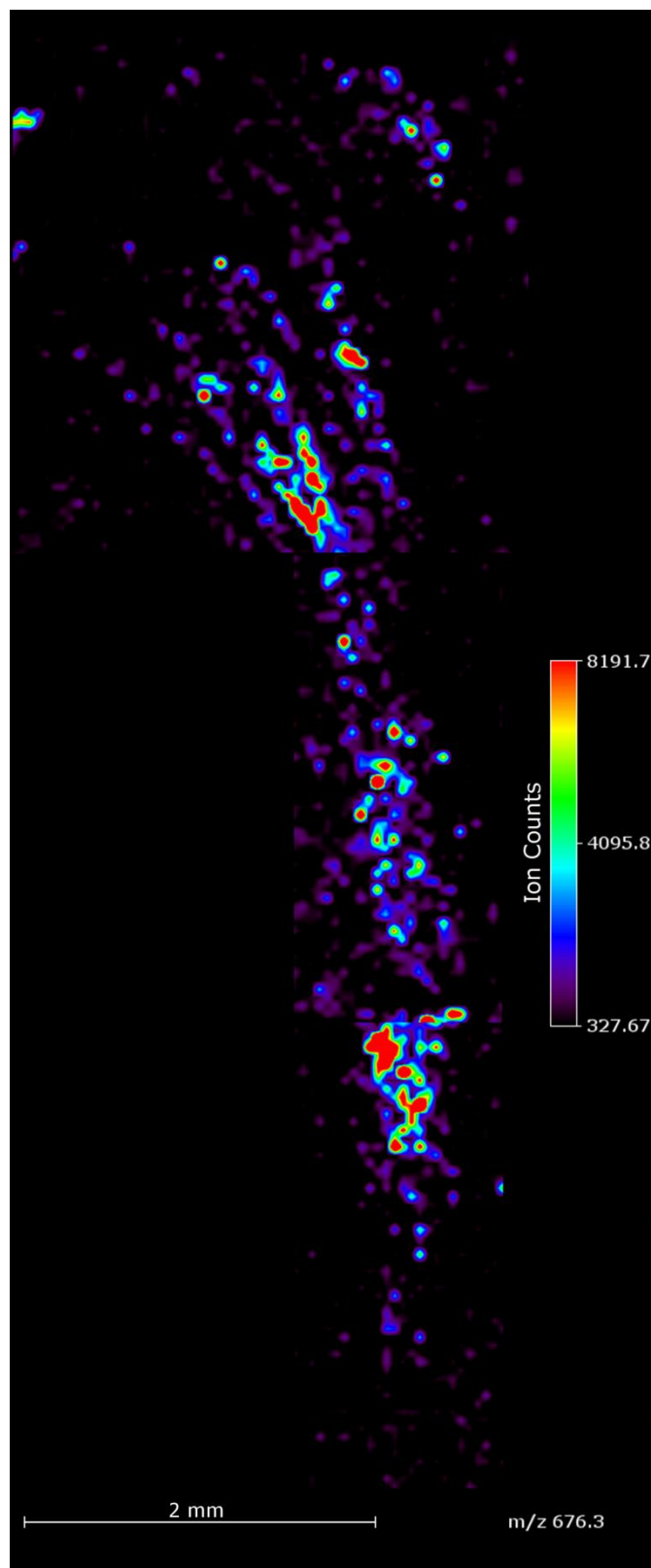


Figure 77: Imaging experiments with the AXIMA TOF² using DHB matrix showing distribution of crocins with two glucose units of stigma A

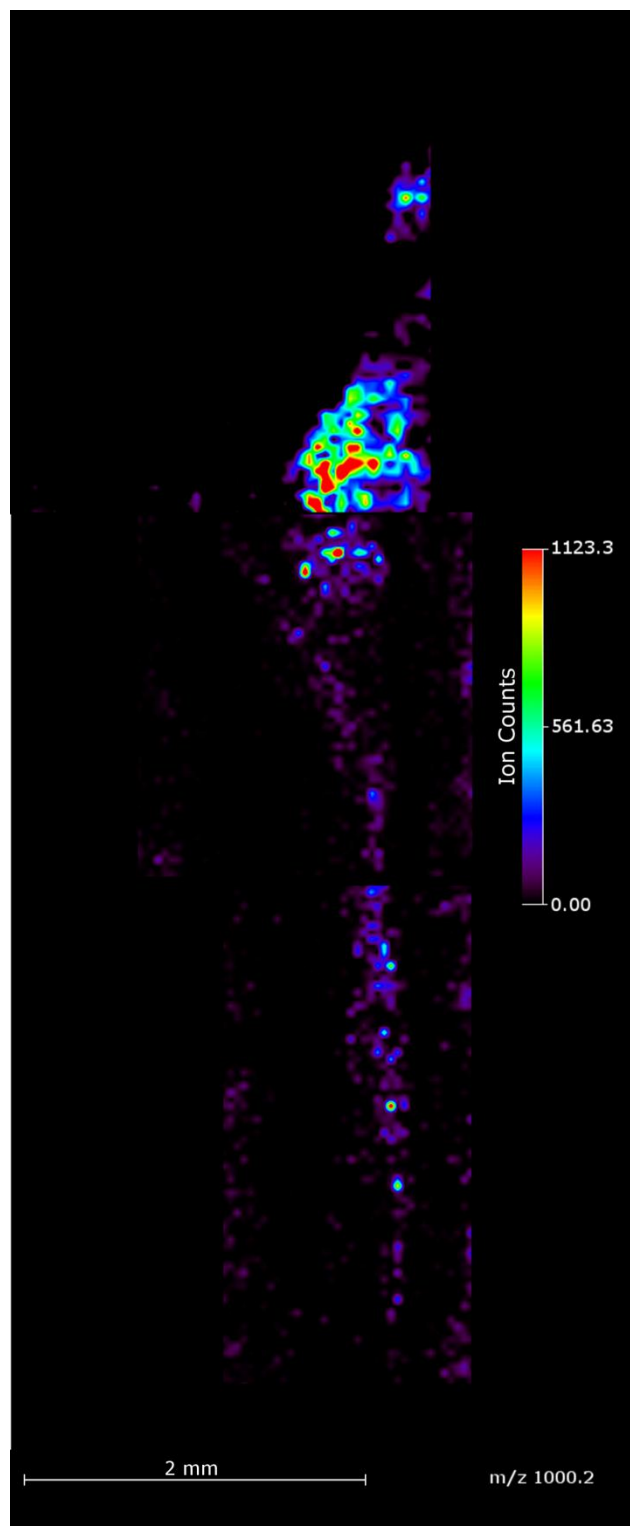


Figure 78: Imaging experiments with the AXIMA TOF² using THAP matrix showing distribution of crocins with four glucose units of stigma A

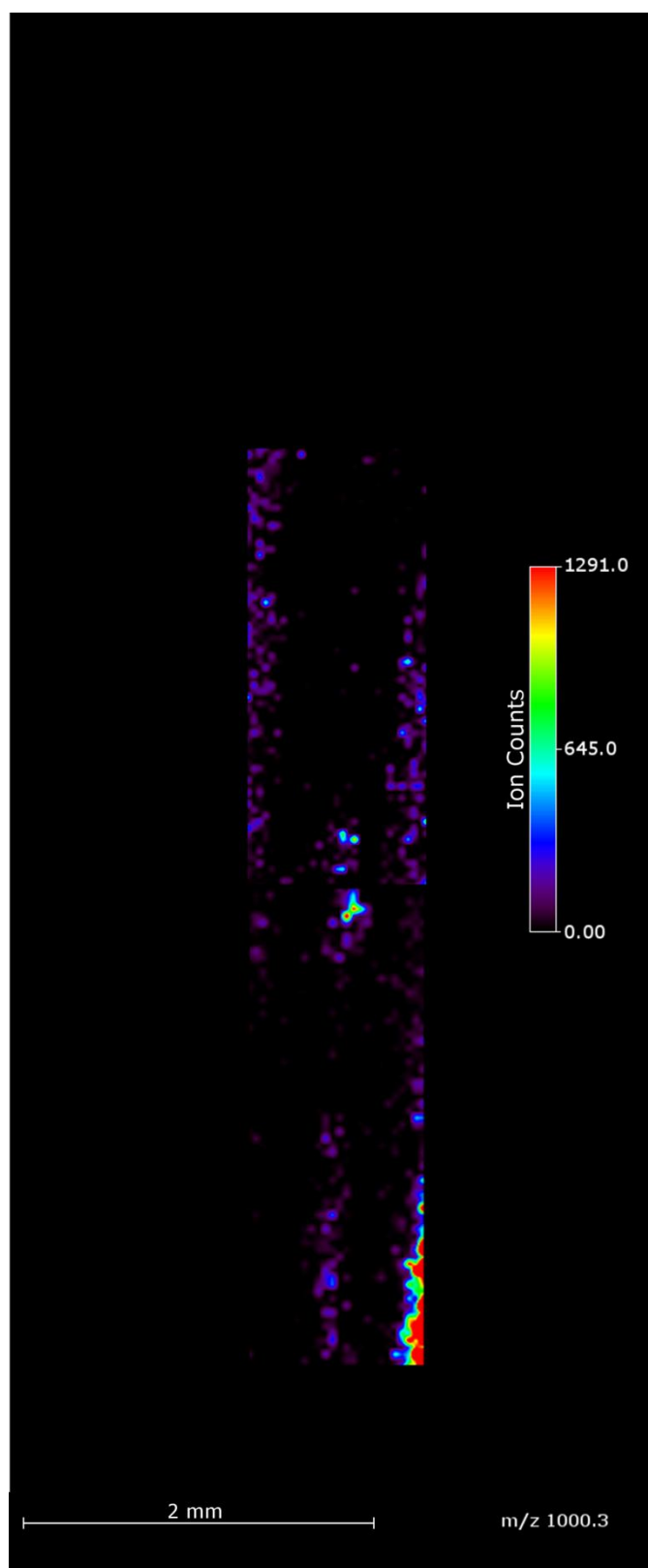


Figure 79: Imaging experiments with the AXIMA TOF² using THAP matrix showing distribution of crocins with four glucose units of stigma

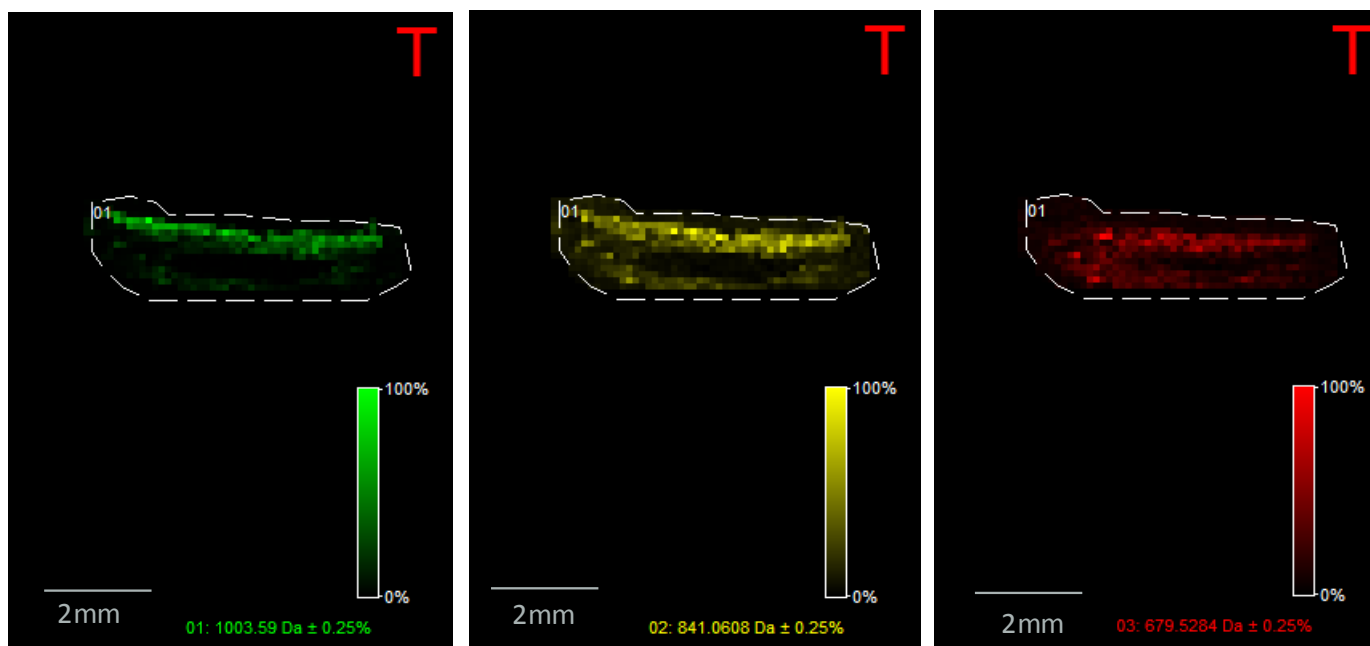


Figure 80: Imaging experiment with the UltrafleXtreme using DHB matrix showing stigma A with different m/z values; Green color represents crocins with four glucose units; Yellow color represents crocins with three glucose units; Red color represents crocins with two glucose unit

10.4 Electron Microscopy results

Figure 81-83 shows electron microscopy results of the saffron stigmas.

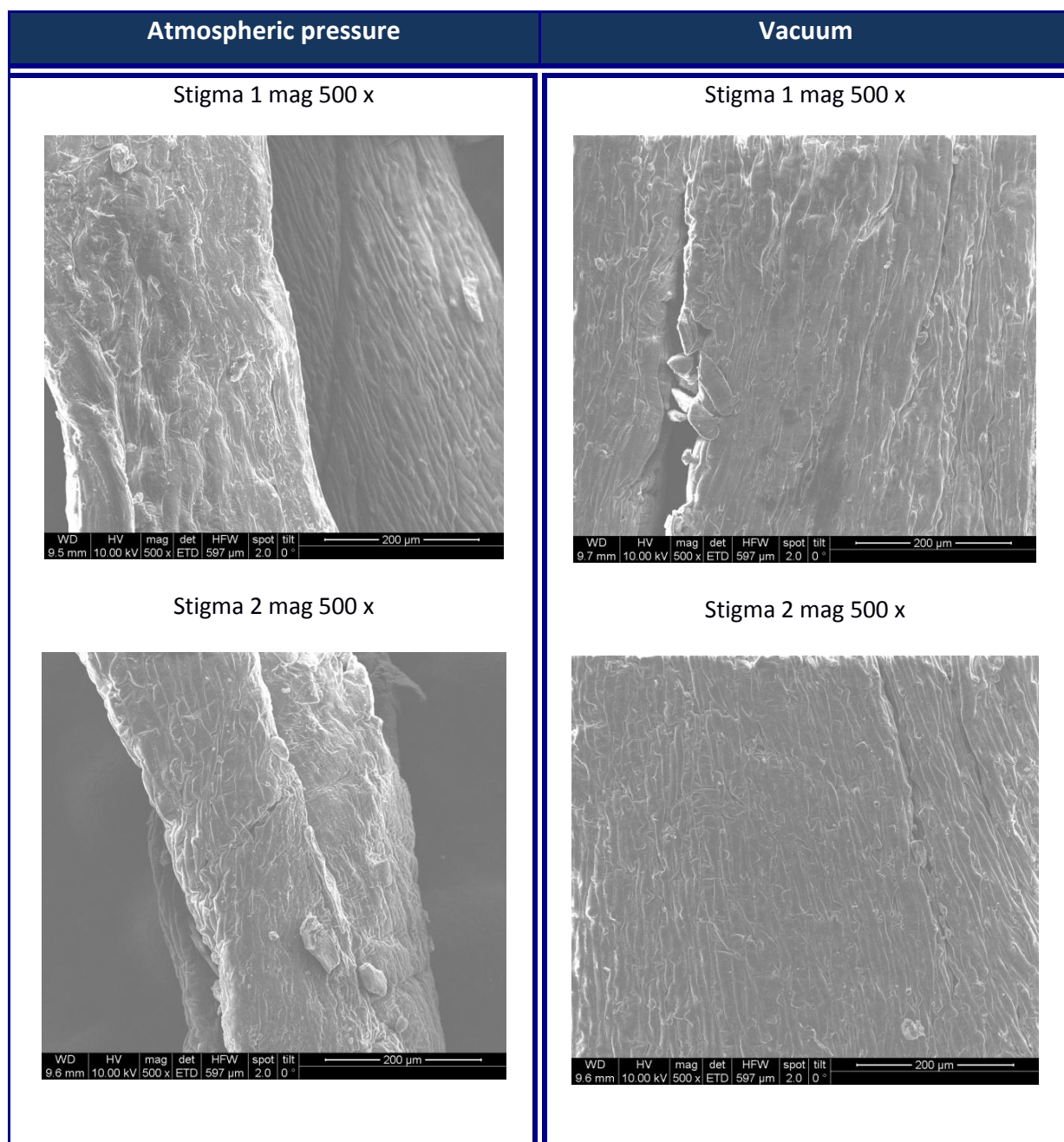


Figure 81: Electron Microscopy images of two saffron stigma (stigma 1 and stigma 2), prepared according to the first approach (see chapter 2.3.1): the left part was stored under atmospheric pressure and the right part in vacuum

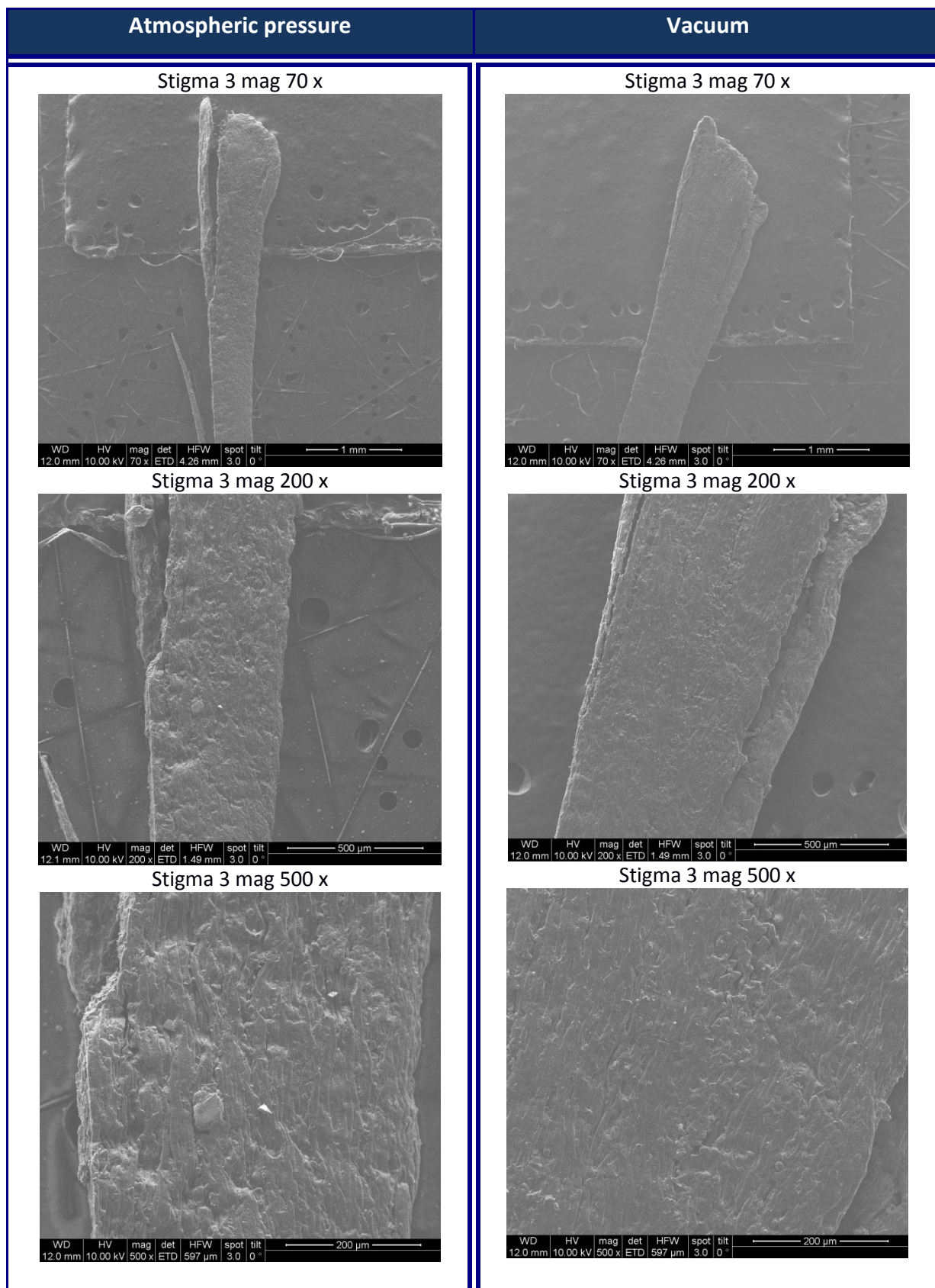


Figure 82: Electron Microscopy images of one saffron stigma (stigma 3), prepared according to the first approach (see chapter 2.3.1): the left part was stored under atmospheric pressure and the right part in vacuum

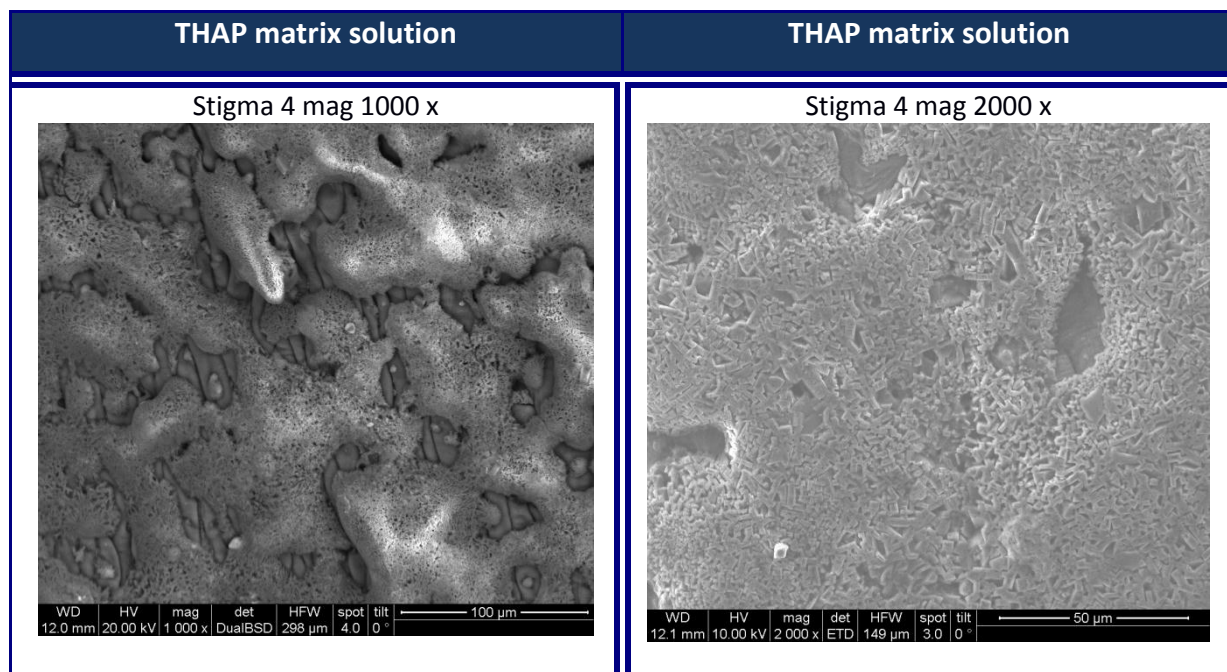


Figure 83: Electron Microscopy images of one saffron stigma (stigma 4) covered with THAP matrix solution, prepared according to the third approach (see chapter 2.3.1)